Modelling of Aqueous Carbon Dioxide Corrosion in Turbulent Pipe Flow

A Thesis

Submitted to the College of Graduate Studies and Research

in Partial Fulfillment of the Requirements

for the Degree of

Doctor of Philosophy

in the Department of Chemical Engineering

University of Saskatchewan

By

Fangyou Wang

Fall 1999

UNIVERSITY OF SASKATCHEWAN

College of Graduate Studies and Research

SUMMARY OF DISSERTATION

Submitted in partial fulfillment

of the requirements for the

DEGREE OF DOCTOR OF PHILOSOPHY

by

Fangyou Wang

Department of Chemical Engineering
University of Saskatchewan

Fall 1999

Examining Committee:

	Dean/Associate Dean/Dean's Designate, Chair, College of Graduate Studies and Research
Dr. D.G. MacDonald	Chair of Advisory Committee, Department of Chemical Engineering
Dr. J. Postlethwaite	Supervisor, Department of Chemical Engineering
Dr. D.J. Bergstrom	Department of Mechanical Engineering
Dr. G.A. Hill	Department of Chemical Engineering
Dr. R. Sumner	Department of Chemical Engineering

External Examiner:

Dr. Paitoon Tontiwachwutikul
Associate Professor
Faculty of Engineering
University of Regina
Regina, Saskatchewan S4S 0A2

In presenting this thesis in partial fulfillment of the requirements for a Postgraduate degree from the University of Saskatchewan, I agree that the Libraries of this University may make it freely available for inspection. I further agree that permission for copying of this thesis in any manner, in whole or in part, for scholarly purposes may be granted by the professor or professors who supervised my thesis work or, in their absence, by the Head of the Department or the Dean of the College in which my thesis work was done. It is understood that any copying or publication or use of this thesis or parts thereof for financial gain shall not be allowed without my written permission. It is also understood that due recognition shall be given to me and to the University of Saskatchewan in any scholarly use which may be made of any material in my thesis.

Requests for permission to copy or to make other use of material in this these in whole or part should be addressed to:

Head of the Department of Chemical Engineering
University of Saskatchewan
Saskatoon, Saskatchewan S7N 5C9
CANADA

Abstract

Carbon dioxide corrosion has long been known to cause severe damage to the production, transportation and refining equipment of crude oil and natural gas. It is a complex phenomenon in which transport, electrochemical and chemical processes occur simultaneously and interactively. In most of the existing CO_2 corrosion mechanistic models, the treatment of transport processes was over-simplified and thus the effects of flow on the corrosion rate cannot be adequately predicted.

This thesis deals with the modelling of aqueous carbon dioxide corrosion of iron in turbulent pipe flow. The objective is to develop a predictive CO_2 corrosion model taking into account the effects of fluid flow on the corrosion processes. The model takes into account diffusion, convection, and charge transfer. It also allows for slow homogeneous chemical reaction of CO_2 hydration and various rapid solution equilibria. Mass transfer is modelled with a two dimensional low Reynolds number k-ε turbulence model by simultaneously solving the conservation equations for mass, axial momentum, radial momentum, kinetic energy of turbulence and its dissipation rate, along with the concentrations of various dissolved species. The effect of the slow homogeneous chemical reaction of CO_2 hydration is incorporated into the model by including an extra source term in the transport equation for carbonic acid. Other homogeneous chemical

reactions are assumed to be in equilibrium with the equilibrium adjusted after each iteration. The cathodic reactions considered are the reduction of carbonic acid, hydrogen ion reduction and the reduction of water. The anodic reaction is iron dissolution. An iterative procedure is employed to calculate CO_2 corrosion rates which ensures that mixed potential theory is satisfied and that the various surface chemical equilibria are preserved. The numerical model is developed in two stages. First, the numerical modelling of the cathodic reactions is performed. The effects of mass transport on the cathodic reactions are studied. Then the anodic reaction of iron dissolution is added into the model to form a corrosion system.

It is shown that at a bulk pH of 4 and very low flow velocities, the reduction of carbonic acid is controlled by the slow homogeneous chemical reaction of CO_2 hydration. The reduction limiting current agrees well with the chemical reaction limiting current given by the Vetter equation (Vetter, 1967). At higher velocities and in the high current density region where Tafel behavior is no longer observed, H_2CO_3 reduction is controlled by the interaction of chemical reaction and mass transfer. At higher current densities, hydrogen ion reduction is controlled by the mass transport of H^+ from the bulk solution to the surface. The H^+ reduction is more flow sensitive than the H_2CO_3 reduction, and CO_2 corrosion is more influenced by flow at pH 4 than at higher pH values due to the fact that the H^+ reduction is the dominant cathodic reaction at pH 4.

Simulation results indicate that the generation of H_2CO_3 by the slow homogeneous chemical reaction of CO_2 hydration enhances the H_2CO_3 mass transport and reduces the H_2CO_3 mass transfer entrance length.

The relative contributions of H_2CO_3, H^+, and H_2O reduction to the corrosion current depend on the solution pH. At pH 4, hydrogen ion reduction and H_2CO_3 reduction are both important. The contribution of water reduction is negligible. At pH 6, the carbonic acid reduction is the dominant cathodic reaction.

The CO_2 corrosion rate is accelerated by flow through an approximate power law: $CR = C \times U_b^n$. At bulk pH 4 the exponent, n, has a value of about 0.4 which is less than 0.8 indicating that the corrosion process is not purely mass transfer controlled. At pH 6, the value of the exponent n is smaller than that for pH 4 which indicates a smaller flow effect at higher pH values. The corrosion rate increases with increasing CO_2 partial pressure. Their relationship is found to be $CR \propto \left(P_{CO_2}\right)^{0.7}$. Present model predictions were tested against experimental results and the de Waard-Lotz model (1993). Good agreement is achieved.

A simplified electrochemical model was also developed for the corrosion of iron in a CO_2-water system. It is built upon the Nesic-Postlethwaite (1994) model and takes into account the following electrochemical reactions: H^+ reduction, H_2CO_3 reduction, H_2O reduction, dissolved oxygen reduction and the iron dissolution. The electrochemical reactions are quantified by using the rate equation that takes into account the effect of

resistance to both charge transfer and mass transfer. Exchange current densities are evaluated based upon the species bulk concentrations. Overall mass transfer coefficients from established correlations for the electroactive species are used in the electrochemical model. Corrosion rates are calculated based on the mixed potential theory. The model is implemented in Microsoft® Excel 97. Corrosion rates are predicted based on the input data such as temperature, pH value, solution velocity, CO_2 partial pressure, and pipe diameter. Using macros and controls through Visual Basic programming, the model is capable of automatically setting up the problem, performing necessary calculations and displaying model predictions in graphs and tables.

Predictions of the present electrochemical model were compared to those of other well-known semi-empirical CO_2 corrosion models and generally good agreement was achieved. The present model is easy to use and, unlike the semi-empirical models, provides the user with a clear picture of the reactions and processes taking place inside the corrosion system. It can be used to study the governing corrosion mechanisms under specified conditions.

Acknowledgments

Thanks are due in the first place to my supervisor, Dr. J. Postlethwaite, for his exceptional support, sound guidance, and financial assistance during all stages of this work.

In addition, I would like to thank my advisory committee members: Dr. D.J. Bergstrom, Dr. G.A. Hill, Dr. D.G. Macdonald and Dr. R.J. Sumner, for their support and supervision.

I would also like to thank my friends and one time co-workers: Dr. Y. Wang and Dr. R. Evitts for their help. Thanks are also due to Mr. Ian MacPhedran, Engineering Computer Center, for his kind assistance.

My special thanks go to Hongbo Zeng, my wife, for her dedication, support and optimism.

Financial support also came from the University of Saskatchewan in the form of a graduate scholarship and computing facilities.

To my Family

Table of Contents

List of Tables

List of Figures

List of Symbols

a_P, a_E, a_W, a_N, a_S transport coefficients in the discretized transport equations

b_a, b_c Tafel slope (anodic and cathodic)

c, C, [] species concentration

$\tilde{c}, c, c'$ instantaneous, mean, and fluctuating species concentration

$C_\mu, C_{\varepsilon 1}, C_{\varepsilon 2}$ turbulence model constants

CR corrosion rate

d straight pipe diameter

D molecular diffusion coefficient

D_t turbulent or eddy diffusivity

E, E_{rev} electrode potential, reversible electrode potential

f fugacity

F Faraday constant (96485 C/mol)

F_{scale} scale factor

f_μ, f_1, f_2 turbulence model functions

i, i_0 current density, exchange current density

J mass flux

$\bar{J}$ Jacobian matrix

k	kinetic energy of turbulence, $\frac{1}{2}\overline{u_i' u_i'}$; local mass transfer coefficient
K	overall mass transfer coefficient
k_b, k_f	rate constants for H_2CO_3 dehydration and CO_2 hydration, respectively
K_H	Henry's law constant
K_{hyd}	equilibrium constant of the CO_2 hydration reaction
l	characteristic length, pipe or cylinder diameter
L	distance from the mass transfer entrance
n	number of electrons involved in overall electrochemical reaction
P	pressure; partial pressure
P'	pressure correction
P_e	Peclet number, $\frac{\rho U \Delta s}{\Gamma}$
P_k	production of turbulence
Q	film correction factor
r	radial coordinate; number of electrons involved in the rate determining step
R	universal gas constant
Re	Reynolds number
R_t	turbulent Reynolds number, $k^2/\nu\varepsilon$
R_Φ	residual for a general variable Φ
S	source term
Sc	Schmidt number, ν/D

S_C, S_P coefficients of the linearized source term

t, T temperature or time

U_i *(U, V, W)* mean velocity components in x, y, and z directions respectively

u_i *(u, v, w)* instantaneous velocity components in x, y, and z directions respectively

u_i' *(u′, v′, w′)* fluctuating velocity components in x, y, and z directions respectively

U_b bulk flow velocity

u^+ dimensionless mean velocity, U/u_τ

u_ε Kolmogorov velocity scale, $(\nu\varepsilon)^{1/4}$

u_τ friction velocity, $(\tau_w / \rho)^{1/2}$

V_{cor} corrosion rate (mm/yr)

x axial coordinate

y distance from the wall

y^* dimensionless distance from wall surface, $u_\varepsilon y/\nu$

y^+ dimensionless distance from wall surface, $u_\tau y/\nu$

δy distance of nearest node from the wall surface

Greek Symbols

$\bar{\alpha}$, $\tilde{\alpha}$ transfer coefficients

β symmetry factor

$\bar{\gamma}$ number of electrons involved in steps preceding the rate determining step

Γ diffusion coefficient

δ boundary layer or reaction layer thickness

ε dissipation of kinetic energy of turbulence

η overpotential, (= $E-E_{rev}$)

μ dynamic viscosity

μ_t turbulent viscosity

ν kinematic molecular viscosity

ν number of times the rate determining step repeated for each occurrence of overall reaction

ρ fluid density

$\sigma_k, \sigma_m, \sigma_\varepsilon$ turbulent Prandtl-Schmidt numbers

Φ general variable

ω rotational speed, equilibrium constant

Subscripts

a anodic

b bulk value; Tafel slope

c cathodic

d diffusion

eff effective value (molecular + turbulent)

f value at the first node from wall

k kinetic energy of turbulence

r	chemical reaction
s	surface value
t	turbulent value

1. Introduction

Carbon dioxide corrosion or sweet corrosion can be defined as the attack of metal by aqueous CO_2 environments. It has long been known that carbon dioxide dissolved in water or aqueous solutions can cause severe corrosion damage to the production, transportation and refining equipment of crude oil and natural gas (Rogers and Shellshear, 1937; Copson, 1951; American Petroleum Institute (API), 1958; Graves and Sullivan, 1966; Schmitt, 1984; Nesic *et al.*, 1997). Carbon dioxide corrosion has in recent years gained new prominence with the advent in particular of enhanced oil recovery techniques based on CO_2 injection into reservoirs and sweet gas production from ever increasing depths (Deberry and Clark, 1979; Gray *et al.*, 1989). Aqueous carbon dioxide corrosion is also a problem in the mineral and food manufacturing industries.

Aqueous CO_2 corrosion is an electrochemical process involving the anodic dissolution of iron and the cathodic evolution of hydrogen. The overall reaction can be written as:

$$Fe + CO_2 + H_2O \rightarrow FeCO_3 + H_2 \qquad (1.1)$$

There have been a number of laboratory as well as field studies of CO_2 corrosion and valuable experimental data have been collected. However, the underlying mechanism of CO_2 corrosion is still not yet well understood. Due to the high cost and long duration of CO_2 corrosion experiments it is imperative that prediction models be developed. Indeed some empirical and semi-empirical models have been developed and are currently being used in the oil and gas industry (e.g., de Waard and Lotz, 1993; Dugstad *et al.*, 1994). These models make use of empirical relationships correlating corrosion rate with some important parameters such as temperature, pH, and CO_2 partial pressure. Since a majority of the empirical relationships were obtained by applying some sort of best-fit technique such as multiple linear regression to a body of experimental data, any extrapolation or sometimes even interpolation of these models can be misleading.

In order to accurately predict a corrosion phenomenon, the models should be based on fundamental theories and equations and involve as few empirical relationships as possible (Nesic *et al.*, 1997). Several electrochemical models have been presented which model the electrochemical reactions and calculate the corrosion current based on fundamental electrochemical principles (e.g., Gray *et al.*, 1990; Nesic *et al.*, 1994). The treatment of transport processes in these mechanistic models, however, was over-simplified. The effects of flow on the corrosion rate were not accurately modelled. The slow homogeneous chemical reaction of CO_2 hydration was either not taken into account or assumed to be always in equilibrium, which is obviously not the case.

The present study deals with aqueous carbon dioxide corrosion of iron and carbon steels in turbulent pipe flow. The objective is to develop a predictive CO_2 corrosion model taking into account the effects of fluid flow on the corrosion processes. All three aspects of the CO_2 corrosion system (mass transport, electrochemical reactions and chemical reactions/equilibria) are incorporated into the present model. Mass transfer is modelled with a low Reynolds number k-ε turbulence model by simultaneously solving the conservation equations for mass, momentum, kinetic energy of turbulence and its dissipation rate as well as species concentrations. The model takes into account diffusion, convection and charge transfer. It also allows for slow homogeneous chemical reaction of CO_2 hydration and various rapid solution equilibria. The generation of H_2CO_3 through the slow homogeneous chemical reaction of CO_2 hydration is incorporated into the model by the inclusion of appropriate source terms. An iterative procedure was used to determine CO_2 corrosion rates by ensuring that various surface chemical equilibria are preserved and that the mixed potential theory is satisfied.

Briefly, the structure of this thesis is as follows. In Chapter 2, the current understanding of carbon dioxide corrosion is reviewed. Important experimental studies as well as some well-known CO_2 corrosion models are presented. Common mitigation measures are also mentioned. The models used in the present study for turbulence, mass transport, chemical equilibria, and corrosion rates are described in Chapters 3, 4, 5, and 6. The mean flow equations and the species transport equations are solved simultaneously with a low Reynolds number model implemented in the near wall

boundary region. Various rapid chemical equilibria are allowed to re-establish after each iteration. In Chapter 7, simulation results are presented. Model predictions are tested against experimental findings and some well-known CO_2 corrosion models. Besides the numerical model that consists of the bulk of this work, a simplified electrochemical model of CO_2 corrosion is also described. In the electrochemical model corrosion rates are determined based on the mixed potential theory. However, unlike the numerical model where the effect of mass transport was modelled through the low Reynolds number k-ε turbulence model, the electrochemical model employs overall mass transfer coefficients from established correlations for the electroactive species. Also, in the electrochemical model the exchange current densities are evaluated based upon the species bulk concentrations. Conclusions of the present study and recommendations for future work are outlined in Chapters 8 and 9.

2. Literature Review

2.1 Introduction

Carbon dioxide corrosion is a complex phenomenon in which several simultaneous and interacting processes occur. Before proceeding to the details of existing studies on CO_2 corrosion, it is appropriate to take a brief look at the properties of carbon dioxide and to present a simplified physical picture of CO_2 corrosion.

Carbon dioxide, CO_2, also known as carbonic anhydride and carbonic acid gas, is a colorless, odorless gas that liquefies at –65 ^{0}C and solidifies as dry ice at –78.2 ^{0}C (Craig and Anderson, 1995). Carbon dioxide does not easily react with other gases in the atmosphere. It does react when in solution with plants, metals, and at elevated temperatures with many other molecules in all forms (Palacios, 1990). As a gas, CO_2 is readily expandable and is soluble in water and various other liquids. The solubility of CO_2 is very dependent on pressure and temperature, and to some extent on the fluid present.

Dry carbon dioxide is non-corrosive. However when dissolved in water, CO_2 is hydrated to form carbonic acid which is responsible for the high corrosion rates of steel

in aqueous CO_2 solutions. It is known that CO_2 hydration is a slow chemical reaction and could become the rate controlling step for the overall corrosion rate (Kern, 1960; Schmitt and Rothman, 1977). A small fraction of carbonic acid is dissociated in two steps to form hydrogen ion, bicarbonate and carbonate ions. These ions eventually reach equilibrium with the undissociated form of carbonic acid.

Electroactive species such as H^+ and H_2CO_3 are transported from the bulk solution to metal surface where the corrosion takes place. The anodic reaction is the iron dissolution and the cathodic reactions include one or more of the following: hydrogen ion reduction, carbonic acid reduction, water reduction and oxygen reduction. Corrosion products such as Fe^{2+} are transported away from the metal surface to the bulk solution.

When the solubility product for a certain salt (e.g. $FeCO_3$) is exceeded, precipitation can occur on the metal surface. Depending on the type of the surface films present and the experimental conditions under which the films were formed, surface films can offer some corrosion protection by reducing mass transfer of the reactants and products in the corrosion process. Iron carbonate precipitation often gives very protective crystalline films at relatively high temperatures (Videm and Dugstad, 1988; Dugstad, 1992). Dugstad (1992) studied film formation on AISI 316 carbon steel in CO_2 saturated aqueous solutions and found that at 80 ^{0}C, protective iron carbonate films were formed after 20-40 hours of exposure and the corrosion rate was reduced by a factor of 7. The scanning electron microscope (SEM) results indicated a $FeCO_3$ film thickness of approximately 160 μm.

2.2 Experimental Studies

2.2.1 Carbon Dioxide Corrosion Mechanisms

In a groundbreaking study, de Waard and Milliams investigated in 1975 the corrosion of X-52 carbon steel in 0.1% NaCl solutions saturated with carbon dioxide (de Waard and Milliams, 1975a). The corrosion rate, which was determined by means of weight loss and polarization resistance measurements, was found to be significantly different from that expected for completely dissociated acids at the same pH. Their theoretical analysis showed that this fact can be quantitatively explained only if the direct reduction of undissociated carbonic acid was involved in the cathodic process:

$$H_2CO_3 + e^- \rightarrow H + HCO_3^- \tag{2.1}$$

The work of de Waard and Milliams provided strong experimental support for the fact that carbonic acid can be more corrosive than a completely dissociated acid at the same pH and had demonstrated that the direct reduction of H_2CO_3 is an important cathodic reaction in CO_2 corrosion.

Efforts had been made to study the cathodic reaction of H_2CO_3 reduction. Schmitt and Rothmann (1977) found through polarization experiments on rotating disk electrodes that the cathodic limiting currents in CO_2-water systems consist of two distinct parts: the diffusion controlled H^+ reduction limiting current and the (CO_2 hydration) chemical reaction-controlled H_2CO_3 reduction limiting current:

$$i_{\lim} = i_{\lim,diffusion(H^+)} + i_{\lim,reaction(H_2CO_3)} \tag{2.2}$$

According to them, the direct reduction of H_2CO_3 is controlled by the preceding slow *heterogeneous* chemical reaction of carbon dioxide hydration:

$$CO_{2(ad)} + H_2O \rightarrow H_2CO_{3(ad)} \tag{2.3}$$

where the subscript "ad" stands for adsorbed. Carbon dioxide is first adsorbed onto the metal surface before the hydration reaction could take place. Experiments of Gray *et al.* (1989) confirmed the composition of cathodic limiting currents. However, Gray *et al.* proposed that it is the slow *homogeneous* chemical reaction of CO_2 hydration that is controlling the H_2CO_3 reduction:

$$CO_{2(aq)} + H_2O \rightarrow H_2CO_{3(aq)} \tag{2.4}$$

where the subscript "aq" denotes aqueous. They argue that similar cathodic limiting currents were observed on metals as different as platinum and iron (Schwenk, 1974; de Waard and Milliams, 1975a). This could not have been possible if the heterogeneous CO_2 hydration was the controlling step as different limiting currents would have been expected due to the different adsorption characteristics of CO_2 on different metals. Gray *et al.* also suggested that in CO_2 corrosion, the charge transfer controlled bicarbonate ion reduction could be the dominant cathodic reaction at pH 6 through 10:

$$2HCO_3^-{}_{(aq)} + 2e^- \rightarrow H_{2(g)} + 2CO_3^{2-}{}_{(aq)} \quad (2.5)$$

Nesic *et al.* (1995) observed through their rotating cylinder experiments that the H_2CO_3 reduction limiting current can be affected by flow. It was found that the H_2CO_3 limiting current (with contributions from chemical reaction and from diffusion) increases with rotational speed at relatively high rotational speed ranges. By introducing a "flow factor" to account for the effect of flow on the reaction limiting current, they have derived a theoretical expression for the superposition of the diffusion and chemical reaction controlled limiting currents. It was suggested that the interaction between diffusion and chemical reaction in CO_2 corrosion is significant at temperatures lower than 40 ^{0}C and velocities higher than 1 m/s when the mass transfer layer is of the similar thickness as the reaction layer. The flow factor will be discussed in greater detail later.

Schmitt and Rothmann (1978) determined that the anodic reaction of iron dissolution follows the three-step pH-dependent mechanism proposed by Bockris *et al.* (1961):

$$Fe + OH^- \Leftrightarrow FeOH + e^- \quad (2.6)$$

$$FeOH \xrightarrow{RDS} FeOH^+ + e^- \quad (2.7)$$

$$FeOH^+ \Leftrightarrow Fe^{2+} + OH^- \quad (2.8)$$

This mechanism of iron dissolution has been assumed in CO_2 corrosion studies by most authors (e.g., de Waard and Milliams, 1975a; Gray *et al.*, 1989; Nesic *et al.*, 1995).

2.2.2 The pH of Aqueous CO_2 Solutions

The pH of a CO_2 saturated aqueous solution is dependent, among other parameters, on the CO_2 partial pressure and temperature. If the second dissociation step of carbonic acid is neglected, the hydrogen ion (H^+) concentration is equal to the bicarbonate ion (HCO_3^-) concentration for a pure CO_2-water solution. According to the definition of the dissociation (equilibrium) constant of carbonic acid, K, the following applies:

$$[H^+]^2 = K[H_2CO_3] \tag{2.9}$$

The concentration of carbonic acid is proportional to the CO_2 partial pressure as described by Henry's law:

$$[H_2CO_3] = K_H P_{CO_2} \tag{2.10}$$

where K_H is the Henry's law constant. Combining equations (2.9) and (2.10) yields:

$$pH = -0.5 \times \log\left(P_{CO_2}\right) + c \tag{2.11}$$

where c is a constant which incorporates the Henry's law constant and the carbonic acid dissociation constant, and obviously it is a function of temperature. De Waard and Milliams (1975a) have measured the pH of a 0.1% NaCl solution as a function of temperature for P_{CO_2} = 1 bar (10^5 Pa) and obtained the following linear relation:

$$pH_{(P_{CO_2}=1\ bar)} = 4.17\times10^{-3}\cdot t + 3.71 \tag{2.12}$$

where t is temperature (^{0}C). Substituting equation (2.12) into equation (2.11) yields:

$$pH = -0.5\times\log\left(P_{CO_2}\right) + 4.17\times10^{-3}\cdot t + 3.71 \tag{2.13}$$

In the expression, P_{CO_2} is the CO_2 partial pressure (bar) and t is the temperature (^{0}C).

2.2.3 Effects of CO_2 Partial Pressure

In the aforementioned study of de Waard and Milliams (1975a), the relationship between corrosion rates and the CO_2 partial pressure at the temperatures studied (15, 25, and 60 ^{0}C) was found to be exponential and the exponent is 0.67:

$$CR = const\cdot\left(P_{CO_2}\right)^{0.67} \tag{2.14}$$

Other authors have found similar power laws between corrosion rates and CO_2 partial pressure with the exponent in the range of 0.5 to 0.8 (e.g., Ikeda *et al.*, 1983; Schmitt, 1983; Videm and Dugstad, 1989).

2.2.4 Effects of Flow

Flow plays an important role in a process with complete or partial mass transfer control. So far it has been established that in CO_2 corrosion, at higher current densities where Tafel behavior is no longer observed, H^+ reduction is mass transfer (diffusion) controlled and H_2CO_3 reduction is controlled by the interaction between mass transfer and chemical reaction at higher velocities. Therefore it is expected that flow will affect the CO_2 corrosion rates.

Generally speaking for corrosion with no protective films present, the acceleration effect of turbulent flow on corrosion rate can be expressed as:

$$CR = const \times U_b^{\,n} \tag{2.15}$$

The value of the exponent, n, is dependent on the corrosion mechanism. Manner and Heitz (1978) determined theoretically that, for a diffusion-controlled transport in a smooth pipe with developed flow, n is equal to 0.8. Videm and Dugstad (1989), through investigations on different steels and under various experimental conditions, found that n varies with the solution pH and that the value of n is in the range of 0.4 to 0.7 which indicated that the corrosion was not under total mass transport control. They also concluded that steels respond differently to flow rate variations in that steels with the lowest corrosion rates are the least influenced by flow.

2.2.5 Effects of Temperature

Temperature has a significant influence on corrosion rates. It is generally agreed that under given CO_2 partial pressure the corrosion rate increases with increasing temperature until a certain temperature is reached. Beyond this temperature protective surface films are formed and the corrosion rates actually decrease with increasing temperature. This means the corrosion rate passes through a maximum at this threshold temperature.

A number of authors have found that above 60 ^{0}C, the corrosion rate was controlled by the formation of protective scales which consist primarily of iron carbonate (e.g., Ikeda *et al.*, 1983; Eriksrud and Søntvedt, 1984; Dunlop *et al.*, 1985; Murata *et al.*, 1985; Hausler, 1985). At temperatures lower than 60 ^{0}C, different surface films may still develop. However, they are not protective due to their open porous structure and poor bond with the substrate metal. This may have been influenced by the experimental conditions under which the films were formed. In fact, Videm and Dugstad (1989) observed three different films in the entire temperature range of 5 to 90 ^{0}C. Studies of Dugstad (1992) indicated that the iron carbonate content in the surface films increases with temperature.

2.2.6 Hydrogen Sulfide and Oxygen Contamination

Autoclave tests conducted by Ikeda *et al.* (1985) to study the effects of hydrogen sulfide and oxygen contamination on CO_2 corrosion found that the presence of even a small amount of H_2S could be very detrimental. Hydrogen sulfide accelerates CO_2 corrosion through the acceleration of the anodic dissolution of iron:

$$Fe + H_2S \rightarrow FeS + 2H^+ + 2e^- \tag{2.16}$$

However, with the increase of H_2S concentration, the possibility of FeS film formation also increases which could decrease the corrosion rate. The presence of oxygen, on the other hand, means the introduction of an additional cathodic reaction (the reduction of oxygen). Therefore it increases the corrosion rate with increasing oxygen concentration.

2.3 Modelling Studies

There are currently many different CO_2 corrosion models in use in the oil and gas industry. Based on how firmly the models are grounded in theory, Nesic *et al.* (1997) have classified them into three categories: mechanistic, semi-empirical, and empirical models. For convenience and clarity, this line of thinking is adopted here.

Mechanistic models have a strong theoretical background. Most of the constants appearing in these models have a clear physical meaning. According to Nesic *et al.* (1997), when calibrated on a reliable experimental database this type of model should

generally produce accurate and physically realistic results. Partially based on theory, semi-empirical models are for practical purposes. Wherever insufficient knowledge is available about a phenomenon, empirical functions are used. Therefore some of the constants used in the models have a clear physical meaning while others may just be best-fit parameters. Calibrated with an adequately large and reliable experimental database, this type of model should enable good interpolation predictions. However, extrapolation could be misleading and questionable. Purely empirical models have little theoretical backing and most or all of the constants have little physical meaning and are just best-fit parameters to the available experimental data. Extrapolation of empirical models could be very risky. Because of the large number of models available and because most models are similar to one another with minor modifications, only a few of the most representative models are discussed in this review.

2.3.1 Mechanistic Models

As pointed out earlier CO_2 corrosion is a complex phenomenon in which several simultaneous and interacting processes occur. These include electrochemical reactions, chemical reactions, and transport processes. An entirely mechanistic model should seamlessly incorporate all three aspects. Unfortunately this is not the case with almost all of the currently available models.

One of the most well-known and widely referenced models is the de Waard and Milliams model (de Waard and Milliams, 1975b). Strictly speaking it is only a partially

mechanistic model. Based on their experimental data from electrochemical studies, they presented a correlation between the corrosion rate and temperature and CO_2 partial pressure:

$$\log(V_{cor}) = 7.96 - \frac{2320}{273+t} - 0.00555 \times t + 0.67 \times \log(P_{CO_2}) \tag{2.17}$$

where V_{cor} is the corrosion rate in mm/yr, t is the temperature in ^{0}C, and P_{CO_2} is the CO_2 partial pressure in bar (10^5 Pa). The authors later revised the model constants based on the experimental results of Dugstad *et al.* (1994) and obtained the following expression:

$$\log(V_{cor}) = 5.8 - \frac{1710}{273+t} + 0.67 \times \log(P_{CO_2}) \tag{2.18}$$

This formula is sometimes referred to as the "de Waard-Milliams equation". Since its inception, the de Waard and Milliams model has been used extensively and reasonably satisfactorily. However serious limitations exist which restrain its applicability.

Equation (2.18) implies that there are no reaction rate limitations from mass transfer effects and thus it could be seen as a "worst case" scenario. The model assumes that all the hydrogen ions in the solution come from the dissociation of carbonic acid and thus the solution pH is dependent on CO_2 partial pressure only. This, in practice, is not true. Other species and corrosion products such as bicarbonate salts and ferrous ions could also influence the pH of the solution. The temperature correlation in equation (2.16) was obtained by assuming an Arrhenius type dependence for a charge transfer

controlled process. Obviously this is questionable as the effect of temperature on mass transfer process was not taken into account.

The original de Waard and Milliams model has subsequently been modified by introducing various correction factors to account for the effects of corrosion product films, velocity, pH, system pressure and some other parameters. The corrosion rate is calculated by multiplying the "base value" with a series of correction factors. This is a typically semi-empirical strategy and will be explained in the next section.

Based on their rotating disk electrode studies on CO_2 corrosion mechanisms, Gray *et al.* (1989, 1990) presented an electrochemical model which takes into account the following electrochemical reactions: iron dissolution, diffusion controlled H^+ reduction, chemical reaction controlled H_2CO_3 reduction, and charge transfer controlled H_2O reduction. The anodic reaction of iron dissolution was assumed to follow the Bockris mechanism (Bockris *et al.*, 1961). The corrosion current was calculated based on the mixed potential theory (Stern and Geary, 1957; Bockris and Reddy, 1970) which states that at corrosion potential E_{corr}, the anodic current is equal to the sum of the cathodic currents and both are equal to the corrosion current i_{corr}:

$$i_{corr} = i_a = \sum |i_c| \tag{2.19}$$

Current densities arising from charge transfer controlled anodic and cathodic reactions were calculated by assuming pure Tafel behavior:

$$i_a = i_{0,a} \exp\left[2.303(E - E_{rev,a}) / b_a\right] \tag{2.20}$$

$$i_c = -i_{0,c} \exp\left[-2.303(E - E_{rev,c}) / b_c\right] \tag{2.21}$$

For cathodic reactions with mixed diffusion and charge transfer control, the current density was given by the following equation (Nagy and Thomas, 1986):

$$\frac{1}{i_c} = -\frac{1}{i_{c,ct}} - \frac{1}{i_{\lim,d}} \tag{2.22}$$

where $i_{c,ct}$ is the charge transfer controlled cathodic current which is given by equation (2.19) and $i_{\lim,d}$ is the diffusion limiting current which was calculated from the Levich equation (Bard and Faulkner, 1980):

$$i_{\lim,d} = 0.62nFD^{2/3}\nu^{-1/6}\omega^{1/2}C \tag{2.23}$$

For cathodic reactions with mixed chemical reaction and charge transfer control, the current density was calculated from a similar equation as equation (2.22) except $i_{\lim,d}$ is now replaced with the chemical reaction limiting current, $i_{\lim,c}$, (Vetter, 1967):

$$i_{\lim,c} = \frac{nFD\left\{[CO_2{}^0{}_{(aq)}] + [H_2CO_3{}^0{}_{(aq)}]\right\}}{\left(\delta_d + \delta_r k_b / k_f\right)} \tag{2.24}$$

where D is the diffusion coefficient for carbonic acid, k_b and k_f are the backward (dehydration) and forward (hydration) reaction rate constants, respectively, for the CO_2 hydration reaction. The diffusion boundary layer thickness, δ_d, and the reaction layer thickness, δ_r, are given by:

$$\delta_d = 1.61 D^{1/3} \nu^{1/6} \omega^{-1/2} \tag{2.25}$$

$$\delta_r = \sqrt{\frac{D}{(k_f + k_b)}} \tag{2.26}$$

where ν is the kinematic viscosity of the solution and ω is the rotational speed. The values of Tafel slopes and exchange current densities, which were initially taken from the literature, were optimized by trial and error until good agreement between the calculated and experimental polarization curves was obtained. The model was developed at pH 4 and 25 ^{0}C and subsequently extended to higher pH's and temperatures. It was the first instance of systematic approach to the electrochemical modelling of CO_2 corrosion.

Following the approach of Gray *et al.*, Nesic *et al.* (1994, 1995) conducted a follow-up study and also presented an electrochemical model of CO_2 corrosion. The Bockris mechanism (Bockris *et al.*, 1961) was not assumed in the model as their experiments found it did not hold true in their specific system at pH higher than 4. Physical constants appearing in the model were obtained from the literature or, when

unavailable, determined from their own rotating cylinder glass cell experiments. The model predictions were successfully compared with independent pipe flow glass loop experiments which demonstrated the model's good extrapolation capability. The model was also tested against two semi-empirical models (de Waard and Lotz, 1993; Dugstad *et al.*, 1994) and its predictions were in most cases in between those of the two semi-empirical models.

It is worth mentioning that Nesic *et al.* (1995) later proposed a correction factor to account for the effect of flow on the H_2CO_3 reduction limiting current. It was called the "flow factor" and was derived theoretically by solving analytically the simplified form of the steady one-dimensional transport equation for H_2CO_3. It is given by the following equation:

$$f = \frac{1+e^{-2\zeta}}{1-e^{-2\zeta}} \tag{2.27}$$

where ζ is the ratio of the diffusion boundary layer thickness, δ_d, to the reaction boundary layer thickness δ_r:

$$\zeta = \frac{\delta_d}{\delta_r} \tag{2.28}$$

The boundary layer thicknesses were estimated by:

$$\delta_d = \frac{D}{k_m} \tag{2.29}$$

$$\delta_r = \sqrt{\frac{D}{k_b}} \tag{2.30}$$

where D is the diffusion coefficient for carbonic acid, k_m is the mass transfer coefficient for straight pipe calculated using the Berger-Hau correlation, and k_b is the backward (dehydration) reaction rate constant for the CO_2 hydration reaction.

While both the Gray *et al.* model and the Nesic *et al.* model described in detail the electrochemical processes taking place on the metal surface, the treatment of the transport processes in the boundary layer was oversimplified. Also the chemical equilibria were not taken into account. In order to accomplish these tasks, a numerical modelling approach is needed.

2.3.1.1 Numerical Modelling

In their work entitled "Modelling of Electrode Processes and Surface Chemistry in Carbon Dioxide Containing Solutions," Turgoose *et al.* (1990) established a numerical approach to the realistic modelling of the cathodic reactions involved in CO_2 corrosion. Following the basic approach given by Bard and Faulkner (1980), the model considers the electron transfer reactions, diffusion, convection, the slow chemical hydration reactions, and rapid solution equilibria on a rotating disk electrode, though

detailed information was not given in the paper. The model was primarily developed to study CO_2 corrosion mechanisms. It demonstrated that the increase in cathodic limiting current at pH values higher than 6 was a result of the solution chemical equilibria and the direct reduction of bicarbonate ions is not necessary to explain the experimental data. This is in contrast to the results of Gray *et al.* (1990) which concluded that in the pH range of 6 to 10, the reduction of bicarbonate ions might be the dominant cathodic reaction.

Another numerical model is the one presented by Nesic (1994). The model considered 7 chemical species (H^+, OH^-, CO_2, H_2CO_3, HCO_3^-, CO_3^{2-} and Fe^{2+}). Four chemical reactions were included in the model which were ionization of water, CO_2 hydration, and the two dissociation steps of H_2CO_3. Mass transport of species was modelled by solving the one-dimensional transient transport equation for all relevant species. The surface concentrations of H^+ and H_2CO_3 were set to zero. The boundary condition at the wall for Fe^{2+} was given by the following flux relation:

$$J_{Fe^{2+}} = -\frac{1}{2}\left(J_{H^+} + J_{H_2CO_3} + J_{HCO_3^-}\right) \tag{2.31}$$

Despite some over-simplifications (e.g., the convective term was omitted in the species transport equation which obviated the computation of the mean flow fields), the approach employed in the model pointed the way to further developments.

The numerical model due to Pots (1995) obtained the species concentration profiles by solving the species conservation equations. The diffusivity was calculated as the sum of the molecular diffusivity and the eddy (turbulent) diffusivity:

$$D = D_{molecular} + D_{turbulent} \tag{2.32}$$

A simple semi-empirical turbulence theory was applied to obtain the eddy diffusivity (Davies, 1972):

$$D_{turbulent} = 0.2 \cdot \left(\frac{y}{\delta_l} \right)^3 \cdot Sc \cdot D_{molecular} \tag{2.33}$$

where y is the distance from the wall, δ_l is the laminar sublayer thickness, and Sc is the Schmidt number. It is obvious that the treatment of the effect of turbulent flow in this manner is inadequate.

2.3.2 Semi-Empirical Models

2.3.2.1 De Waard and Lotz Model

As mentioned earlier, the original de Waard and Milliams model (de Waard and Milliams, 1975b) has subsequently been modified on several occasions (de Waard, Lotz, and Milliams, 1991; de Waard and Lotz, 1993) by introducing correction factors to account for the effects of various parameters. The corrosion rate is calculated by

multiplying the "base value" with a series of correction factors. Only some major correction factors are explained below.

Protective films: A scale factor was obtained by applying multi-dimensional regression analysis to the high temperature CO_2 corrosion experimental data of Ikeda *et al.* (1984) to find a best-fit:

$$\log F_{scale} = \frac{2400}{T} - 0.6 \times \log(f_{CO_2}) - 6.7 \tag{2.34}$$

where T is absolute temperature (K) and f_{CO_2} is the CO_2 fugacity (bar). The maximum value for F_{scale} is 1.

System pressure: The effect of high total system pressure was modelled by employing a fugacity coefficient to account for the non-ideality of the natural gas. The fugacity coefficient can be calculated by solving the equation of state for the mixture of CO_2 and natural gas. After the fugacity coefficient is determined, CO_2 fugacity instead of the CO_2 partial pressure was used in the model calculations.

Flow velocity: The effect of velocity in the absence of surface protective films was modelled through a so-called resistance model (Lotz, 1990):

$$\frac{1}{V_{cor}} = \frac{1}{V_r} + \frac{1}{V_m} \tag{2.35}$$

In the expression, the first term on the right-hand side represents the activation-controlled reaction rate and the second term denotes the effect of mass transfer rate.

2.3.2.2 Dugstad *et al.* Model

Based on their extensive experimental studies on CO_2 corrosion mechanisms, Dugstad *et al.* (1994) presented a semi-empirical model which, according to the authors, is valid in one phase water flow and over the following parameter ranges: T (20 – 90 ^{0}C), P_{CO_2} (0.05 – 1.0 MPa), and pH (3.5 – 6). The corrosion rate was assumed to be a function of CO_2 partial pressure, pH, temperature, shear stress, steel chromium content, and film properties:

$$CR = f(P_{CO_2}, pH, T, \tau, Cr, Q) \tag{2.36}$$

Based on their experiments, the influence of CO_2 partial pressure was modelled by assuming a power law:

$$CR \propto P_{CO_2}{}^{0.7} \tag{2.37}$$

where CR is the corrosion rate in mm/yr and P_{CO_2} is the CO_2 partial pressure in MPa. The temperature effect at 0.1 MPa CO_2 partial pressure and shear stress of 350 Pa was given by:

$$CR = 3.04 - 8.243\times10^{-2}t + 1.352\times10^{-2}t^2 - 1.228\times10^{-4}t^3 \tag{2.38}$$

In the expression, CR is the corrosion rate (mm/yr) in unbuffered/pure solutions and t is temperature in ^{0}C. When the surface shear stress was reduced from 350 Pa to 19 Pa, the corrosion rate can be expressed as:

$$CR \propto Q \times 10^{-(350-\tau)t \times 0.00001} \tag{2.39}$$

where Q is a film correction factor. Q is 1 at temperatures above 20 ^{0}C at shear stresses from 19 to 350 Pa. At 20 ^{0}C and below, Q = 1.2 at shear stresses above 19 Pa. When the shear stress is reduced from 19 Pa to 0.02 Pa, the corrosion film becomes more protective and Q is therefore less than 1 as expressed below:

$$CR \propto \frac{\tau^{0.2}}{19} \tag{2.40}$$

The effect of the steel's chromium content has been studied at 60 ^{0}C and 0.2 MPa of CO_2 partial pressure only. Dugstad *et al.* (1994) proposed the following preliminary expression to account for the influence of chromium content in wt% for shear stresses from 19 Pa to 350 Pa:

$$CR \propto \frac{1}{0.88 + 1.5Cr} \tag{2.41}$$

Their experiments indicated that corrosion rate was always reduced when pH was increased. However, it was difficult to use a simple formulae to describe the pH effect although they did present the following expression to roughly estimate the corrosion rate

reduction factor, R, for temperature range 20 to 40 ^{0}C and shear stresses from 19 to 150 Pa:

$$\log R \propto -0.13 \times (pH - pH_{pure})^{1.6} \tag{2.42}$$

where pH_{pure} is the pH of the unbuffered CO_2-water solution. It is a function of CO_2 partial pressure and can be determined from Henry's law. The corrosion rate reduction factor, R, is more linear at higher temperatures and higher shear stresses (> 150 Pa):

$$CR \propto \left[1 + 0.33 \times \left(pH_{pure} - pH\right)\right] \tag{2.43}$$

The authors caution that equations (2.41) and (2.42) are only indicative and must be used with care.

Like the de Waard and Lotz (1993) model, the Dugstad *et al.* (1994) model provides a useful tool in estimating CO_2 corrosion rates under different service conditions. However, as knowledge of shear stress is required, the Dugstad *et al.* (1994) model may prove to be more cumbersome to use in practice.

2.3.3 Empirical Models

Few purely empirical CO_2 corrosion models exist in the open literature. One such model was the multi-variable linear regression model by Adams *et al.* (1993). However, as the purely empirical models essentially disregard the corrosion mechanism and all the

reactions and processes, it is questionable that one such simple linear model can satisfactorily represent the highly nonlinear and coupled processes in CO_2 corrosion, especially when interpolation and/or extrapolation of model predictions are involved.

2.4 Control Measures

Carbon dioxide corrosion mitigation measures are briefly outlined below. Firstly, design and operating techniques can be used to combat corrosion. The original design can be chosen to reduce the severity of corrosion and to allow mitigation procedures to be easily implemented if necessary. Secondly, corrosion inhibitors are used extensively in both oil and gas wells to reduce corrosion damage to subsurface equipment. In some situations, inhibitors may be the most economical means to control corrosion. The most widely used commercial CO_2 corrosion inhibitors are amines and their salts. These are nitrogen-based organic surfactants. They form, through surface adsorption, a thin layer on the metal surface which acts as a barrier between the metal and the corrosive environment. Factors such as the adsorption/desorption characteristics, the inhibitor film thickness and stability all affect the performance and effectiveness of the inhibitor. Lastly, protective coatings and materials selection (use of more corrosion-resistant materials) can also be used in controlling corrosion. Choice of any specific control measure or a combination of the measures should be based on thorough investigation of the situation in question and is a tradeoff among cost, performance, and ease of implementation and operation.

3. Modelling Turbulent Flow

3.1 Introduction

Flows of practical relevance are almost always turbulent. This means that the fluid motion is highly random, unsteady and three-dimensional. Despite these complexities, the exact equations describing the turbulent motion are known. The origin of these equations is the conservation laws for mass and momentum. For incompressible flows, these laws can be expressed as:

Mass conservation (continuity equation):

$$\frac{\partial u_i}{\partial x_i} = 0 \tag{3.1}$$

Momentum conservation (Navier-Stokes equations):

$$\rho \frac{\partial u_i}{\partial t} + \rho u_j \frac{\partial u_i}{\partial x_j} = -\frac{\partial p}{\partial x_i} + \mu \frac{\partial^2 u_i}{\partial x_j \partial x_j} \tag{3.2}$$

These instantaneous flow equations form a closed set and describe all the details of the turbulent motion. However, these equations cannot at present be solved for

turbulent flows of practical relevance due to the prohibitive computing time required. Therefore the mean flow approach is employed.

3.2 Mean-Flow Equations

As proposed by Reynolds (1895), the instantaneous values of the velocity, u_i, and the pressure, p, can be decomposed into the mean and fluctuating quantities:

$$u_i = U_i + u_i' \tag{3.3}$$

$$p = P + p' \tag{3.4}$$

The mean quantity is a time-averaged value as defined below:

$$U_i = \frac{1}{t_2 - t_1}\int_{t_1}^{t_2} u_i dt \tag{3.5}$$

$$P = \frac{1}{t_2 - t_1}\int_{t_1}^{t_2} p dt \tag{3.6}$$

The averaging time (t_2-t_1) is long compared with the time scale of the turbulent motion (and is small compared with the time scale of the mean flow in transient problems). The time average of the fluctuating quantities is zero. Introducing equations (3.3) and (3.4) into equations (3.1) and (3.2) and subsequently time-averaging yields the time averaged conservation equations for mass and momentum:

$$\frac{\partial U_i}{\partial x_i} = 0 \tag{3.7}$$

$$\rho \frac{\partial U_i}{\partial t} + \rho U_j \frac{\partial U_i}{\partial x_j} = -\frac{\partial P}{\partial x_i} + \frac{\partial}{\partial x_j}\left(\mu \frac{\partial U_i}{\partial x_j} - \rho \overline{u_i' u_j'} \right) \tag{3.8}$$

These mean flow equations are also exact since no assumptions have been made in deriving them. However, the time averaging process has introduced one additional unknown, $-\rho \overline{u_i' u_j'}$, and as a result these equations no longer form a closed set. Physically the new unknown, $-\rho \overline{u_i' u_j'}$, represents the transport of momentum by the fluctuating (turbulent) motion. It acts as a stress on the fluid and is known as the turbulent stress or Reynolds stress.

In order to solve the mean flow equations, the turbulence correlations $\overline{u_i' u_j'}$ must be somehow specified. This task can be accomplished by a turbulence model which is a set of algebraic or differential equations which determines the turbulent transport terms in the mean flow equations and thus closes the system of equations.

3.3 Model of Turbulence

The eddy-viscosity concept proposed by Boussinesq in 1877 has been employed in most turbulence models in use today. It assumes that, in analogy to the viscous

stresses in laminar flows, the turbulent stresses are proportional to the mean velocity gradients:

$$-\overline{u_i'u_j'} = \nu_t\left(\frac{\partial U_i}{\partial x_j}+\frac{\partial U_j}{\partial x_i}\right)-\frac{2}{3}k\delta_{ij} \tag{3.9}$$

where ν_t is the turbulent or eddy viscosity. It should be noted that, unlike molecular viscosity, ν_t is not a fluid property but depends strongly on the state of turbulence. The value of turbulent viscosity may vary significantly from one point in the flow to another and also from flow to flow. The second term involving the Kronecker delta, δ_{ij}, and k has been added in order to make the expression also applicable to the normal stresses since by definition the sum of all normal stresses is twice the kinetic energy k of the fluctuating motion. And since this term constitutes a pressure, it can be absorbed by the pressure gradient term when equation (3.9) is used to eliminate $\overline{u_i'u_j'}$ in the momentum equation. Therefore, the appearance of k in equation (3.9) does not necessitate the determination of k. The quantity that has to be determined now is the eddy viscosity, ν_t.

Because of the analogy between the molecular motion and the turbulent motion, the eddy viscosity can be considered proportional to a velocity characterizing the fluctuating motion, $\hat{u}$, and to a typical length of this motion, l, which Prandtl called the mixing length (Prandtl, 1925). Therefore,

$$\nu_t = \hat{u}l \tag{3.10}$$

The simplest turbulent models specify the eddy viscosity or $\hat{u}$ and l either directly from experiments or by relating it to the mean velocity distribution. In order to account for the transport of turbulence, models have been developed which employ transport equations for quantities characterizing the turbulence. Some models use only one transport equation for the single velocity scale $\hat{u}$ (one-equation models) while others also use an equation for the length scale l (two-equation models). There are also more sophisticated models that use multiple transport equations for more than one velocity scale or length scale.

In one-equation models, $\sqrt{k}$ is used as the velocity scale where k is the kinetic energy of the turbulent motion (per unit mass) as defined by the following expression:

$$k = \frac{1}{2}\overline{u_i' u_i'} = \frac{1}{2}\left(\overline{u_1'^2} + \overline{u_2'^2} + \overline{u_3'^2}\right) \tag{3.11}$$

The choice of $\sqrt{k}$ as the velocity scale is physically meaningful because according to equation (3.11), k is a direct measure of the intensity of the turbulent fluctuations in three directions. With $\sqrt{k}$ being the velocity scale, equation (3.10) now becomes:

$$\nu_t = c_\mu \sqrt{k} l \tag{3.12}$$

where c_μ is an empirical constant. This equation is known as the Kolmogorov-Prandtl expression. The distribution of eddy viscosity can be determined after the length scale is specified and the transport equation for k is solved.

Two-equation models employ a length scale equation in addition to the k-equation. There exist several two-equation models with different specifications of the length scale. The most widely tested and successfully applied turbulence model is the k-ε model in which the turbulence length scale is prescribed as $l = k^{\frac{1}{2}} / \varepsilon$. In the expression, ε is the dissipation rate of kinetic energy of turbulence. It is defined by the following correlation:

$$\varepsilon = \nu \overline{\frac{\partial u_i'}{\partial x_j} \frac{\partial u_i'}{\partial x_j}} \tag{3.13}$$

The eddy viscosity is determined from the kinetic energy of turbulence, k, and its dissipation rate, ε, as expressed below:

$$\nu_t = c_\mu f_\mu \frac{k^2}{\varepsilon} \tag{3.14}$$

where f_μ is the damping function. It is equal to one in the fully turbulent flow region and is less than one in the near-wall region where the flow is directly affected by the molecular viscosity. The expression for the damping function is given in Section 3.5.1.

Equations (3.11) and (3.13) give the definitions of the kinetic energy of turbulence (per unit mass) and its dissipation rate. The problem now is reduced to the determination of the transport equations for k and ε. Two methods (Hinze, 1975; Wilcox, 1993) can be used to derive the transport equation in exact form for the kinetic energy of turbulence. The exact transport equation can be derived from the Navier-Stokes equations for the fluctuating vorticity and thus for the dissipation rate, ε (Tennekes and Lumley, 1972). However, these exact equations for k and ε are of little use in a turbulence model since they contain new unknown complex correlations whose behavior is little known and fairly drastic model assumptions must be introduced for these terms. Therefore, the exact equations are omitted here; instead their final modelled form will be presented in Section 3.4.

In the past two decades, the k-ε model has been extensively applied with much success in specific situations. In particular the limiting behavior of flow in the near-wall region can be satisfactorily predicted with the low Reynolds number model used in the near-wall region. It offers the best compromise between model performance and computational economy and is therefore used in the present study.

3.4 Two-Dimensional Flow Model

Now that all the preparations are completed, we are in a position to present the final modelled form of all equations that we attempt to solve. We will limit our

discussion to a steady-state two-dimensional turbulent pipe flow. In an axisymmetric cylindrical coordinate system, the transport equations are given below:

Continuity equation:

$$\frac{\partial}{\partial x}(\rho U)+\frac{1}{r}\frac{\partial}{\partial r}(r\rho V)=0 \tag{3.15}$$

Momentum equation in axial direction:

$$\begin{aligned}\frac{\partial}{\partial x}(\rho U^2)+\frac{1}{r}\frac{\partial}{\partial r}(r\rho UV)=&\frac{\partial}{\partial x}\left(\mu_{eff}\frac{\partial U}{\partial x}\right)+\frac{1}{r}\frac{\partial}{\partial r}\left(r\mu_{eff}\frac{\partial U}{\partial r}\right)\\&+\frac{\partial}{\partial x}\left(\mu_{eff}\frac{\partial U}{\partial x}\right)+\frac{1}{r}\frac{\partial}{\partial r}\left(r\mu_{eff}\frac{\partial V}{\partial x}\right)-\frac{\partial P}{\partial x}\end{aligned} \tag{3.16}$$

Momentum equation in radial direction:

$$\begin{aligned}\frac{\partial}{\partial x}(\rho UV)+\frac{1}{r}\frac{\partial}{\partial r}(r\rho V^2)=&\frac{\partial}{\partial x}\left(\mu_{eff}\frac{\partial V}{\partial x}\right)+\frac{1}{r}\frac{\partial}{\partial r}\left(r\mu_{eff}\frac{\partial V}{\partial r}\right)\\&+\frac{\partial}{\partial x}\left(\mu_{eff}\frac{\partial U}{\partial r}\right)+\frac{1}{r}\frac{\partial}{\partial r}\left(r\mu_{eff}\frac{\partial V}{\partial r}\right)-2\mu_{eff}\frac{V}{r^2}-\frac{\partial P}{\partial r}\end{aligned} \tag{3.17}$$

Equation for kinetic energy of turbulence:

$$\frac{\partial}{\partial x}(\rho Uk)+\frac{1}{r}\frac{\partial}{\partial r}(r\rho Vk)=\frac{\partial}{\partial x}\left[\left(\mu+\frac{\mu_t}{\sigma_k}\right)\frac{\partial k}{\partial x}\right]+\frac{1}{r}\frac{\partial}{\partial r}\left[r\left(\mu+\frac{\mu_t}{\sigma_k}\right)\frac{\partial k}{\partial r}\right]+P_k-\rho\varepsilon \tag{3.18}$$

Equation for dissipation rate of kinetic energy of turbulence:

$$\frac{\partial}{\partial x}(\rho U\varepsilon)+\frac{1}{r}\frac{\partial}{\partial r}(r\rho V\varepsilon)=\frac{\partial}{\partial x}\left[\left(\mu+\frac{\mu_t}{\sigma_\varepsilon}\right)\frac{\partial \varepsilon}{\partial x}\right]+\frac{1}{r}\frac{\partial}{\partial r}\left[r\left(\mu+\frac{\mu_t}{\sigma_\varepsilon}\right)\frac{\partial \varepsilon}{\partial r}\right] + \frac{\varepsilon}{k}\left(C_1 f_1 P_k - C_2 f_2 \rho\varepsilon\right) \tag{3.19}$$

In equations (3.16) and (3.17), μ_{eff} is the effective viscosity. It is equal to the sum of molecular viscosity and turbulent viscosity:

$$\underbrace{\mu_{eff}}_{effective} = \underbrace{\mu}_{molecular} + \underbrace{\mu_t}_{turbulent} \tag{3.20}$$

The generation of kinetic energy of turbulence, P_k, in equations (3.18) and (3.19) is:

$$P_k = \mu_t\left\{2\left[\left(\frac{\partial U}{\partial x}\right)^2+\left(\frac{\partial V}{\partial r}\right)^2+\left(\frac{V}{r}\right)^2\right]+\left(\frac{\partial U}{\partial r}+\frac{\partial V}{\partial x}\right)^2\right\} \tag{3.21}$$

The cylindrical coordinate system is employed in the above fluid flow equations (3.15) to (3.19). Note that for programming purposes, it can be conveniently converted to the Cartesian *x-y* coordinate system by setting the following in the flow equations:

$$\frac{\partial}{\partial r}=\frac{\partial}{\partial y}, \qquad r=1, \qquad \frac{1}{r^2}=0 \tag{3.22}$$

3.5 Boundary Conditions

The set of flow equations (3.15) to (3.19) are elliptic partial differential equations. In order to solve these equations, boundary conditions are required for all

variables on all boundaries of the computational domain: inlet, outlet, wall, and symmetry axis.

At the inlet the mean axial velocity profile, U, can be taken from established values for fully developed flow in straight pipes. The inlet mean radial velocity, V, is zero. The inlet turbulent kinetic energy, k, and its dissipation rate, ε, are specified as follows (Schlichting, 1979):

$$k = \frac{3}{2} T_u^2 U^2, \qquad \varepsilon = C_\mu^{0.75} \frac{k^{1.5}}{0.015d} \tag{3.23}$$

where $T_u = \frac{u'}{U}$ is the turbulence intensity and d is the pipe diameter.

Zero gradients can be set for velocities, kinetic energy of turbulence, and its dissipation rate at the outlet (exit) of an adequately long computational domain:

$$\frac{\partial U}{\partial x} = \frac{\partial V}{\partial x} = \frac{\partial k}{\partial x} = \frac{\partial \varepsilon}{\partial x} = 0 \tag{3.24}$$

At the symmetry axis, zero gradients can be assumed:

$$\frac{\partial U}{\partial y} = \frac{\partial V}{\partial y} = \frac{\partial k}{\partial y} = \frac{\partial \varepsilon}{\partial y} = 0 \tag{3.25}$$

On the wall, all velocities are zero and so is the kinetic energy of turbulence.

$$U = V = k = 0 \tag{3.26}$$

The strict boundary condition for ε at the wall is $\varepsilon = \nu \left.\frac{\partial^2 k}{\partial y^2}\right|_{wall}$. This can be derived from the transport equation of kinetic energy of turbulence (3.18). This type of boundary conditions is, however, unstable in the initial stage of the calculation because the second-order derivative cannot be guaranteed to provide a positive value. Therefore the following modified form of the boundary condition is used in the present study:

$$\varepsilon = \nu \frac{2k_1}{(\delta y)^2} \tag{3.27}$$

where k_1 represent the value of the turbulence energy at the first (nearest) node from the wall and δy is the distance of first node from the wall surface. It can be shown that equation (3.27) is valid when the first node from the wall is placed close enough to the wall (Abe *et al.*, 1994). This condition is satisfied in the present study as the distance between wall and the first node is less than 1 μm.

3.5.1 Low Reynolds Number Model

The k-ε turbulence model presented so far is generally valid for high Reynolds number flows where local isotropy prevails. It cannot be applied in the near wall region without modification because of both the viscous and the wall effects in the vicinity of walls.

To account for the viscous effect in the near wall region, the low Reynolds number (LRN) model is used which enables the application of the k-ε turbulence model all the way to the wall. The low Reynolds number model uses empirical damping functions f_μ, f_1, and f_2 to account for the wall proximity effect by modifying the original high Reynolds number k-ε model so that turbulence gradually fades out as the wall is approached. This is important because for flows with high Schmidt numbers the diffusion-controlled mass transfer sublayer is deep inside the hydrodynamic viscous sublayer (Levich, 1962) and it is imperative to capture the wall limiting behavior.

The first low Reynolds number model was proposed by Jones and Launder (1972 and 1973). Since then several versions have been developed by different authors. Among them the model proposed by Nagano and Tagawa (NT) (1990) can reproduce the near-wall limiting behavior and provide accurate predictions for attached turbulent flows. In this study the LRN model proposed by Abe, Kondoh and Nagano (AKN) (1994) is used. The AKN model is a modification from the NT model (1990). The main improvement is achieved by the introduction of the Kolmogorov velocity scale, $u_\varepsilon \equiv (\nu\varepsilon)^{1/4}$, instead of the friction velocity, u_τ, to account for the near-wall and low-Reynolds-number effects in both attached and detached flows. The model constants and model functions used in the AKN model are listed in Table 3.1.

Table 3.1 Constants and functions in the AKN low Reynolds number model (Abe *et al.*, 1994).

C_μ	$C_{\varepsilon 1}$	$C_{\varepsilon 2}$	σ_k	σ_ε
0.09	1.5	1.9	1.4	1.4
$f_\mu = \left[1-\exp\left(-\frac{y^*}{14}\right)\right]^2\left[1+\frac{5}{R_t^{0.75}}\exp\left\{-\left(\frac{R_t}{200}\right)^2\right\}\right]$				
$f_1 = 1$				
$f_2 = \left[1-0.3\exp\left(-\left(\frac{R_t}{6.5}\right)^2\right)\right]\left[1-\exp\left(-\frac{y^*}{3.1}\right)\right]^2$				

3.6 Discretization of the Partial Differential Equations

In this study the partial differential equations are discretized based on the control volume approach as proposed by Patankar (1980). The computational domain is divided into a finite number of control volumes with each containing only one grid point. The partial differential equations are integrated over each control volume resulting in a discretization equation containing the values of the unknown variables for a set of grid points. The discretization equation expresses the conservation principles over the finite control volume just as the differential equation does for an infinitesimal control volume.

To illustrate the process, the discretizing procedure is discussed only for Cartesian coordinates. A typical control volume for an arbitrary grid point P is shown in Figure 3.1 by dashed lines. For the grid point P, points W and E (denoting west and east) are its x-direction neighbors, and N and S (standing for north and south) are its y-direction neighbors. The lowercase letters w, e, s, and n indicate the faces of the control volume on the west, east, south, and north sides. The dimensions of the control volume are Δx and Δy with the third dimension being unity.

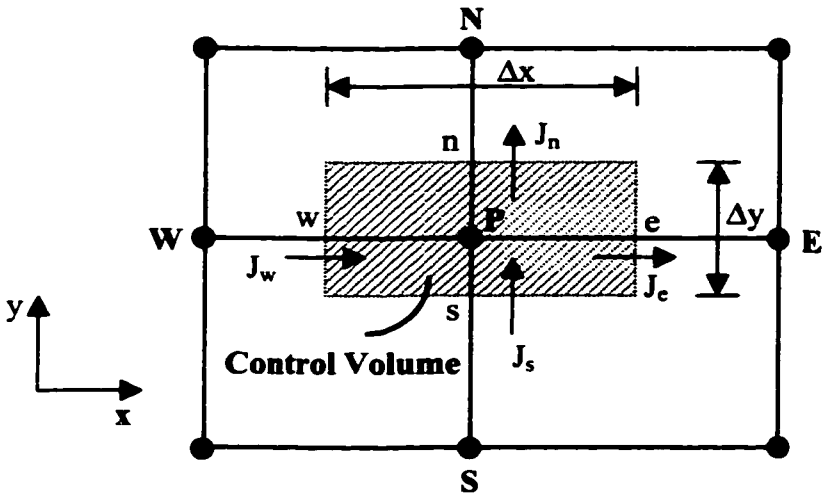

Figure 3.1 Control volume for a general variable in the two dimensional computational domain.

The general transport equation in a Cartesian coordinate system is:

$$\frac{\partial}{\partial x}(\rho U\Phi) + \frac{\partial}{\partial y}(\rho V\Phi) = \frac{\partial}{\partial x}(\Gamma_\Phi \frac{\partial \Phi}{\partial x}) + \frac{\partial}{\partial y}(\Gamma_\Phi \frac{\partial \Phi}{\partial y}) + S_\Phi \tag{3.28}$$

The left-hand side represent the convection terms. The first two terms on the right hand side are the diffusion terms. All other modes of transport of the general variable Φ are contained in the source term S_Φ including the production and destruction of Φ. It can be expected that this source term is often significant compared to the convective and diffusion terms and is usually a function of Φ or its derivatives. Patankar (1980) suggested an effective way to linearize the source term:

$$S_\Phi = S_C + S_P\Phi \tag{3.29}$$

The coefficients S_C and S_P are constants and S_P must be non-positive in order to ensure a stable and convergent solution procedure.

The general equation (3.28) can be rewritten as:

$$\frac{\partial}{\partial x}(\rho U\Phi - \Gamma_\Phi \frac{\partial \Phi}{\partial x}) + \frac{\partial}{\partial y}(\rho V\Phi - \Gamma_\Phi \frac{\partial \Phi}{\partial y}) = S_\Phi \tag{3.30}$$

If we define the fluxes:

$$J_x = \rho U\Phi - \Gamma_\Phi \frac{\partial \Phi}{\partial x} \tag{3.31}$$

$$J_y = \rho V\Phi - \Gamma_\Phi \frac{\partial \Phi}{\partial y} \tag{3.32}$$

Then equation (3.30) can be further written as

$$\frac{\partial J_x}{\partial x} + \frac{\partial J_y}{\partial y} = S_\Phi \tag{3.33}$$

When this equation is integrated over the control volume in Figure 3.1 the following results:

$$J_e(\Delta y) - J_w(\Delta y) + J_n(\Delta x) - J_s(\Delta x) = (S_C + S_P\Phi)\Delta x\Delta y \tag{3.34}$$

Now let's take a look at the discretization of the continuity equation. By setting $\Phi = 1$ and $S_\Phi = 0$ in the the general equation (3.28), the continuity equation is obtained:

$$\frac{\partial}{\partial x}(\rho U) + \frac{\partial}{\partial y}(\rho V) = 0 \tag{3.35}$$

Integrating the continuity equation over the control volume (Figure 3.1) yields:

$$(\rho U)_e(\Delta y) - (\rho U)_w(\Delta y) + (\rho V)_n(\Delta x) - (\rho V)_s(\Delta x) = 0 \tag{3.36}$$

Denote F as the mass flow rate and the above equation becomes:

$$F_e - F_w + F_n - F_s = 0 \tag{3.37}$$

If the discretized continuity equation (3.37) is multiplied by Φ_P and then subtracted from the discretized general transport equation (3.34), we obtain:

$$\begin{aligned}&(J_e\Delta y - F_e\Phi_P) - (J_w\Delta y - F_w\Phi_P) + (J_n\Delta x - F_n\Phi_P) - (J_s\Delta x - F_s\Phi_P)\\ &= (S_C + S_P\Phi)\Delta x\Delta y\end{aligned} \tag{3.38}$$

According to Patankar (1980) the fluxes in brackets in equation (3.38) can be expressed as:

$$J_e\Delta y - F_e\Phi_P = a_E(\Phi_P - \Phi_E) \tag{3.39}$$

$$J_w\Delta y - F_w\Phi_P = a_W(\Phi_W - \Phi_P) \tag{3.40}$$

$$J_n\Delta x - F_n\Phi_P = a_N(\Phi_P - \Phi_N) \tag{3.41}$$

$$J_s\Delta x - F_s\Phi_P = a_S(\Phi_S - \Phi_P) \tag{3.42}$$

The coefficients a_E, a_W, a_N and a_S represent the convection and diffusion influence on the four faces of the control volume. The choice of these transport coefficients can transform the equations (3.39) to (3.42) into a central difference, upwind, hybrid, power law or other discretization scheme (Patankar, 1980). In the present study the hybrid scheme is used. It is a combination of a central difference scheme for low Peclet numbers $(|P_e| \le 2)$ and an upwind scheme outside this range. Use of the hybrid scheme

ensures that the transport coefficients are always positive which, as argued by Patankar (1980), is required if physically realistic solutions are to be produced.

Finally equations (3.39) to (3.42) are substituted into equation (3.38) to obtain the final form of the two dimensional discretization equation for a general variable Φ:

$$a_P\Phi_P = a_E\Phi_E + a_W\Phi_W + a_N\Phi_N + a_S\Phi_S + S_C\Delta x\Delta y \tag{3.43}$$

where

$$a_P = a_E + a_W + a_N + a_S - S_P\Delta x\Delta y \tag{3.44}$$

The discretized equation (3.43) for each variable Φ is written for each and everyone of the control volumes in the computational domain resulting in a set of algebraic equations.

3.6.1 The Momentum Equation

The discretization method presented so far enables the solution of a general transport equation. But a difficulty is encountered when this method is used to calculate the velocity profiles. The difficulty is caused by the unknown pressure field. The problem with the pressure as well as with the continuity equation is that first derivatives are discretized. If pressure and velocities are calculated for the same point, this will require interpolation of the fluxes on the control volume faces which can yield completely unrealistic wavy pressure and velocity fields (Patankar, 1980).

A remedy for this is to use the staggered grid (Figure 3.2). The control volume for velocities are different from the ones used for the discretization of the other equations (contunuity, k, ε, concentraion, ...). The control volumes for U are staggered in the x direction and the control volumes for V are staggered in the y direction only. The staggered grid system is arranged so that the velocity components are calculated for control volumes which are located on the faces of the scalar control volume around grid point P. This ensures that the pressure difference calculated between two adjacent grid points naturally becomes the driving force for the velocity component located between the two grid points. Another advantage is that if the continuity equation is integrated over the main control volume, the discretized form will contain the velocity difference of adjacent velocity components which will prevent a wavy velocity field.

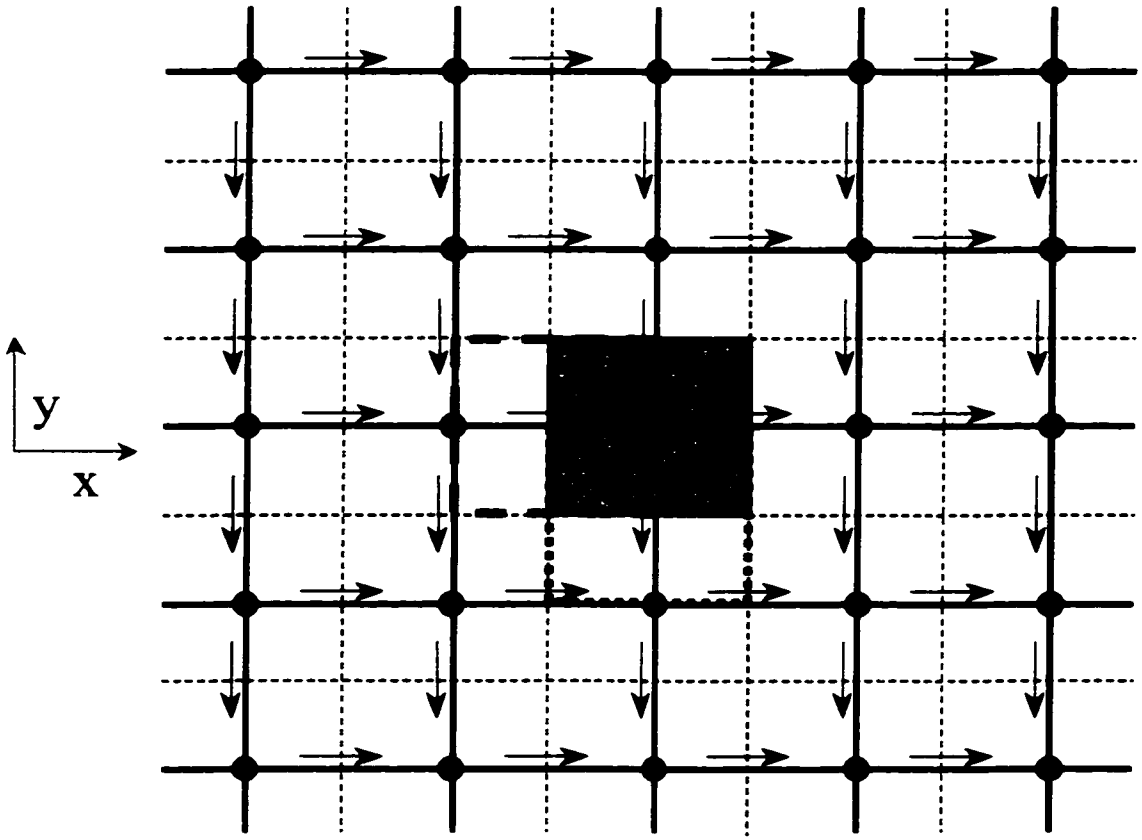

Figure 3.2 Staggered grid. Control volumes for U and V are the areas enclosed by the dash line and square dot line, respectively. The horizontally shaded area is the control volume for a general variable (P, k, ε, c, ...).

Now we are ready to face another problem: linking the continuity equation with the momentum equations via pressure. Pressure appears in the momentum equations but not in the continuity equation and there is no obvious equation to solve for the pressure field. We note that only with a correct pressure field will the velocity profiles determined from the momentum equations satisfy the continuity equation. This means that the pressure field is indirectly specified via the continuity equation. In this study, the SIMPLE (Semi-Implicit Method for Pressure Linked Equation) algorithm (Patankar and Spalding, 1972; Patankar, 1980) is used to link pressure with the continuity equation. The essence of the SIMPLE algorithm is the concept of a pressure correction, P', and the velocity correction, U', as defined below:

$$P = P^* + P' \tag{3.45}$$

$$U = U^* + U' \tag{3.46}$$

where P^* and U^* are guessed pressure and velocity fields, and P and U are real (correct) pressure and velocity fields respectively. Pressure correction and velocity correction are related to each other so that, after substituting the velocities with the pressure, the continuity equation now becomes the pressure correction equation from which values of pressure correction are calculated. The boundary conditions for the pressure correction equation are based on the definition of the pressure correction. Since

in this study the velocity components are known or specified at all the boundaries (inlet, outlet, symmetry axis and wall), their values do not need to be corrected. Therefore no change of the pressure correction on these boundaries is necessary.

$$\frac{\partial P'}{\partial x} = 0, \quad \text{or} \quad \frac{\partial P'}{\partial y} = 0 \tag{3.47}$$

The guessed velocity is corrected in response to the pressure correction until the pressure correction is zero or an adequately small number. The procedure is as follows:

1. Start with a guessed pressure, P^*;

2. Solve the momentum equations for the velocities;

3. Solve the pressure correction equation for the new pressure correction, P', and calculate the new pressure field, P, from equation (3.45);

4. Treat P as a new guessed pressure and return to Step 2. Iteration continues until the absolute value of the pressure correction is a prescribed small number or zero.

3.7 Solution of the Discretized Equations

A set of algebraic equations containing $n_i \times n_j$ equations for each variable are obtained after the discretization procedure, where n_i and n_j are the number of grid points

in the x- and y-direction respectively for the flow domain. Because of the large number of grid points involved in this study, it is impractical to solve the algebraic equations simultaneously using a direct method. An iterative method (point iterative or line iterative) has to be employed. The point iterative method is easy to implement but convergence is very slow because the information at the boundaries is transmitted at a rate of one grid interval per iteration. Therefore a line iterative method is used as convergence is reached much faster. When the general discretization equation (3.43) is applied to all the grid points within one line, a system of linear equations is obtained which has a tridiagonal coefficient matrix because the values of the grid point's two off-line neighbors are either known from the previous iteration level or have just been calculated in the present iteration level. The resulting system of equations is solved using the Tri-Diagonal Matrix Algorithm.

In this study we have applied the line by line iteration method in the y direction since the dependent variables change values more drastically in this direction. Also, a left to right sweep was used in this study as a sweep from upstream to downstream produces faster convergence than a sweep against the stream.

3.8 Convergence Criteria

One problem that remains to be clarified is when to declare the achievement of a convergent solution. The choice of an appropriate convergence criterion depends on the nature of the problem and on the objectives of the computation. A common procedure is

to examine the most significant quantities given by the solution and to require the iterations be continued only until the relative change in these quantities between two successive iterations is smaller than a certain small number. This type of criterion can be misleading. In this study, under-relaxation is used to ensure a stable and convergent solution as the equations we are solving contain strongly nonlinear terms. Therefore the change in the dependent variables between successive iterations is intentionally slowed down; this may create an illusion of convergence though the solution may be far from being converged. A more meaningful method is to examine how perfectly the discretization equations are satisfied by the current values of the dependent variables.

As presented earlier the two-dimensional general discretization equation is:

$$a_P\Phi_P = a_E\Phi_E + a_W\Phi_W + a_N\Phi_N + a_S\Phi_S + S_C\Delta x\Delta y \tag{3.48}$$

where Φ is the general variable and a_j are the coefficients. For each grid point, a residual R_Φ is defined and calculated from:

$$R_\Phi = \left(a_E\Phi_E + a_W\Phi_W + a_N\Phi_N + a_S\Phi_S + S_C\Delta x\Delta y\right) - a_P\Phi_P \tag{3.49}$$

Obviously the residual, R_Φ, will be zero when the discretization equation is perfectly satisfied. In practice, it is adequate to require it to be smaller than a certain given number.

In this study the sum of the absolute values of residuals for all control volumes for each variable in the computational domain is calculated and then normalized. The normalization for the continuity equation is performed with the inlet fluid flowrate, and for the momentum equation with the inlet momentum rate. This normalized residual is subsequently monitored and required to be smaller than 0.001. Also, one or more locations in the flow domain are monitored to ensure there is no abrupt changes in any variable during the iteration procedure.

3.9 Overall Algorithm

The computer program used in this study is based on the TEACH algorithm proposed by Patankar and Spalding (1972). It has been modified to include the low-Reynolds-number model, the mass transfer model, the corrosion model, and subroutines to solve various chemical equilibria. The block diagram of the overall algorithm is shown in Figure 3.3. The computational steps are briefly outlined below.

1. First input parameters. Set grid parameters and program control constants. Set inlet boundary conditions including the surface concentrations of the reacting species. Call subroutine INIT to calculate geometry and initialize variables. Set initial guessed pressure field.

2. Call PROPS to calculate initial flow properties (effective viscosity, effective diffusivity, turbulent Reynolds number, the damping function, etc.)

3. Call CALCU and CALCV to solve the momentum equations for the axial velocity and the radial velocity.

4. The pressure correction equation (modified continuity equation) is solved and the pressure field is updated by calling CALCP.

5. Call CALCTE and CALCED to solve the kinetic energy of turbulence equation and the energy dissipation rate equation.

6. Call CALCMH to solve the mass transport (species concentration) equation. Adjusting of various chemical equilibria is accomplished by calling the subroutine EQUIL. Chemical equilibrium will be discussed in detail in Chapter 5.

7. Subroutine PROPS is called to update the flow properties.

8. Check convergence. If a convergent solution is not reached, return to step 3 for the next iteration; if the solution has converged, continue to the next step.

9. Check if the mixed potential theory is satisfied. If yes, iteration ends. Otherwise change the surface concentrations of the reacting species and go back to step 3 to start a new round of iteration. The mixed potential theory will be discussed in Chapter 6.

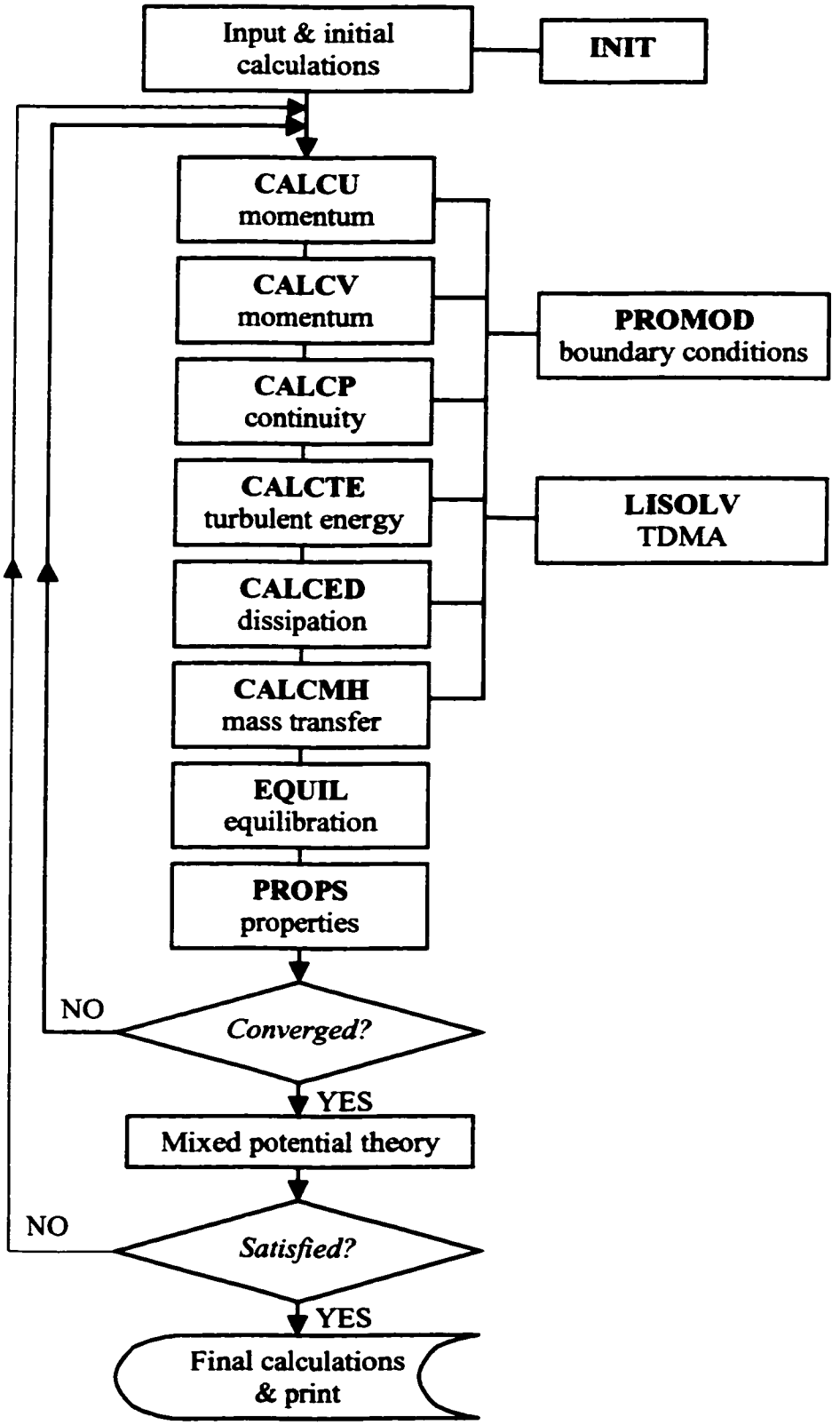

Figure 3.3 Block diagram of the overall algorithm.

Subroutines CALCU, CALCV, CALCP, CALCTE, CALCED, and CALCMH all have a similar code structure with each having the following main computational steps:

1) Calculation of the area and volume for each control volume

2) Calculation of the convection and the diffusion coefficients

3) Calculation of the source term coefficients S_C and S_P

4) Calculation of the main coefficients a_E, a_W, a_N and a_S

5) Subroutine PROMOD (denoting problem modification) is called to introduce the boundary conditions (inlet, wall, symmetrical axis and outlet) so that the main coefficients and source term coefficients at the boundaries are modified.

6) Calculation of the coefficient a_P and the residuals

7) Subroutine LISOLV is called to solve the resulting set of algebraic equations by using the Tri-Diagonal Matrix Algorithm.

4. Modelling Mass Transport

Mass transport is a crucial aspect of the corrosion process. The corrosion rates are ultimately dependent upon the distribution of relevant species concentrations in the system, which in turn is determined by the flow structure and the nature of the species being transported.

4.1 Governing Transport Equation

Knowledge about the flow fields is obtained by solving the flow equations presented in Chapter 3. Mass transport information can be obtained by solving the mass transport equation simultaneously with the flow equations. The steady state instantaneous transport equation for species concentration is:

$$u_i \frac{\partial \tilde{c}}{\partial x_i} = \frac{\partial}{\partial x_i}\left(D \frac{\partial \tilde{c}}{\partial x_i} \right) + S_{\tilde{c}} \tag{4.1}$$

where $\tilde{c}$ is the instantaneous species concentration and $S_{\tilde{c}}$ is the source term for this species. Using the same statistical approach described earlier, the instantaneous species concentration can be separated into mean and fluctuating components:

$$\tilde{c} = c + c' \tag{4.2}$$

Introducing the above equation into the instantaneous equation and subsequent time-averaging yields the following equation:

$$U_i \frac{\partial c}{\partial x_i} = \frac{\partial}{\partial x_i}\left(D\frac{\partial c}{\partial x_i} - \overline{c'u_i'} \right) + S_c \tag{4.3}$$

The term $\overline{c'u_i'}$, multiplied by the fluid density, represents the transport of mass due to the fluctuating (turbulent) motion. It is the transport of mass in the direction of x_i and is therefore a turbulent mass flux. In order to solve for the mean values of concentration, this correlation (turbulent mass flux) must be determined in some way.

In direct analogy to the turbulent momentum transport, the turbulent heat or mass transport is often assumed to be related to the gradient of the transported quantity:

$$-\overline{c'u_i'} = D_t \frac{\partial c}{\partial x_i} \tag{4.4}$$

where D_t is the turbulent or eddy diffusivity. Like the turbulent viscosity, the turbulent diffusivity depends on the state of turbulence and is not a fluid property. Turbulent viscosity and turbulent diffusivity are linked by the Reynolds analogy which compares the momentum transfer process with the heat/mass transfer process and states that the eddy diffusivity for heat/mass transfer is equal to the eddy diffusivity for momentum. By definition,

$$\sigma_m = \frac{\nu_t}{D_t} \tag{4.5}$$

where σ_m is the turbulent Prandtl (heat) or Schmidt (mass) number. Therefore the Reynolds analogy corresponds to a turbulent Prandtl/Schmidt number of one. Experimental evidence, at least for air, suggests that σ_m is in fact 1.00 although a value near 0.9 is perhaps a little closer to the correct value over most of the boundary layer (Kays and Crawford, 1980). In this study the value of σ_m was therefore set at 0.9.

Similar to the effective viscosity, μ_{eff}, an effective diffusivity, D_{eff}, can be defined as the sum of the molecular and turbulent diffusivities:

$$\underbrace{D_{eff}}_{effective} = \underbrace{\frac{\mu}{\rho S_c}}_{molecular} + \underbrace{\frac{\mu_t}{\rho \sigma_m}}_{turbulent} \tag{4.6}$$

With the above assumptions and preparations, the two dimensional time-averaged mass transport equation in a cylindrical coordinate system becomes:

$$\frac{\partial}{\partial x}(Uc) + \frac{1}{r}\frac{\partial}{\partial r}(rVc) = \frac{\partial}{\partial x}(D_{eff}\frac{\partial c}{\partial x}) + \frac{1}{r}\frac{\partial}{\partial r}(rD_{eff}\frac{\partial c}{\partial r}) + S_c \tag{4.7}$$

In this equation, S_c is the source term. It describes the rate of production or consumption of a species through a *homogeneous* chemical reaction which means the chemical reaction takes place inside the solution (fluid) where the mass transport equation applies. Generation or consumption of a species through electrochemical

reactions at the metal surface (*heterogeneous* reactions) are taken into account via the boundary conditions and should not be included in the source term in equation (4.7). The above equation (4.7) is written for all the electroactive species resulting in a set of mass transport equations. The electroactive species include hydrogen ion, carbonic acid and ferrous ion. H^+ and H_2CO_3 are reduced on the wall, and ferrous ion is the product of iron dissolution.

4.1.1 Source Term for Species Conservation – H_2CO_3

Carbonic acid is produced through the chemical reaction of carbon dioxide hydration. Because of the special characteristics of this reaction as explained below, there will be generation of carbonic acid throughout the boundary layer, which is accommodated by a source term.

Consider the CO_2 hydration reaction:

$$CO_{2(aq)} + H_2O \underset{k_b}{\overset{k_f}{\Leftrightarrow}} H_2CO_3 \tag{4.8}$$

where, k_f and k_b are the rate constants for the forward (hydration) and backward (de-hydration) reactions, respectively. The forward reaction is known to be much slower than the backward reaction, at 25 ^{0}C, k_f= 0.03 s^{-1} and k_b = 20 s^{-1} (Kern, 1960). Assuming CO_2 hydration is a first order chemical reaction, then the homogeneous rate of formation of carbonic acid is (Vetter, 1967; Nesic *et al.*, 1995):

$$v = \underbrace{k_f c_{CO_{2(aq)}}}_{hydration} - \underbrace{k_b c_{H_2CO_3}}_{de-hydration} \tag{4.9}$$

In an open system, we can, for all practical purposes, assume that the concentration of dissolved carbon dioxide is constant under a given temperature and denote the rate of hydration with a constant, v_0:

$$v = v_0 - k_b c_{H_2CO_3} \tag{4.10}$$

At equilibrium, there is no net generation, $v = 0$, therefore

$$v_0 = k_b c_{H_2CO_{3(b)}} \tag{4.11}$$

where the subscript (b) stands for bulk concentration. Combining equations (4.10) and (4.11) yields:

$$v = k_b c_{H_2CO_{3(b)}} - k_b c_{H_2CO_3} \tag{4.12}$$

For simplicity, the subscript can be dropped and the source term for the conservation equation of carbonic acid is obtained:

$$v = k_b (c_b - c) \tag{4.13}$$

The above equation shows that wherever the carbonic acid concentration is below its equilibrium concentration, there will be generation of carbonic acid. Since there is plenty of aqueous CO_2 present in the solution, there is always a tendency to

replenish the carbonic acid so that the equilibrium concentration is reached. However because the forward reaction is very slow, the CO_2 hydration/H_2CO_3 dehydration reaction will not be in equilibrium and carbonic acid cannot attain its equilibrium concentration.

It should be pointed out that, as explained earlier, there are no source terms arising from the electrochemical reactions for any of the electroactive species. Further, no source terms are included for all the rapid chemical reactions such as the carbonic acid dissociation steps (see Section 5.1). The effects of these chemical reactions are accounted for through calculation of the chemical equilibria which is described in Chapter 5.

4.2 Solution of the Mass Transport Equations

The mass transport equation (4.7) has the same general form as all other mean flow equations discussed in Chapter 3. After the boundary conditions are specified, they are solved simultaneously with the mean flow equations using the same discretization and solution procedure presented there.

4.2.1 Boundary Conditions

For mass transport equations the boundary conditions are specified in a similar manner as for mean flow equations. At the pipe inlet, fully developed concentration profile can be used. At the symmetry axis and exit, zero concentration gradients are set.

At the wall, species concentrations are determined through electroneutrality and chemical equilibria as described in detail in Chapter 6. When cathodic limiting currents are being studied, surface concentrations of the species involved in the cathodic reactions are set to zero. As indicated in Chapter 3, the low Reynolds number model is implemented in the near wall region. This approach enables the determination of species concentrations all the way from the bulk solution to the corroding surface.

4.3 Calculation of Species Surface Mass Flux

As the low Reynolds number approach enables the application of the k-ε turbulence model all the way to the wall, species concentration profiles from the wall to the bulk solution can be obtained. The surface mass flux of a species is determined according to Fick's first law:

$$J = D\left.\frac{\partial c}{\partial y}\right|_{y=0} \tag{4.14}$$

where c is the species concentration and y is the distance from wall. As previously pointed out, the first near-wall node is placed very close to the wall such that it is within the diffusion controlled portion of the mass transfer sublayer. Therefore the surface mass flux can be calculated by rewriting the above equation:

$$J = D\frac{(c_f - c_s)}{(\delta y)} \tag{4.15}$$

where c_f, c_s and δy are the concentration at the first node from wall, surface (wall) concentration, and the distance of nearest node from the wall surface, respectively.

Two grid systems were used to evaluate the effects of the first node distance from the wall on evaluation of surface mass flux (Figure 4.1). The results indicate that the concentration profile is approximately linear within the diffusion-controlled boundary layer. Equation (4.15) can be used to estimate adequately the first derivative of the concentration profile.

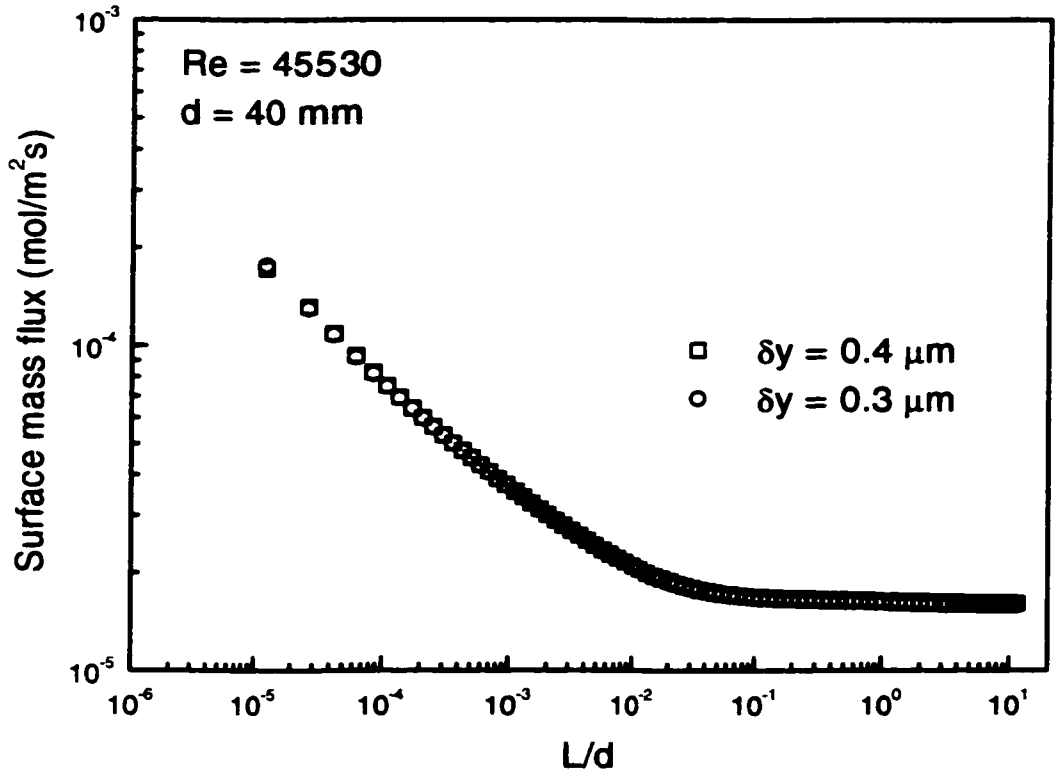

Figure 4.1 Effect of first node distance from wall on the evaluation of the surface H_2CO_3 mass flux. $Re = 45530$; $d = 40$ mm.

4.4 Aqueous Solution Properties and Species Diffusion Coefficients

For the dilute solution of CO_2-water system, its density and viscosity can be taken to be the same as those of pure water. Water density as a function of temperature is (Gray *et al.*, 1990):

$$\rho = -0.5116 \times T + 1152.3 \tag{4.16}$$

where T is the absolute temperature and ρ is density in kg/m^3. This gives a water density of 999.77 kg/m^3 at 25 ^{0}C. Water viscosity is calculated as (Lide and Frederikse, 1997):

$$\mu = \mu_{ref} 10^{\frac{1.3272(t_{ref}-t)-0.00153(t_{ref}-t)}{t+105}} \tag{4.17}$$

where t is temperature in degree Celsius. At 20 ^{0}C, water viscosity is 1.002×10^{-3} kg/ms (Lide and Frederikse, 1997). This is used as the reference viscosity value for water.

Because of the relatively small temperature range in this study, diffusion coefficients of species are calculated using the following relationship (Reid *et al.*, 1977):

$$\frac{D_i \mu}{T} = constant \tag{4.18}$$

where μ is the fluid viscosity and T is the absolute temperature. In order to use this correlation, the species diffusion coefficient at a reference temperature must be known. This information usually comes from experimental findings.

At 25 ^{0}C, the diffusion coefficient for H^+ is 9.31×10^{-9} m^2/s (Atkins, 1986). For ferrous ion, the diffusion coefficient is calculated by using the following equation:

$$D_i = \frac{2.662 \times 10^{-7}}{|z_i|} \lambda_i \tag{4.19}$$

For Fe^{2+} ion at 25 ^{0}C, $z_i = 2$ and $\lambda_i = 53.5$ (Parsons, 1959). This gives a value of $D_{Fe^{2+}} = 7.12 \times 10^{-6}$ cm^2/s, or, 7.12×10^{-10} m^2/s.

The difficulty lies with carbonic acid. It is a weak acid and there is very little information available in the literature with respect to its diffusion coefficient. As carbonic acid is present in aqueous solution as hydrated carbon dioxide, it is reasonable to assume that the diffusion coefficient of carbon dioxide is a good approximation of that of carbonic acid. The value of D_{CO_2} at 25 ^{0}C is experimentally found to be 2.00×10^{-9} m^2/s (Reid *et al.*, 1977). This reference value is used for carbonic acid in this study.

5. Modelling Chemical Equilibrium

5.1 Solution Chemistry

Chemical reactions in a CO_2 corrosion system can have a significant impact on the corrosion rates by modifying the local concentrations of reactants and products throughout the solution. In order to correctly simulate the corrosion phenomenon, various chemical reactions must be taken into account. In this study the following chemical reactions and chemical equilibria are incorporated into the corrosion model.

Firstly, carbon dioxide is dissolved into water:

$$CO_{2(g)} \Leftrightarrow CO_{2(aq)} \tag{5.1}$$

The equilibrium constant for this reaction (Henry's law constant) as a function of temperature is (Roberts and Tremaine, 1985):

$$\log K_H = 3482.89 / T + 8.3068 \ln T - 2.790 \times 10^{-4} T - 60.3994 \tag{5.2}$$

where T is absolute temperature. For most practical applications, it is appropriate to assume that the concentration of dissolved carbon dioxide is constant throughout the

solution under a given temperature (Vetter, 1967). A small fraction of the dissolved CO_2 reacts with water to give carbonic acid. This is the CO_2 hydration reaction:

$$CO_{2(aq)} + H_2O \underset{k_b}{\overset{k_f}{\Leftrightarrow}} H_2CO_3 \tag{5.3}$$

where, k_f and k_b are the rate constants for the forward (hydration) and backward (de-hydration) reactions, respectively. The forward reaction is known to be much slower than the backward reaction, at 25 ^{0}C approximately $k_f = 0.03$ s^{-1} and $k_b = 20$ s^{-1} (Kern, 1960). The equilibrium constant for CO_2 hydration is 2.58×10^{-3} and does not change in the temperature range of 10 - 150 ^{0}C (Palmer and Eldik, 1983). The rate constant of the forward reaction, k_f, is calculated from (Palmer and Eldik, 1983):

$$\log k_f = 195.3 - 63.590 \log T - 11715.8 / T \tag{5.4}$$

The carbonic acid (hydrated carbon dioxide) undergoes dissociation in two steps:

$$CO_{2(aq)} + H_2O \Leftrightarrow H^+ + HCO_3^- \tag{5.5}$$

$$HCO_3^- \Leftrightarrow H^+ + CO_3^{2-} \tag{5.6}$$

The corresponding dissociation constants K_{a1} and K_{a2} are given by the following equations (Roberts and Tremaine, 1985):

$$\log K_{a1} = 29688.2 / T + 81.8401 \ln T - 0.0896488T - 2.04679 \times 10^6 / T^2 - 519.873 \tag{5.7}$$

$$\log K_{a2} = -2730.7 / T - 0.02199T + 5.388 \tag{5.8}$$

Other chemical reactions include the water dissociation and the two-step hydrolysis reactions of ferrous ions:

$$H_2O_{(l)} \Leftrightarrow H^+ + OH^- \tag{5.9}$$

$$Fe^{2+} + H_2O \Leftrightarrow Fe(OH)^+ + H^+ \tag{5.10}$$

$$Fe(OH)^+ + H_2O \Leftrightarrow Fe(OH)_{2(aq)} + H^+ \tag{5.11}$$

The ionization constant of water K_w is (Sweeton *et al.*, 1974):

$$\log K_w = 31286 / T + 94.9734 \ln T - 0.0976117T - 2.17087 \times 10^6 / T^2 - 606.522 \tag{5.12}$$

The equilibrium constants for the hydrolysis reactions of ferrous ions are calculated from the following equations (Baes and Mesmer, 1976):

$$\log K_1 = \frac{1}{2.303 \times 1.98717}\left[-15143 / T - 6.46 \times (\ln T - 1) + 38.49\right] \tag{5.13}$$

$$\log(K_1 K_2) = \frac{1}{2.303 \times 1.98717}\left[-31491 / T - 9.81 \times (\ln T - 1) + 57.64\right] \tag{5.14}$$

As indicated earlier, CO_2 hydration is very slow compared to the reverse half reaction so that the hydration /dehydration reaction will not be in equilibrium where the local carbonic acid concentration is different than its bulk concentration. The generation

of carbonic acid through this slow homogeneous chemical reaction is incorporated into the model by the inclusion of an appropriate source term for the H_2CO_3 transport equation. All other chemical reactions are assumed to be always in equilibrium with the equilibria adjusted after each iteration.

5.2 Solution of Simultaneous Chemical Equilibria

Coupled non-linear algebraic equations are often very difficult to solve. Iteration methods are most commonly used to find roots of algebraic equations. In these procedures, a guess is made at the root and an algorithm refines the guess repeatedly until a small difference in the value of the root between consecutive iterations is achieved.

5.2.1 Newton-Raphson Method

The Newton-Raphson method is one of the most popular and effective iterative methods for solving coupled algebraic equations as it converges quadratically. Once close to a root, the number of significant digits doubles with each iteration.

In order to illustrate the numerical techniques used in the models, consider the following general chemical reactions:

$$A + B \Leftrightarrow C + D \qquad (K_{eq,1} = \omega) \tag{5.15}$$

$$E + F \Leftrightarrow C + G \qquad (K_{eq,2} = \xi) \tag{5.16}$$

All seven species A, B, C, D, E, F, and G are at equilibrium as prescribed by the equilibrium constants $K_{eq,1}$ and $K_{eq,2}$. If a disturbance is introduced, the system will no longer be at equilibrium and new values of concentrations of all species will have to be determined.

Denote aa, bb, cc, dd, ee, ff, and gg as the initial unequilibrated concentrations of species A, B, C, D, E, F, and G, respectively; and AA, BB, CC, DD, EE, FF, GG as the equilibrated concentrations of the corresponding species, respectively. Also let X be the number of moles of A that are consumed to form C and D; let Y be the number of moles of E that are consumed to form C and G. The following equations can be established:

$$K_{eq,1} = \frac{(CC)(DD)}{(AA)(BB)} = \omega \tag{5.17}$$

$$K_{eq,2} = \frac{(CC)(GG)}{(EE)(FF)} = \xi \tag{5.18}$$

$$aa - AA = X \tag{5.19}$$

$$bb - BB = X \tag{5.20}$$

$$cc - CC = -X + Y \tag{5.21}$$

$$dd - DD = -X \tag{5.22}$$

$$ee - EE = Y \tag{5.23}$$

$$ff - FF = Y \tag{5.24}$$

$$gg - GG = -Y \tag{5.25}$$

For this system there are now nine equations and nine unknowns (AA, BB, CC, DD, EE, FF, GG, X and Y) and therefore it is a closed system. The Newton-Raphson method can be used to solve the algebraic equations. It is a two step procedure. Guesses at the roots, $\bar{x}_{old}$, are first chosen and changes in these values, $\delta\bar{x}$, are updated by the following equation:

$$\bar{J}(\delta\bar{x}) = -\bar{F} \tag{5.26}$$

where $\bar{J}$ is the Jacobian matrix and $\bar{F}$ is the vector of functions:

$$\bar{J} = \begin{bmatrix} \frac{\partial F_1}{\partial x_1} & \frac{\partial F_1}{\partial x_2} & \cdots & \frac{\partial F_1}{\partial x_n} \\ \frac{\partial F_2}{\partial x_1} & \frac{\partial F_2}{\partial x_2} & \cdots & \frac{\partial F_2}{\partial x_n} \\ \vdots & & & \\ \frac{\partial F_n}{\partial x_1} & \frac{\partial F_n}{\partial x_2} & \cdots & \frac{\partial F_n}{\partial x_n} \end{bmatrix}, \quad \bar{F} = \begin{bmatrix} F_1(x_1, x_2, \cdots, x_n) \\ F_2(x_1, x_2, \cdots, x_n) \\ \vdots \\ F_n(x_1, x_2, \cdots, x_n) \end{bmatrix} \tag{5.27}$$

Improved guesses, $\bar{x}_{new}$, are then obtained:

$$\bar{x}_{new} = \bar{x}_{old} + (\delta\bar{x}) \tag{5.28}$$

The iteration continues until some tolerance is met (Press *et al.*, 1992).

5.2.2 Modified Gauss-Seidel Method

If the chemical equilibria are initially treated as being independent, the equations can be simultaneously solved by the following procedure. Consider the previously given general chemical equilibrium (equation 5.15). If the four species A, B, C, and D with unequilibrated concentrations aa, bb, cc, and dd respectively are not at equilibrium, and the concentrations are δ mol/l away from their equilibrium values, then

$$\frac{(cc+\delta)(dd+\delta)}{(aa-\delta)(bb-\delta)} = \omega \tag{5.29}$$

The above equation is subsequently written in quadratic form and solved for δ. Numerical experimentation has shown that, of the two roots, the one with the smallest absolute value should be chosen. The species concentrations are then updated using the residual δ. The new concentrations of A, B, C, and D are now (aa-δ), (bb-δ), (cc+δ), and (dd+δ), respectively, and they are closer towards equilibrium than the initial concentrations. This procedure is repeated for all chemical equilibria in a sequential manner using the values of the common species calculated by the previous equilibrium

relationship. The whole procedure is then iterated until the total change in the sum of the absolute values of the residual is negligible. For chemical reactions with stoichiometric coefficients other than unity, the procedure is still the same except that the resultant algebraic equation will not be quadratic. In that case, a procedure such as the Secant method (e.g., Maron, 1987) is used to determine the value of the residual δ during each iteration.

The modified Gauss-Seidel Method is easier to implement than the Newton-Raphson method. It is also less demanding in terms of computer resources. Therefore it is used in this study. The Newton-Raphson technique has been used to cross-check the results of the Gauss-Seidel method.

6. Modelling Corrosion Rates

6.1 Basic Corrosion Kinetics

Corrosion is the degradation and deterioration of a material by chemical or electrochemical reaction with its environment. Virtually all known instances of metallic corrosion are electrochemical in nature. The metallic corrosion process involves at least one anodic reaction where electrons are produced and one cathodic reaction where electrons are consumed. For instance, in the case of iron immersed in a deaerated dilute hydrochloric acid, the anodic reaction is iron dissolution and the cathodic reaction is hydrogen evolution.

$$Fe \rightarrow Fe^{2+} + 2e^{-} \tag{6.1}$$

$$2H^{+} + 2e^{-} \rightarrow H_2 \tag{6.2}$$

An electrochemical reaction is essentially a multi-step process in nature. A typical electrochemical reaction involves the following sequence. First the reactants such as H^+ are transported from the bulk of the solution to the corroding metal/solution interface. The electronation (electron consuming) or de-electronation (electron producing) reaction then takes place at the surface. Metal is corroded through dissolution

and oxidants are reduced. Finally, the electrochemical reaction products such as Fe^{2+} are transported away from the metal/interface to the bulk solution. There may also be adsorption and desorption steps before and after the electronation/de-electronation reaction. The slowest step in the reaction sequence controls the overall reaction rate and is called the rate-determining step (RDS).

6.1.1 General Rate Equation

The rate at which an electrochemical reaction proceeds depends on temperature, the exchange current density of the reaction concerned, i_0 (based on the surface concentrations), and the overpotential of the electrode, η (also based on the surface concentrations), as expressed in the general Butler-Volmer equation (Bockris and Reddy, 1970):

$$i = \vec{i} - \overleftarrow{i} = i_0\left[\exp\left(\frac{\vec{\alpha}F\eta}{RT}\right) - \exp\left(-\frac{\overleftarrow{\alpha}F\eta}{RT}\right)\right] \tag{6.3}$$

where $\vec{\alpha}$ and $\overleftarrow{\alpha}$ are the transfer coefficients for the electrochemical reaction. These transfer coefficients determine the slope of the log(i) versus η curve, i.e., the Tafel slope of a multi-step reaction, and are of primary importance in mechanism determinations. They are defined as follows:

$$\vec{\alpha} = \frac{n - \vec{\gamma}}{\nu} - r\beta \tag{6.4}$$

$$\bar{\alpha} = \frac{\bar{\gamma}}{\nu} + r\beta \tag{6.5}$$

where n is the total number of electrons transferred in the overall electrochemical reaction, $\bar{\gamma}$ is the number of electrons transferred in the steps that precede the rate determining step, r is the number of electrons involved in the rate determining step, ν is the number of times the rate-determining step is required to repeat for each occurrence of the overall reaction, and β is the symmetry factor. Combining equations (6.4) and (6.5) yields:

$$\bar{\alpha} + \bar{\alpha} = \frac{n}{\nu} \tag{6.6}$$

It is evident from above description that mass transport (flow) can have a major impact on the corrosion rate by modifying the *surface concentrations* of reactants and products. From a mathematical point of view, the values of the parameters such as the exchange current density and overpotential in equation (6.3) are directly influenced by the surface concentrations of the relevant electroactive species and thus also by mass transport.

6.1.2 Mixed Potential Theory

The mixed potential theory (Stern and Geary, 1957; Bockris and Reddy, 1970) is a fundamental principle in corrosion science and engineering. It was developed by

Wagner and Traud (1938) to deal with several electrochemical reactions that are proceeding simultaneously at the same metal/solution interface. For a corrosion system with multiple anodic and/or cathodic reactions, mixed potential theory states that the corrosion potential, E_{corr}, will be attained at which the sum of all anodic currents is equal to the sum of all cathodic currents and both are equal to the corrosion current, i_{corr}:

$$\Sigma i_a = \Sigma i_c = i_{corr} \tag{6.7}$$

With the corrosion current, i_{corr}, being known, the corrosion rate can be determined by applying Faraday's laws. The mixed potential theory provides an effective way to calculate corrosion potential and corrosion rates.

6.2 Modelled Electrochemical Reactions

In the present study the anodic reaction is iron dissolution, and the cathodic reactions considered are the reduction of hydrogen ion, the direct reduction of carbonic acid and the reduction of water:

$$Fe \rightarrow Fe^{2+} + 2e^- \tag{6.8}$$

$$2H^+ + 2e^- \rightarrow H_2 \tag{6.9}$$

$$2H_2CO_3 + 2e^- \rightarrow H_2 + 2HCO_3^- \tag{6.10}$$

$$2H_2O + 2e^- \rightarrow H_2 + 2OH^- \tag{6.11}$$

6.2.1 Anodic Dissolution of Iron

For the anodic reaction of iron dissolution it is assumed that iron dissolution follows the three-step pH-dependent mechanism proposed by Bockris *et al.* (1961):

$$Fe + OH^- \Leftrightarrow FeOH + e^- \tag{6.12}$$

$$FeOH \xrightarrow{RDS} FeOH^+ + e^- \tag{6.13}$$

$$FeOH^+ \Leftrightarrow Fe^{2+} + OH^- \tag{6.14}$$

The anodic current is calculated according to the general rate equation (6.3):

$$i_a = i_0 \left(10^{\frac{E-E_{rev}}{b_a}} - 10^{\frac{E-E_{rev}}{b_c}} \right) \tag{6.15}$$

In the rate equation, the exchange current density, i_0, and the reversible potential, E_{rev}, are calculated based on the surface concentration of ferrous ions. The Tafel slopes b_a and b_c are:

$$b_a = \frac{2.303RT}{\bar{\alpha}F}, \quad b_c = \frac{2.303RT}{\bar{\alpha}F} \tag{6.16}$$

According to Bockris and Reddy (1970) for iron dissolution, $\bar{\alpha} = 1.5$ and $\bar{\alpha} = 0.5$. This gives $b_a = 0.04$ V and $b_c = 0.12$ V at 25 ^{0}C.

The dependence of the exchange current density on Fe^{2+} concentration is modelled by:

$$\frac{\partial \log i_0}{\partial \log[Fe^{2+}]} = 0.75 \tag{6.17}$$

And the pH dependence of the exchange current density is:

$$\frac{\partial \log i_0}{\partial \mathrm{pH}} = n \tag{6.18}$$

where n is pH dependent. According to Bockris *et al.* (1961), $n = 1$ in strong acid solutions and is close to zero at pH values over 4. The reference i_0 value used for iron dissolution is 5×10^{-4} A/m^2 at 25 ^{0}C, pH 4, and [Fe^{2+}] = 7.2×10^{-7} M (Gray *et al.*, 1989).

6.2.2 Hydrogen Ion Reduction

The rate equation for hydrogen ion reduction is given by

$$i_c = i_0 \left(10^{-\frac{E-E_{rev}}{b_c}} - 10^{\frac{E-E_{rev}}{b_a}} \right) \tag{6.19}$$

where i_0 and E_{rev} are calculated based on H^+ surface concentration. According to Bockris and Reddy (1970), $\bar{\alpha} = 0.5$, $v = 1$. From equation (6.4), $\bar{\alpha} = (2/1) - 0.5 = 1.5$. Therefore

at 25 ^{0}C, $b_c = 0.12$ V and $b_a = 0.04$ V. A value of 5×10^{-2} A/m^2 at pH 4, 20 ^{0}C and 0.1 MPa H_2 is used as the reference exchange current density for H^+ reduction (Nesic *et al.*, 1996). The pH dependence of the exchange current density is (Bockris *et al.*, 1961):

$$\frac{\partial \log i_0}{\partial \mathrm{pH}} = -0.5 \tag{6.20}$$

6.2.3 Carbonic Acid Reduction

Similarly for carbonic acid reduction the reaction rate is calculated by:

$$i_c = i_0 \left(10^{-\frac{E-E_{rev}}{b_c}} - 10^{\frac{E-E_{rev}}{b_a}} \right) \tag{6.21}$$

As demonstrated by Gray *et al.* (1989) the reversible potentials for the reduction of hydrogen ion, water, and carbonic acid are all thermodynamically equivalent and are given by:

$$E_{rev} = -\frac{2.303RT}{F}\mathrm{pH} - \frac{2.303RT}{2F}\log P_{H_2} \tag{6.22}$$

where P_{H_2} is the partial pressure of hydrogen. The Tafel slopes b_a and b_c are assumed to be the same as those for hydrogen ion reduction which was confirmed by the experiments of de Waard and Milliams (1975a). The exchange current density is proportional to the carbonic acid concentration and the hydrogen ion concentration (Nesic *et al.*, 1996):

$$i_0 \propto [H_2CO_3] \times [H^+]^{-0.5} \tag{23}$$

A value of 6×10^{-2} A/m^2 at pH 4, 20 ^{0}C, 0.1 MPa CO_2 and 0.1 MPa H_2 is used as the reference exchange current density for H_2CO_3 reduction (Nesic *et al.*, 1996). The pH dependence of the exchange current density is therefore:

$$\frac{\partial \log i_0}{\partial \mathrm{pH}} = 0.5 \tag{6.24}$$

6.2.4 Water Reduction

The reduction of water can be important in high overpotential regions. The reduction rate is calculated with the following equation:

$$i_c = i_0 \left(10^{-\frac{E-E_{rev}}{b_c}} - 10^{\frac{E-E_{rev}}{b_a}} \right) \tag{6.25}$$

As pointed out earlier the reduction of water and the reduction of hydrogen ions are thermodynamically equivalent, the reversible potential for water reduction is the same as that of H^+ reduction and is calculated using equation (6.22). The same values of Tafel slopes used for H^+ reduction are employed here. It has been experimentally determined (Stern, 1955) that the water reduction kinetics on iron surface is independent of the pH values of the solution. The exchange current density for water reduction is modelled as

being independent of pH. Gray *et al.* (1989) found the exchange current density is 1×10^{-4} A/m^2 at 25 ^{0}C. This is used as the reference value for water reduction.

6.3 Calculation of Corrosion Rates

The corrosion rates were calculated using an iterative procedure. An initial value of carbonic acid surface concentration was chosen. This value should be between its bulk concentration and zero (limiting condition). Based on this initial guess surface concentrations of other species were determined according to the following surface chemical equilibria and electroneutrality:

$$H_2CO_3 \Leftrightarrow H^+ + HCO_3^- \tag{6.26}$$

$$HCO_3^- \Leftrightarrow H^+ + CO_3^{2-} \tag{6.27}$$

$$H_2O_{(l)} \Leftrightarrow H^+ + OH^- \tag{6.28}$$

$$Fe^{2+} + H_2O \Leftrightarrow Fe(OH)^+ + H^+ \tag{6.29}$$

$$Fe(OH)^+ + H_2O \Leftrightarrow Fe(OH)_{2(aq)} + H^+ \tag{6.30}$$

$$Fe^{2+} + CO_3^{2-} \Leftrightarrow FeCO_3 \tag{6.31}$$

$$[H^+] + 2[Fe^{2+}] + [Fe(OH)^+] = [HCO_3^-] + 2[CO_3^{2-}] + [OH^-] \tag{6.32}$$

The surface concentrations of the electroactive species were then used as boundary conditions for the corresponding species conservation equations. After numerically solving all the conservation equations and the chemical equilibria, the species concentration profiles were determined, and the surface fluxes of the electroactive species were calculated.

With the surface concentrations known, the mixed potential theory was applied to determine the corrosion current. The reversible potentials and exchange current densities in the calculation of the corrosion current were determined at the surface concentrations.

A convergence check was performed after each iteration. Iteration continued until the surface flux of the electroactive species involved in the anodic reaction was balanced by the fluxes of the cathodic species also the mixed potential theory was satisfied. When these criteria are met, steady state is achieved and the corrosion current (corrosion rate) determined.

7. Simulation Results and Discussion

7.1 Introduction

The development of a carbon dioxide corrosion numerical model is broken down into two steps. First the numerical modelling of the cathodic reactions is performed. This will enable the understanding of the effects of flow on each individual cathodic reaction. Species concentration profiles are obtained and cathodic limiting currents are studied. Then the anodic reaction of iron dissolution is added into the model to form a corrosion system. Kinetic corrosion diagrams are constructed. Corrosion currents and corrosion rates are calculated. The effects of turbulent flow on the corrosion processes are investigated. The effects of parameters such as pH, temperature, CO_2 partial pressure on the corrosion rates are also studied.

Additionally an interactive simplified electrochemical CO_2 corrosion model has been developed and implemented in Microsoft® Excel 97. It is suitable for practical use in the oil and gas production and transportation. The electrochemical model, like the numerical model, also calculates the corrosion rates based on electrochemistry. However, overall mass transfer coefficients from established correlations for the electroactive species are used in the electrochemical model. Using macros and controls

through Visual Basic programming, the model can automatically set up the problem, perform necessary calculations and display model predictions in graphs and tables.

7.2 Numerical Modelling of Cathodic Reactions in CO_2 Corrosion

7.2.1 Introduction and Preparation

As described in Chapter 6, the cathodic reactions considered in the present study are the hydrogen ion reduction, carbonic acid reduction and the reduction of water. Oxygen reduction is negligible in most practical cases due to the very small oxygen concentrations. Water molecules are present in nearly unlimited quantities throughout the solution and the reduction of water can be simply assumed to be solely charge transfer controlled. Therefore, the H^+ reduction and H_2CO_3 reduction are the only two cathodic reactions that need our attention for now.

7.2.1.1 Computational Domain

The computational domain for the present study is shown in Figure 7.1. Fully developed flow conditions are introduced at the inlet. To study the cathodic limiting currents, the species concentrations at the pipe wall were set to zero for both hydrogen ion and carbonic acid. At the symmetrical axis of the pipe, zero concentration gradients were specified. The pipe diameter used is 40 mm. Non-uniform staggered grids were

used with most nodes clustered in the near wall region and mass transfer entrance region. The first near-wall node was placed at y = 0.4 μm which ensured that the dimensionless wall distance y^+ is less than 0.1 for all the flow velocities considered in this study. The first node close to the mass transfer entrance was placed at x = 0.5 μm.

7.2.1.2 Grid Dependence of Computational Results

Two grid systems, 120 × 60 and 90 × 45, have been used to test the grid dependence of the computational results (Figure 7.2). It is seen that the grid system 90 × 45 is adequately accurate to model the mass transport and is therefore used for the rest of the study.

7.2.1.3 The Law of the Wall

In order to evaluate the numerical technique employed in this study, a flat axial velocity profile is used at the inlet for a straight pipe. With an adequately long computational domain in the straight pipe, fully developed velocity profiles are obtained at the outlet of the computational domain. Figures 7.3-7.4 illustrate the velocity profiles for Re = 45530. It is shown that within the viscous sublayer ($y^+ < 5$), the velocity has a linear profile; In the fully turbulent region the velocity follows a logarithmic profile. This is known as the law of the wall (e.g., Schlichting, 1979).

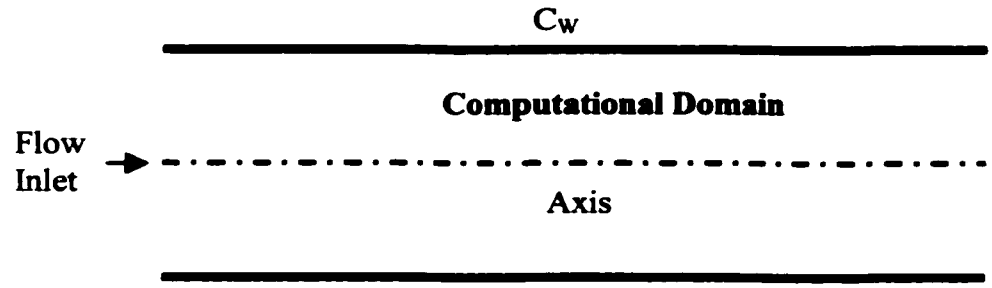

Figure 7.1 Computational domain. Fully developed flow at inlet. Zero concentration gradient on symmetrical axis. Pipe diameter $d = 40$ mm.

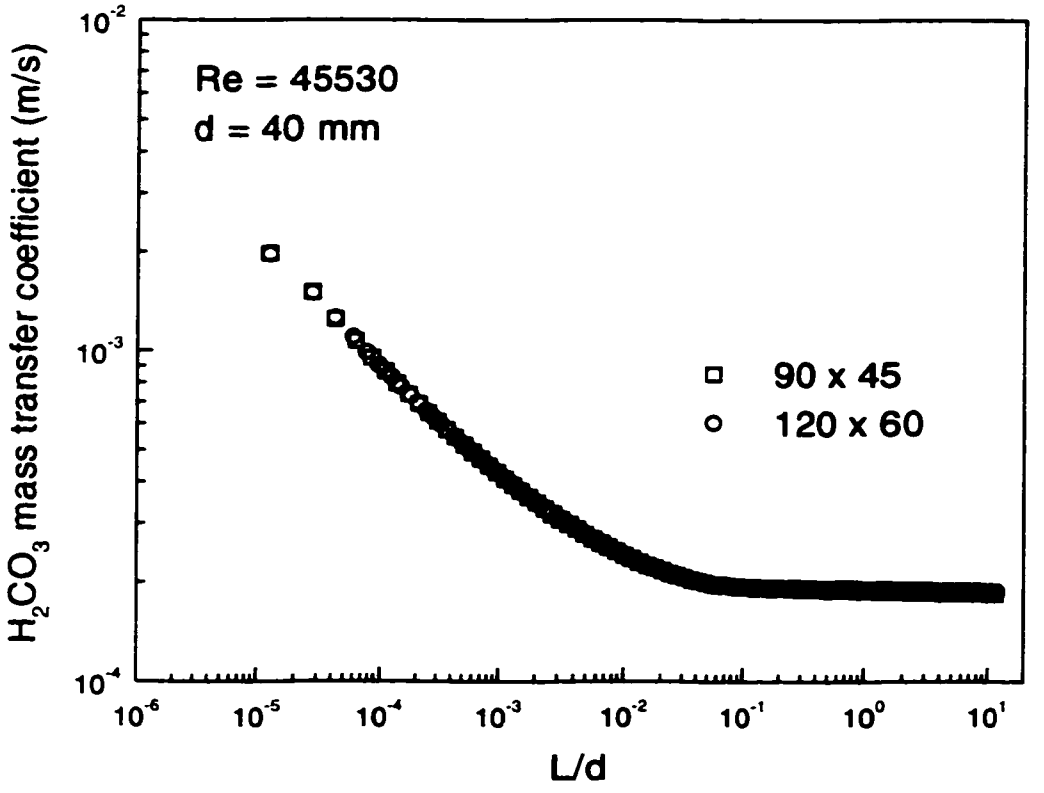

Figure 7.2 Evaluation of grid dependence on computational results. *Re* = 45530; *d* = 40 mm.

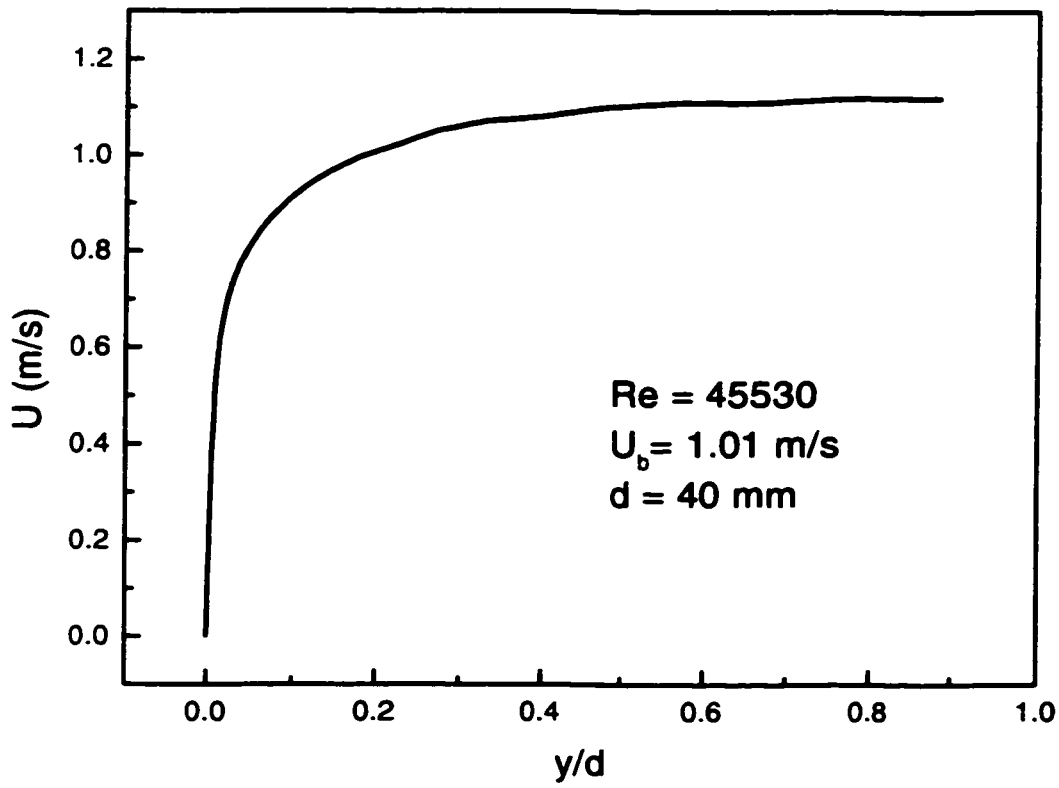

Figure 7.3 Calculated axial velocity profile. $Re = 45530$; $U_b = 1.01$ m/s; $d = 40$ mm.

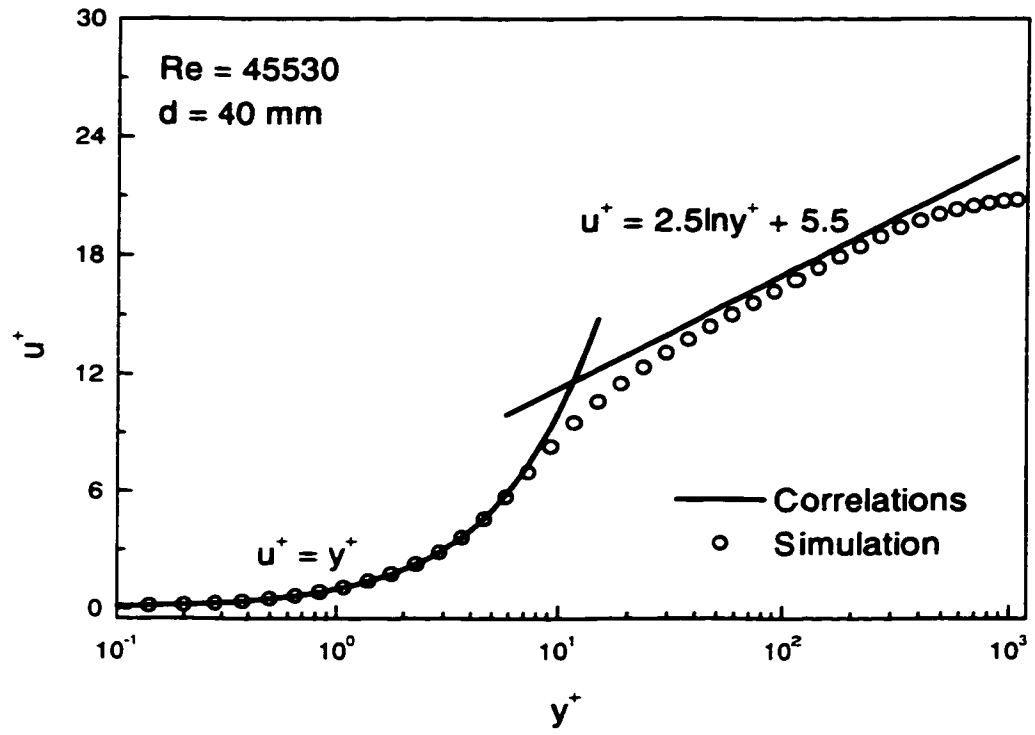

Figure 7.4 Comparison of velocity profile with known correlations. *Re* = 45530; *d* = 40 mm.

7.2.2 Equilibrium Distribution of Carbonate Species

Before the species concentration profiles can be solved for, the equilibrium (bulk) concentrations of the species must first be determined. Using the vapor-liquid equilibrium and relevant chemical equilibrium equations and correlations presented in Chapter 5, it is possible to calculate the distribution of different species in equilibrium in an open system of CO_2 saturated aqueous solution as a function of pH. Figures 7.5-7.8 present such equilibrium distributions of the major carbonate species for four different temperatures 10 ^{0}C, 25 ^{0}C, 40 ^{0}C, and 60 ^{0}C, all at a CO_2 partial pressure of 0.1 MPa (1 bar).

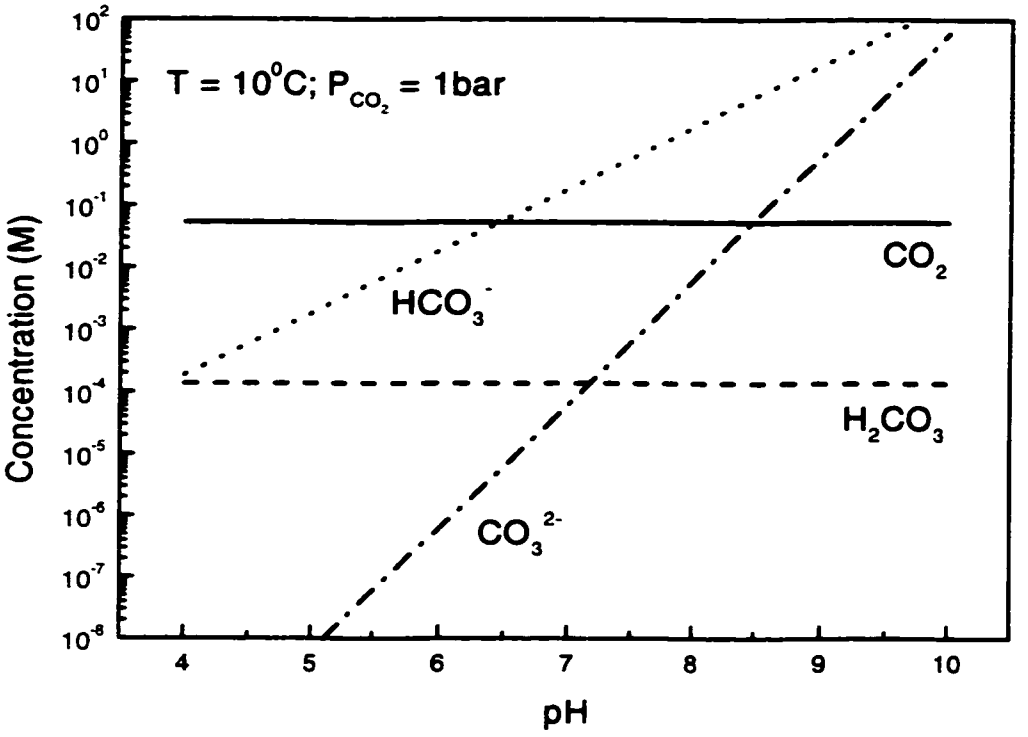

Figure 7.5 Equilibrium distribution of carbonate species in bulk solution. T = 10 ^{0}C; P_{CO_2} = 0.1 MPa.

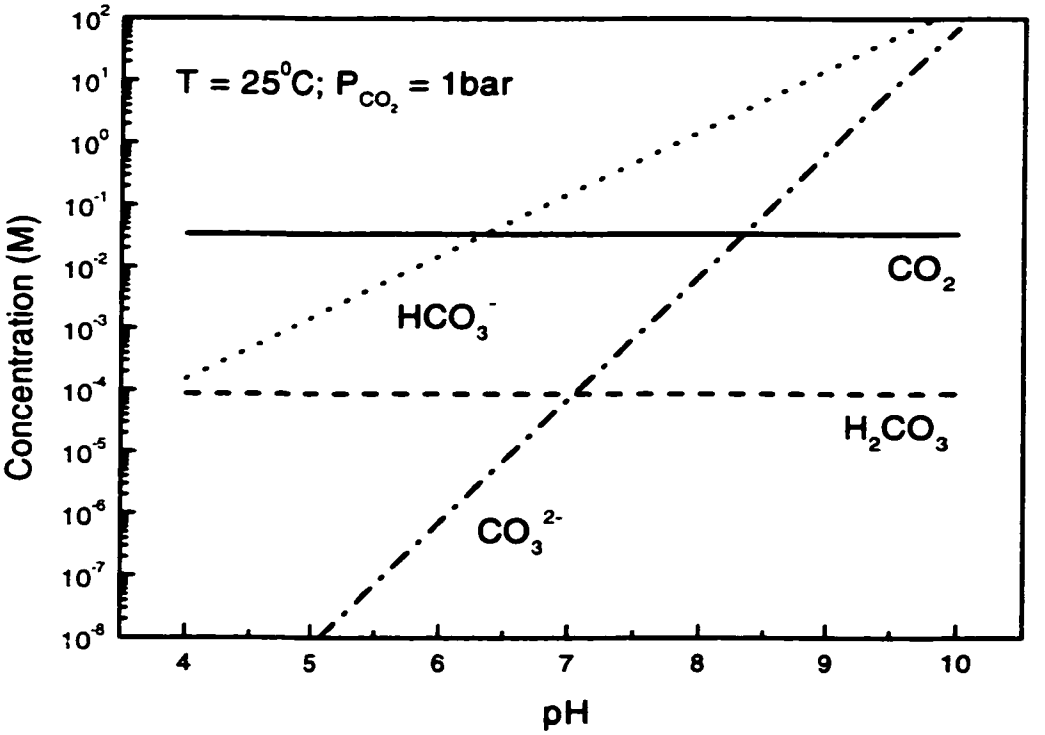

Figure 7.6 Equilibrium distribution of carbonate species in bulk solution. T = 25 ^{0}C; P_{CO_2} = 0.1 MPa.

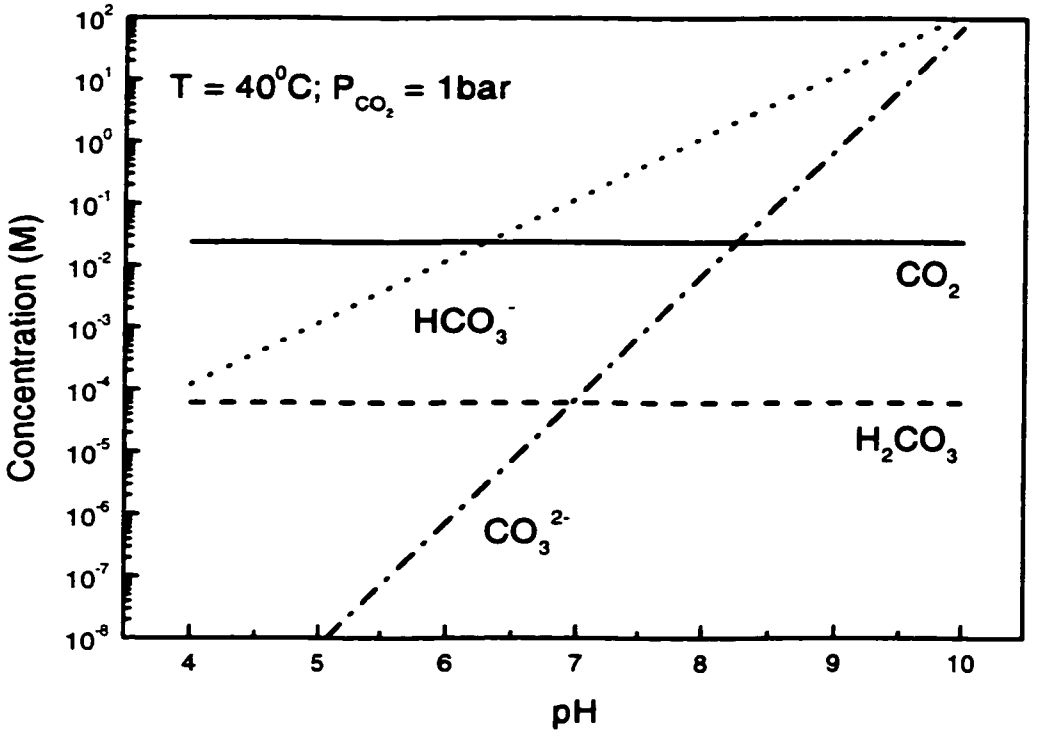

Figure 7.7 Equilibrium distribution of carbonate species in bulk solution. T = 40 ^{0}C; P_{CO_2} = 0.1 MPa.

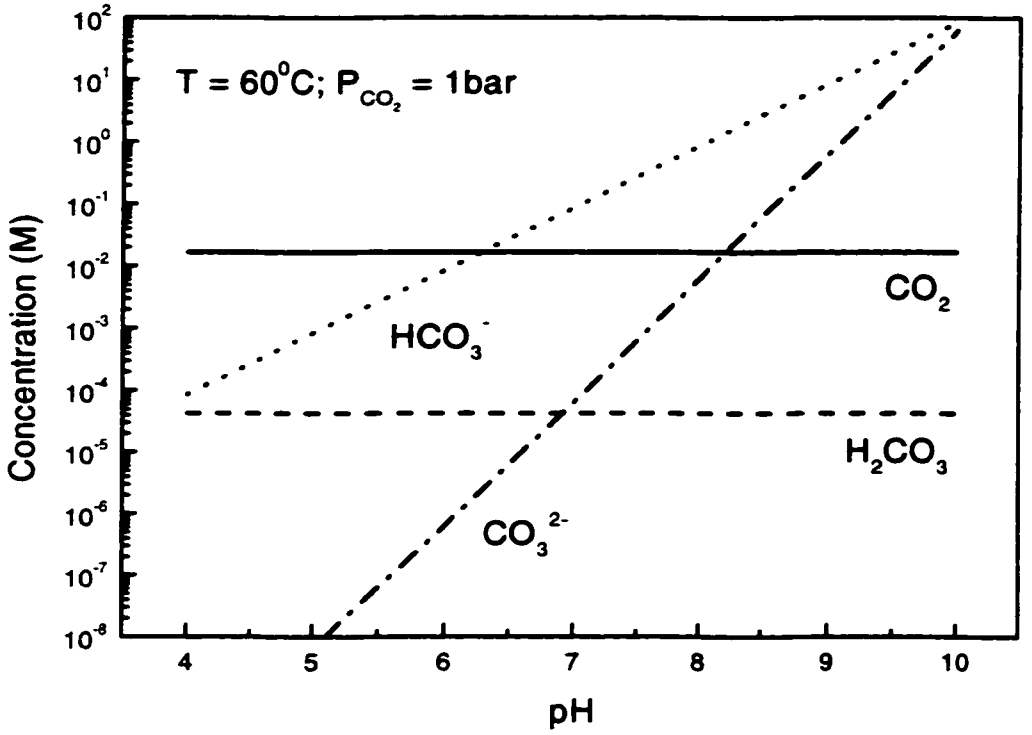

Figure 7.8 Equilibrium distribution of carbonate species in bulk solution. T = 60 ^{0}C; P_{CO_2} = 0.1 MPa.

7.2.3 Species Concentration Profiles

Because of the application of the low Reynolds number k-ε turbulence model, the concentration profiles of various dissolved species can be determined from the bulk solution to the surface. The fully developed carbonic acid concentration profiles at bulk pH 4 and 25 ^{0}C are given in Figure 7.9. It is seen that the concentration profile at U_b = 1.01 m/s differs little from that at U_b = 0.10 m/s. At higher velocities, the concentration profile becomes more flow sensitive. Higher velocities bring the H_2CO_3 bulk concentration closer to the wall resulting in a thinner concentration boundary layer. The H_2CO_3 concentration profiles at different temperatures (40 and 60 ^{0}C) and at a different pH value (pH 6) exhibit the same behavior, as illustrated in Figures 7.10-12.

The hydrogen ion profiles (Figures 7.13 and 7.14) are very flow dependent. The profile is quite different at different mean velocities at a given temperature, and higher velocities bring the bulk H^+ concentration closer to the wall. This is expected for a wholly mass transfer controlled process.

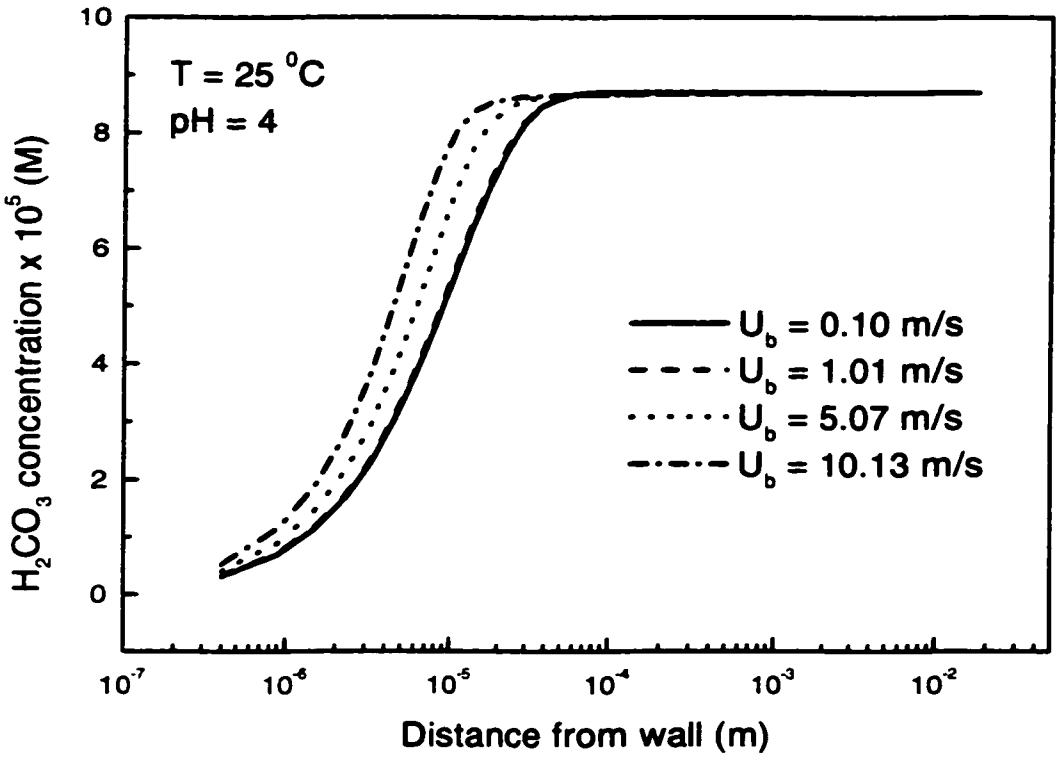

Figure 7.9 Variation of fully developed H_2CO_3 concentration profiles with mean flow. T = 25 °C; $pH = 4$; $P_{CO_2} = 0.1$ MPa.

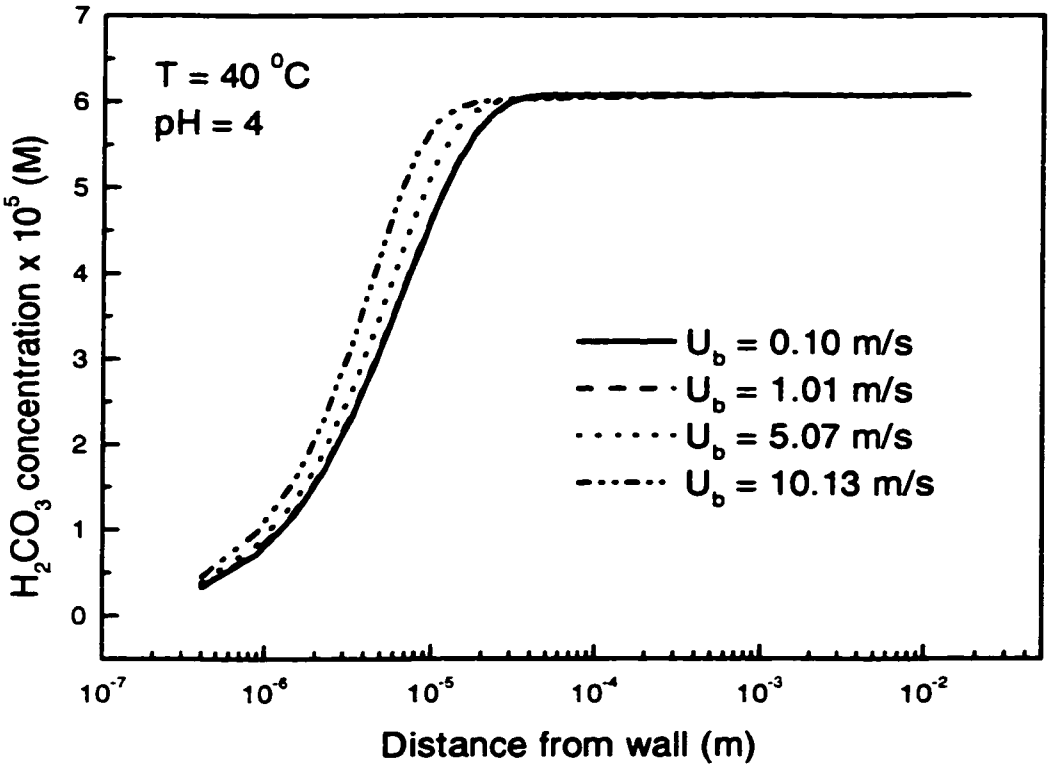

Figure 7.10 Variation of fully developed H_2CO_3 concentration profiles with mean flow. $T = 40\ ^0C$; $pH = 4$; $P_{CO_2} = 0.1$ MPa.

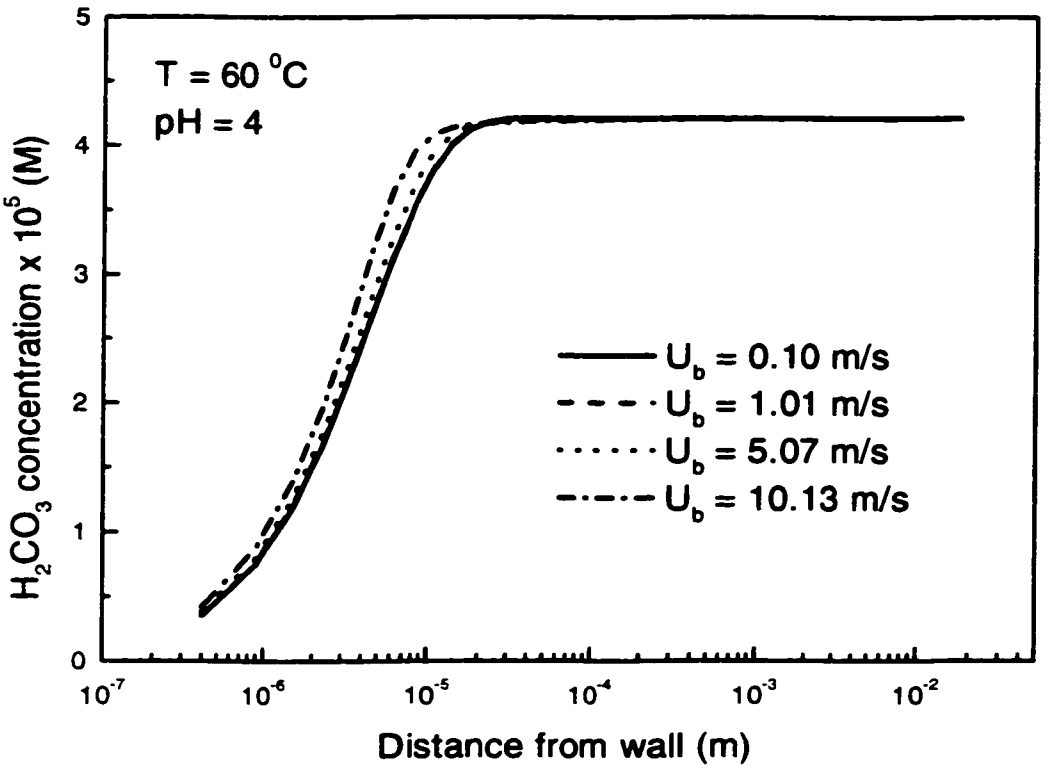

Figure 7.11 Variation of fully developed H_2CO_3 concentration profiles with mean flow. $T = 60\ ^0C$; $pH = 4$; $P_{CO_2} = 0.1$ MPa.

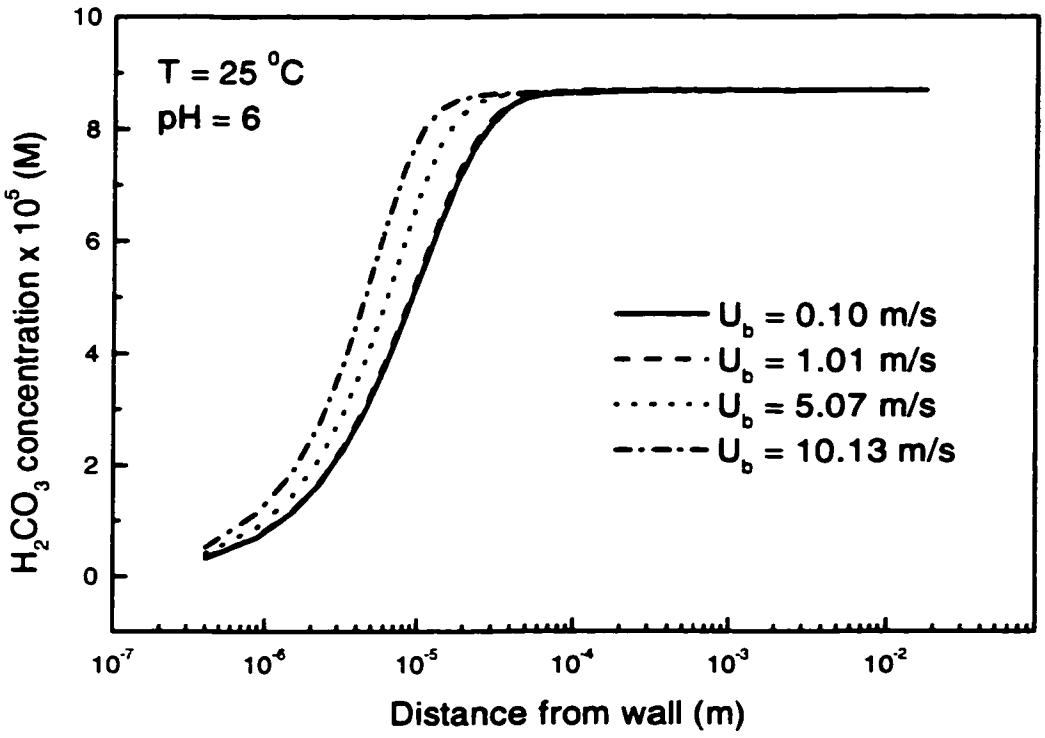

Figure 7.12 Variation of fully developed H_2CO_3 concentration profiles with mean flow. $T = 25\ ^0C$; $pH = 6$; $P_{CO_2} = 0.1$ MPa.

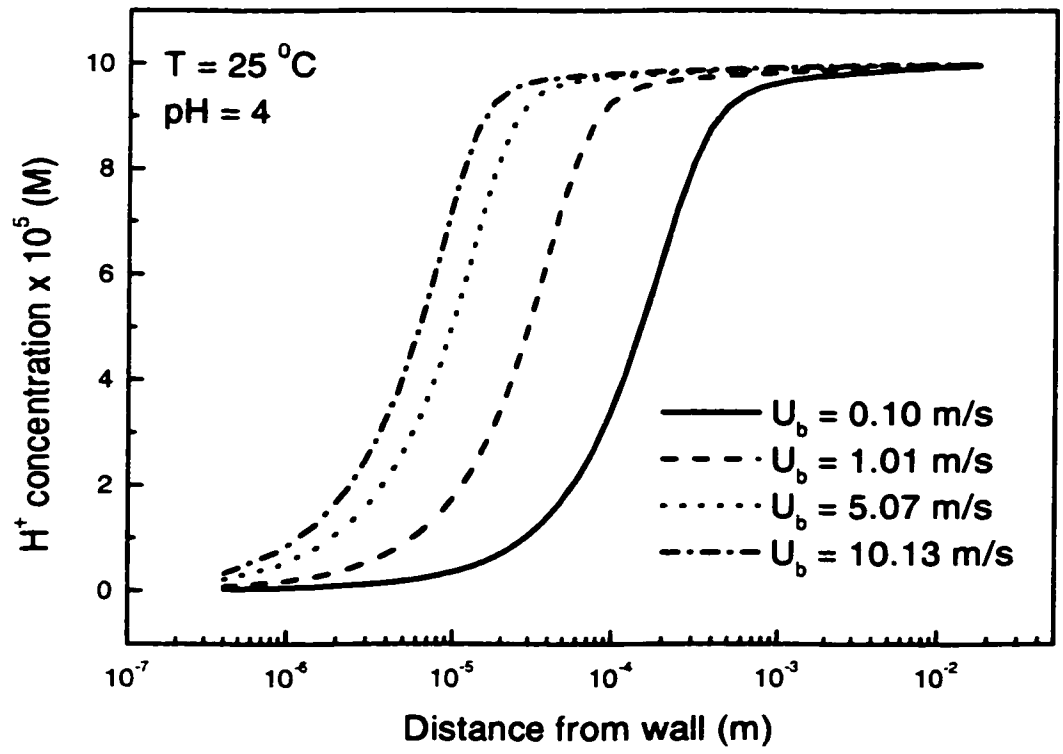

Figure 7.13 Variation of fully developed H^+ concentration profiles with mean flow. T = 25 ^{0}C; $pH = 4$; $P_{CO_2} = 0.1$ MPa.

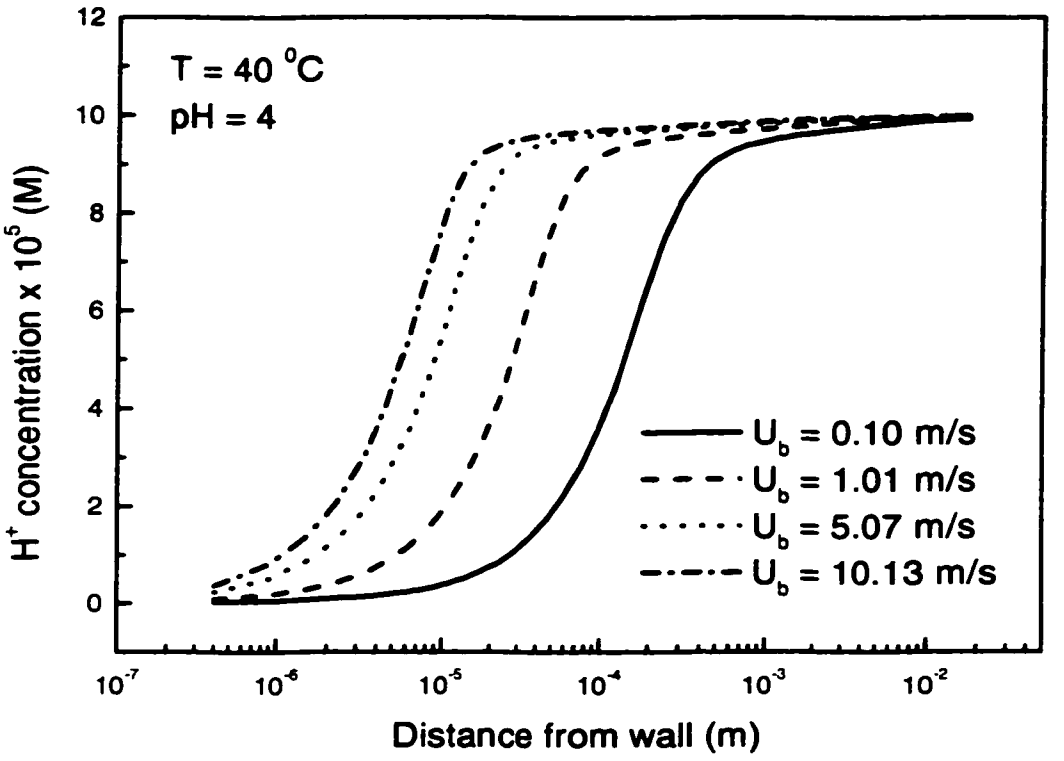

Figure 7.14 Variation of fully developed H^+ concentration profiles with mean flow. T = 40 ^{0}C; $pH = 4$; P_{CO_2} = 0.1 MPa.

Changes in carbonic acid and hydrogen ion concentrations also lead to changes in bicarbonate and carbonate ions concentrations. The bicarbonate ion concentration profiles pass through a maximum value as the wall is approached (Figures 7.15-7.17). Modelling cathodic limiting currents in CO_2 corrosion for a rotating disk electrode system, Turgoose *et al.* (1990) also found the same bicarbonate ion concentration pattern at a bulk pH value of 6.5. The peaks are especially noticeable at lower velocities. At higher velocities, the concentration change within the boundary layer is less significant.

Figure 7.18 presents the fully developed concentration profile for carbonate ion at 25 ^{0}C and bulk pH 4. The CO_3^{2-} concentration increases when the wall surface is approached. Figure 7.19 shows the CO_3^{2-} concentration profiles at U_b = 1.01 m/s and bulk pH 4 for four different temperatures (10, 25, 40, and 60 ^{0}C). Examination of these concentration profiles indicates that CO_3^{2-} concentrations very close to the wall increase with increasing temperature as a result of the rapid chemical equilibria. This suggests that formation of ferrous carbonate films is possible at higher temperatures when the solution is saturated with the carbonate and ferrous ions.

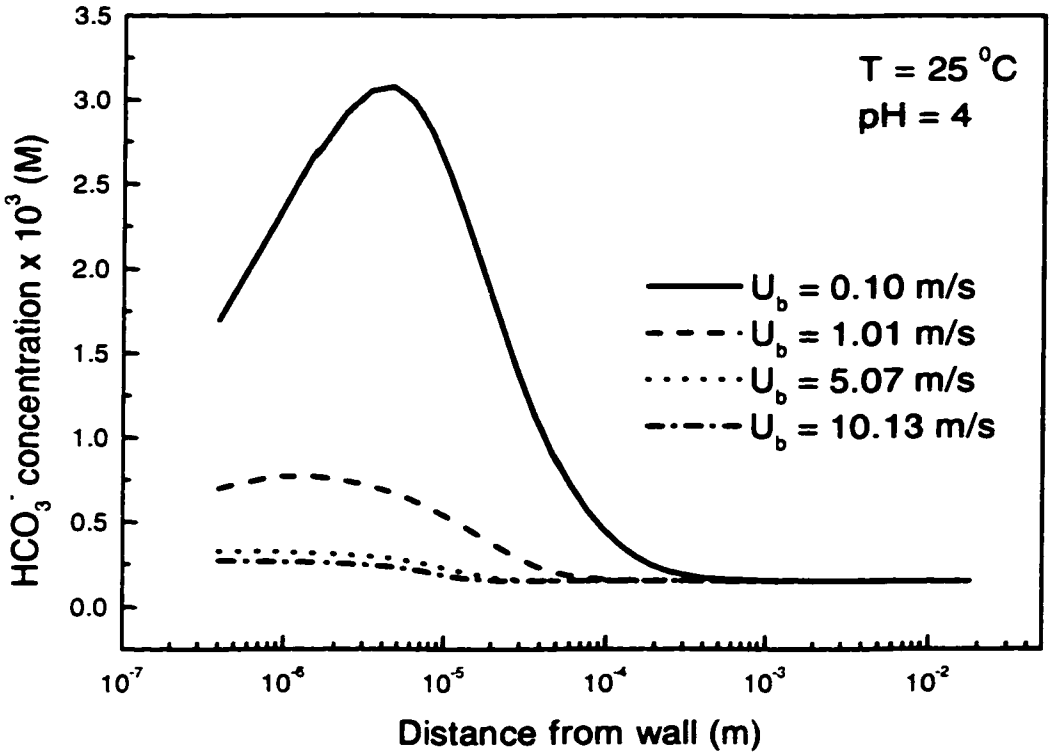

Figure 7.15 Variation of fully developed HCO_3^- concentration profiles with mean flow. $T = 25\ ^0C$; $pH = 4$; $P_{CO_2} = 0.1$ MPa.

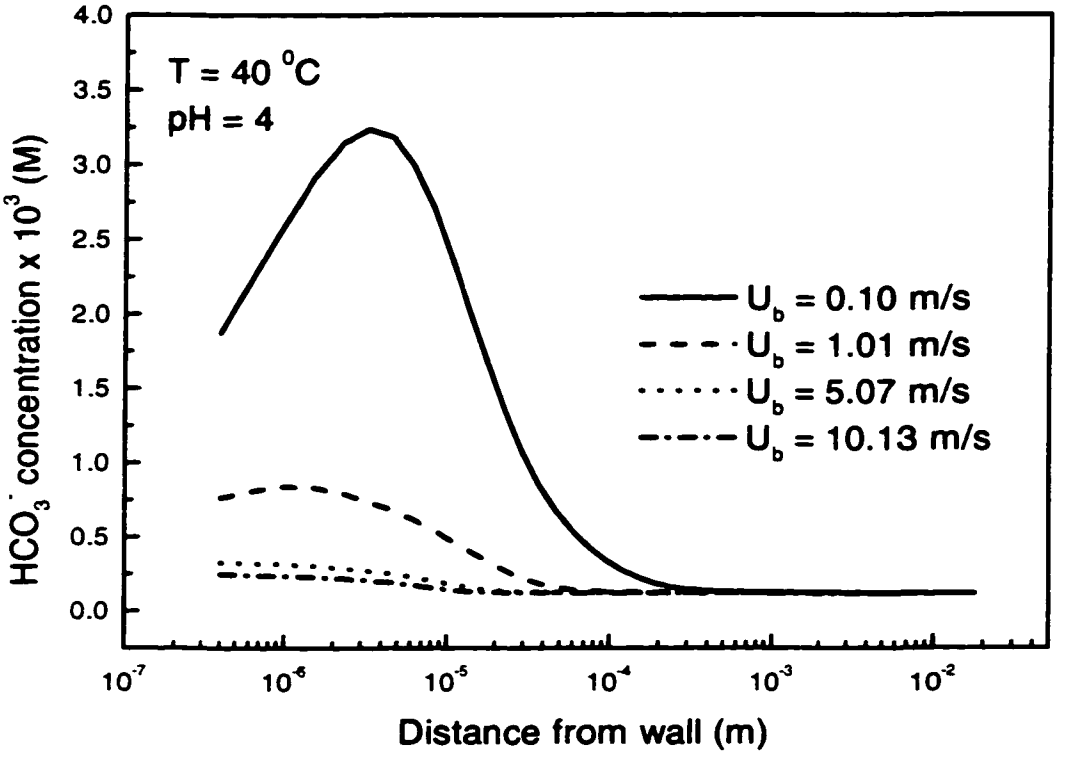

Figure 7.16 Variation of fully developed HCO_3^- concentration profiles with mean flow. $T = 40\ ^0C$; $pH = 4$; $P_{CO_2} = 0.1$ MPa.

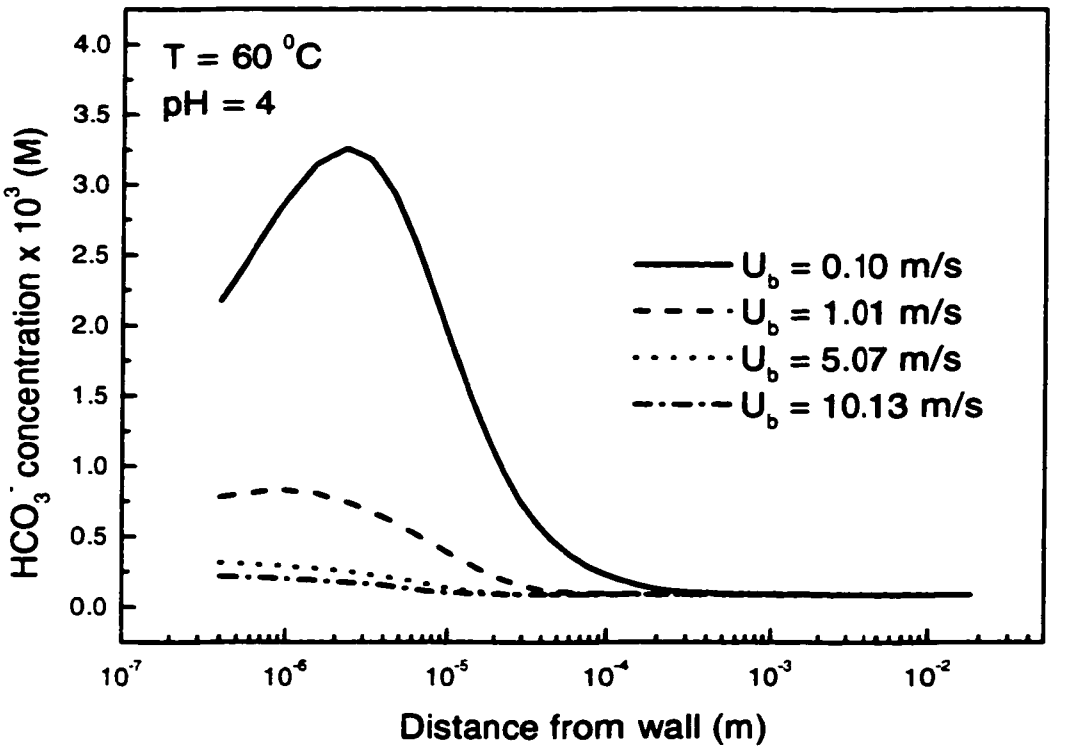

Figure 7.17 Variation of fully developed HCO_3^- concentration profiles with mean flow. $T = 60\ ^0C$; $pH = 4$; $P_{CO_2} = 0.1$ MPa.

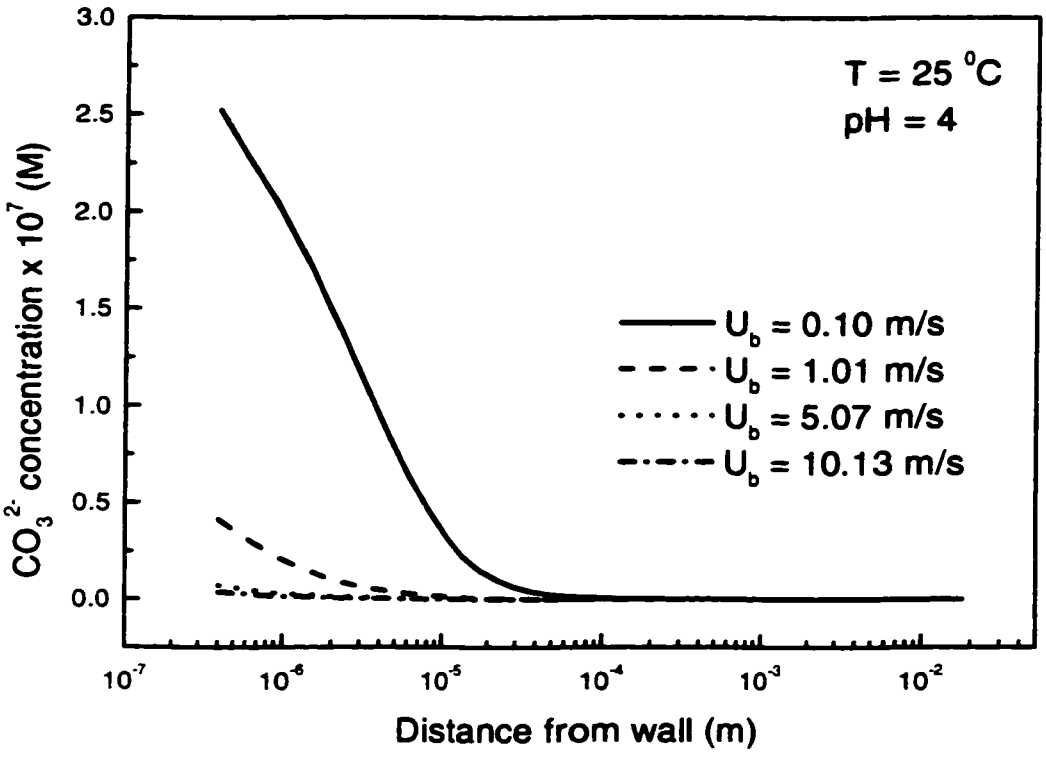

Figure 7.18 Variation of fully developed CO_3^{2-} concentration profiles with mean flow. T = 25 °C; pH = 4; P_{CO_2} = 0.1 MPa.

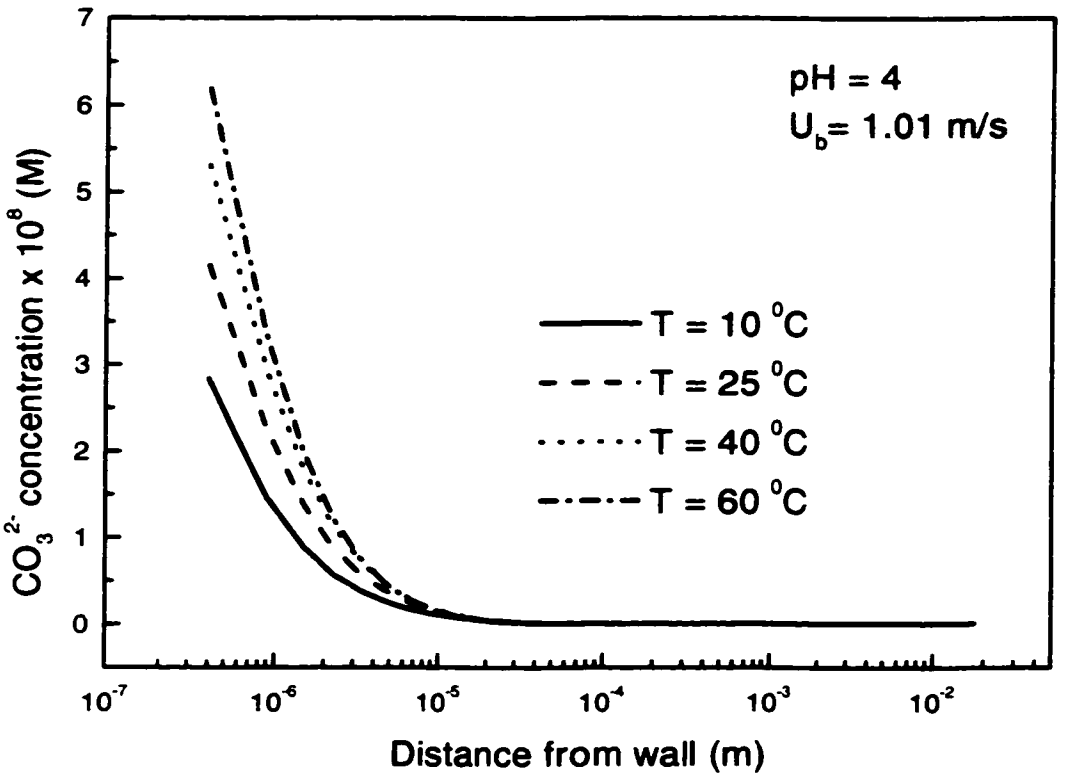

Figure 7.19 Variation of fully developed CO_3^{2-} concentration profiles with temperature. U_b = 1.01 m/s; pH = 4; P_{CO_2} = 0.1 MPa.

7.2.4 Cathodic Limiting Currents

Cathodic currents are generated at the surface through cathodic reactions such as the reduction of hydrogen ion and the reduction of carbonic acid. The carbonic acid is supplied to the surface by mass transport with generation of H_2CO_3 by CO_2 hydration along the mass transfer path.

7.2.4.1 H_2CO_3 Reduction

The H_2CO_3 reduction limiting current is shown as a function of mean flow velocity at 25 ^{0}C in Figure 7.20. For comparison, the diffusion limiting current, with no reaction, and chemical reaction limiting current are also plotted. The latter was calculated from the Vetter equation (Vetter, 1967). At very low velocities, the reduction current agrees well with that given by the Vetter equation which is valid for strictly stagnant solutions when the reaction layer is deep inside the diffusion layer. At higher velocities, the limiting current deviates increasingly from the chemical reaction limiting current. This suggests that at low velocities the reduction of carbonic acid is controlled by the slow chemical reaction of CO_2 hydration. At higher velocities, the diffusion layer becomes thinner and its thickness becomes comparable with that of the reaction layer, the H_2CO_3 reduction is controlled by the interaction of chemical reaction and diffusion. The contribution from diffusion increases with velocity. It is also shown that the

superposition of chemical reaction and diffusion is not the simple addition of the two. Figures 7.21-7.23 show the carbonic acid limiting current at other temperatures studied (10, 40 and 60 ^{0}C). The same pattern is observed.

This notion of mixed control by diffusion and chemical reaction is shared by Nesic *et al.* (1995) who have investigated experimentally the cathodic reactions in CO_2 corrosion. In order to account for the observed increase in H_2CO_3 limiting current with mean flow at higher velocities, they have proposed a "flow factor" to elucidate the effects of flow velocity (diffusion) on the limiting current by multiplying the limiting current with the flow factor (See Chapter 2). The comparison (Figure 7.24) indicates the present model predictions agree well with their results.

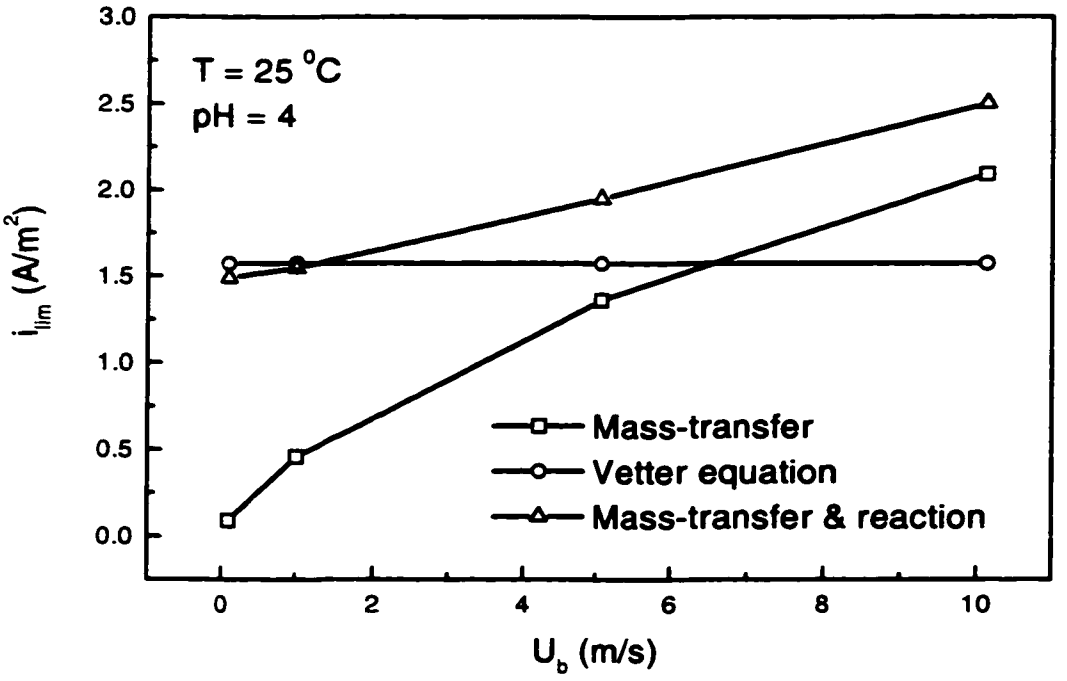

Figure 7.20 Carbonic acid reduction limiting current as a function of mean flow. $T = 25$ ^{0}C; $pH = 4$; $P_{CO_2} = 0.1$ MPa.

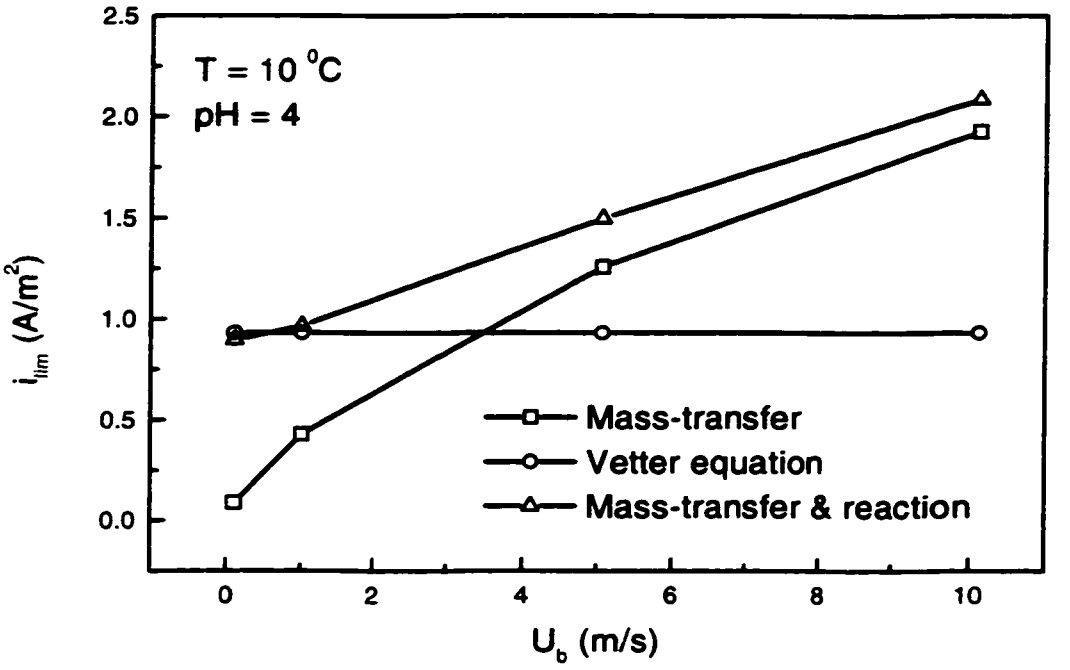

Figure 7.21 Carbonic acid reduction limiting current as a function of mean flow. T = 10 ^{0}C; pH = 4; P_{CO_2} = 0.1 MPa.

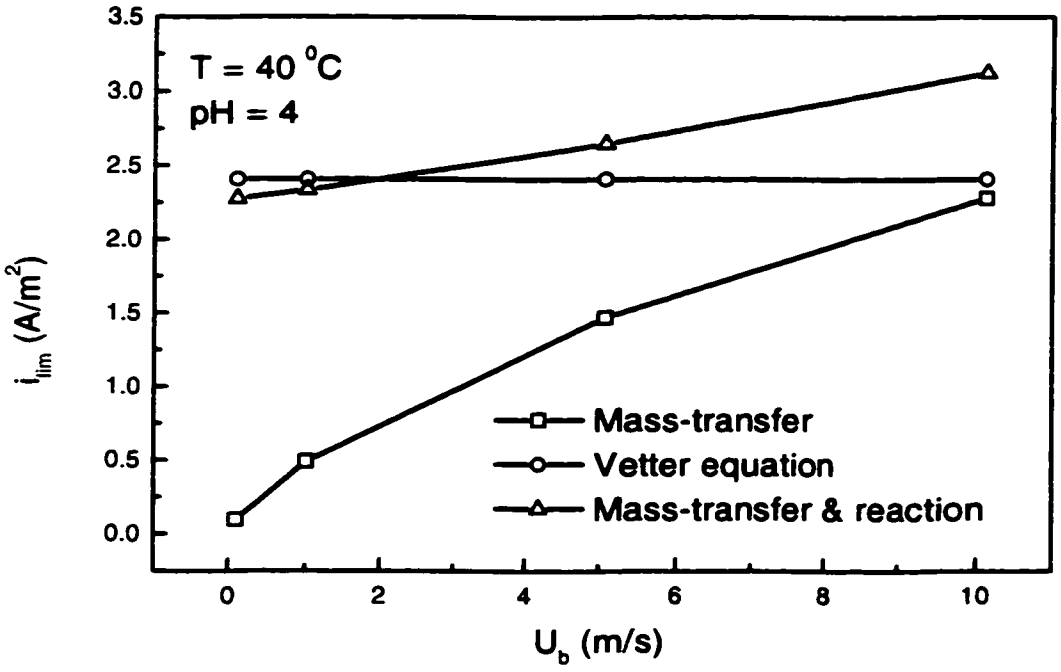

Figure 7.22 Carbonic acid reduction limiting current as a function of mean flow. $T = 40$ ^{0}C; $pH = 4$; $P_{CO_2} = 0.1$ MPa.

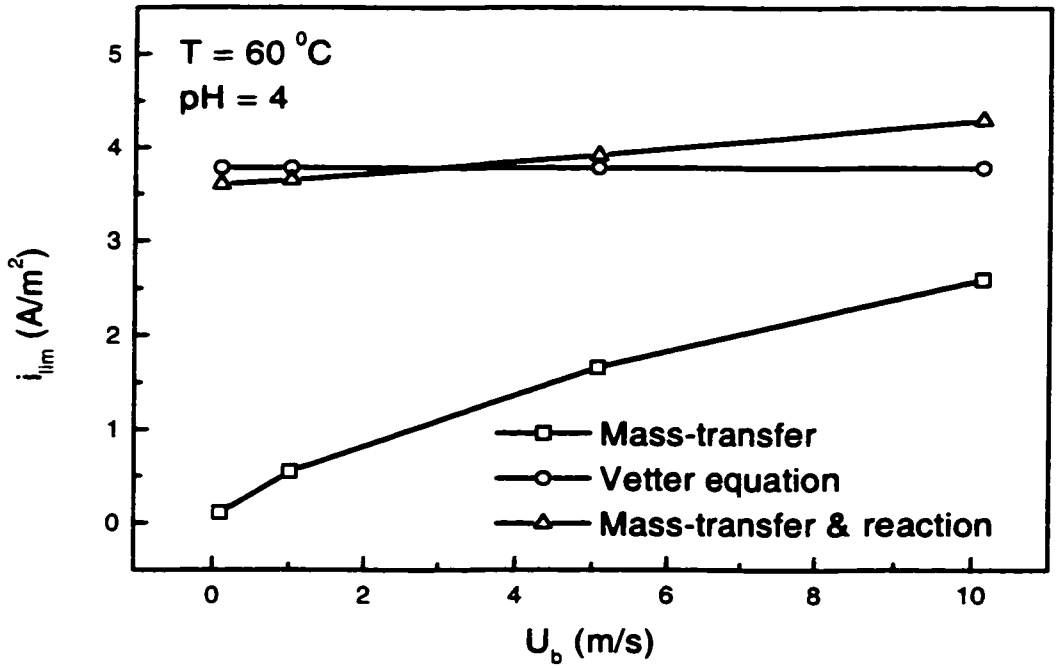

Figure 7.23 Carbonic acid reduction limiting current as a function of mean flow. $T = 60$ ^{0}C; $pH = 4$; $P_{CO_2} = 0.1$ MPa.

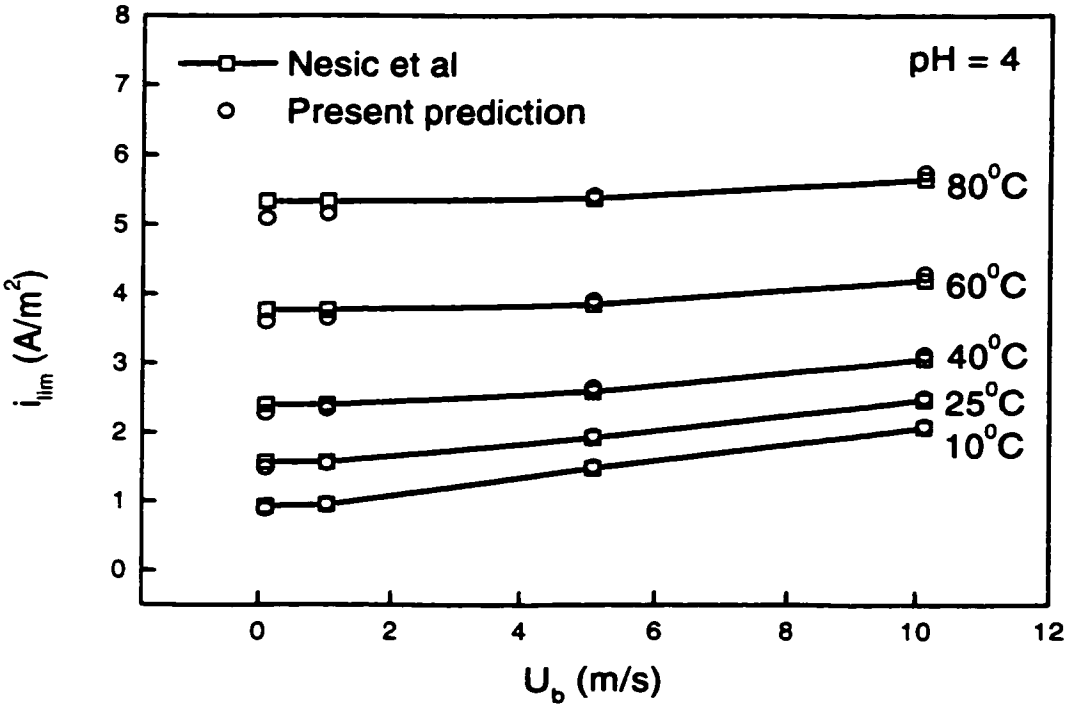

Figure 7.24 Comparison of model prediction with Nesic *et al.* (1995): H_2CO_3 reduction limiting current. $pH = 4$; $P_{CO_2} = 0.1$ MPa.

7.2.4.2 H^+ Reduction

The limiting current for the reduction of hydrogen ion is controlled by the transport of H^+ from the bulk solution to the surface. Figures 7.25 - 7.28 plot the H^+ reduction limiting currents at bulk pH 4 for four different temperatures (10, 25, 40, 60 ^{0}C). For comparison, the H_2CO_3 limiting current is also plotted, and so is the total cathodic current which will be discussed later on. It is seen from the graphs that H^+ limiting current increases with mean flow velocity which is to be expected since higher velocities, for a mass transfer controlled process, result in enhanced mass transfer and greater mass transport coefficients. It is also obvious from the graphs that the H^+ limiting current curves have far bigger slopes than the H_2CO_3 limiting current curves. Therefore it can be concluded that H^+ reduction is much more flow-sensitive than H_2CO_3 reduction.

7.2.4.3 Total Cathodic Limiting Current

The total cathodic limiting current is calculated by adding the H_2CO_3 limiting current to the H^+ limiting current. This is possible because the interactions between H+ and H_2CO_3 (and other species) throughout the boundary layer have been taken into account in the present study through chemical equilibria. Our model allows for all the relevant species to modify the concentration profiles of one another.

Figures 7.25 – 7.28 show that at pH 4, H^+ limiting current constitutes a substantial part of the total cathodic current except at very low velocities where H_2CO_3 limiting current is more important. Turgoose *et al.* (1990), in modelling a rotating disk system with a calculated pH value of 3.85 to 4.45, found that the relationship between the total limiting current and the square root of rotational speed is approximately linear only at relatively high rotational speeds; at low rotational speeds, the current stays nearly constant. This is in agreement with the present findings that at low velocities CO_2 corrosion is controlled by the slow chemical reaction of CO_2 hydration, and is controlled at higher velocities by H^+ diffusion and the interaction of chemical reaction and H_2CO_3 diffusion. It is noted that the model predictions of Turgoose *et al.* (1990) closely reproduced the experimental results obtained by Schmitt and Rothmann (1977).

Figure 7.29 compares the predicted cathodic limiting currents from this study with Eriksrud and Søntvedt (1984) experimental results. Excellent agreement is shown with the experimental results being over-predicted by less than 5%.

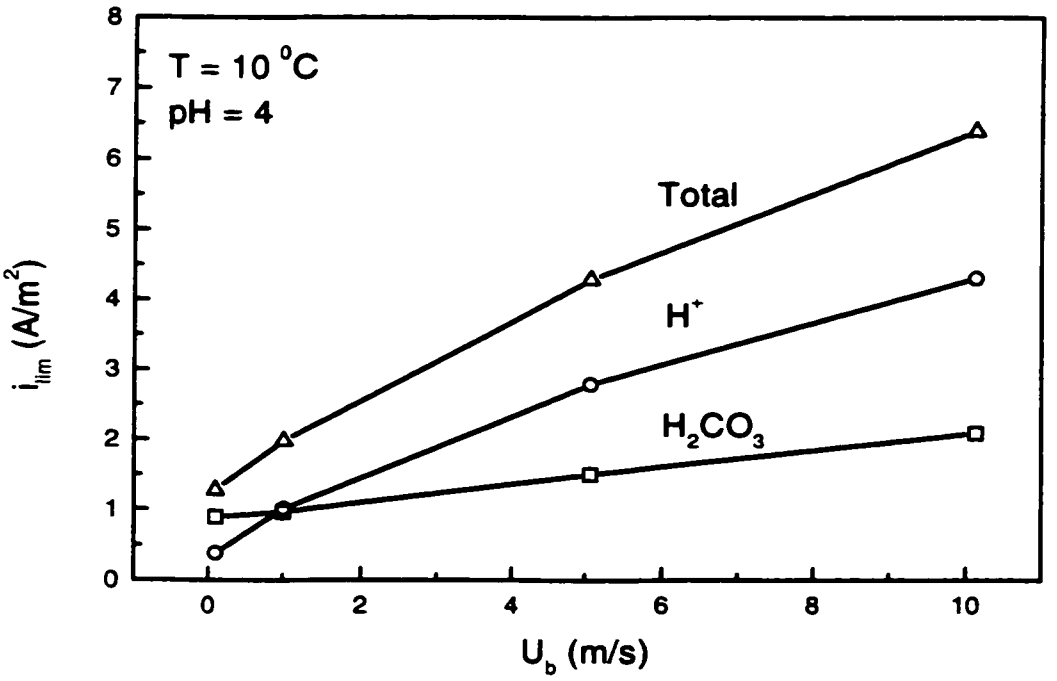

Figure 7.25 Cathodic limiting currents as a function of mean flow. T = 10 ^{0}C; pH = 4; P_{CO_2} = 0.1 MPa.

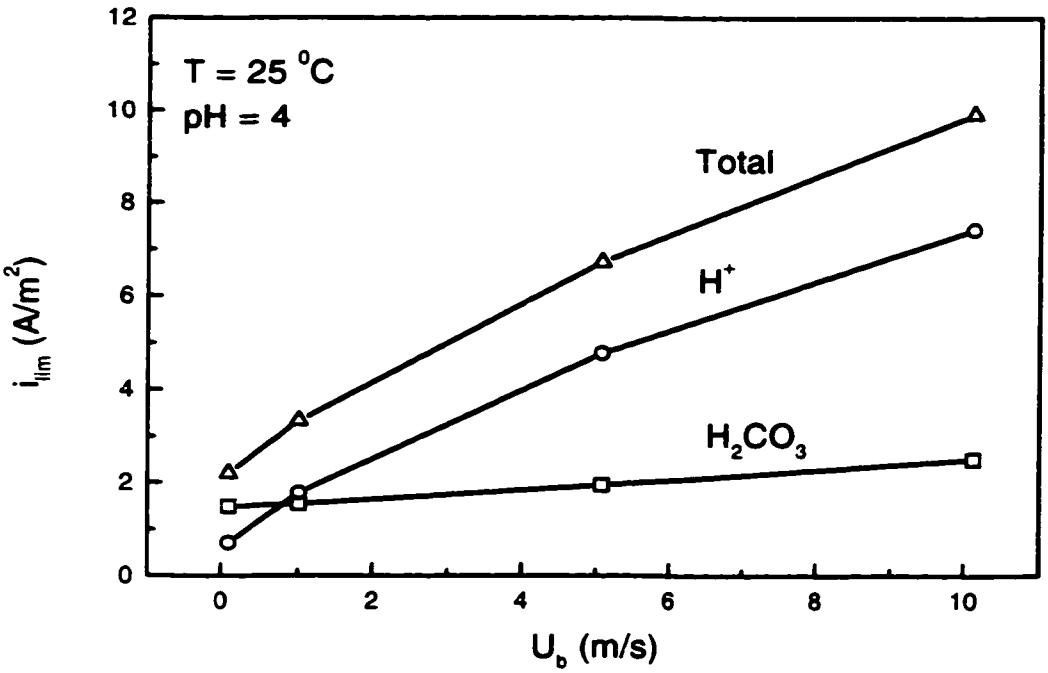

Figure 7.26 Cathodic limiting currents as a function of mean flow. T = 25 ^{0}C; pH = 4; P_{CO_2} = 0.1 MPa.

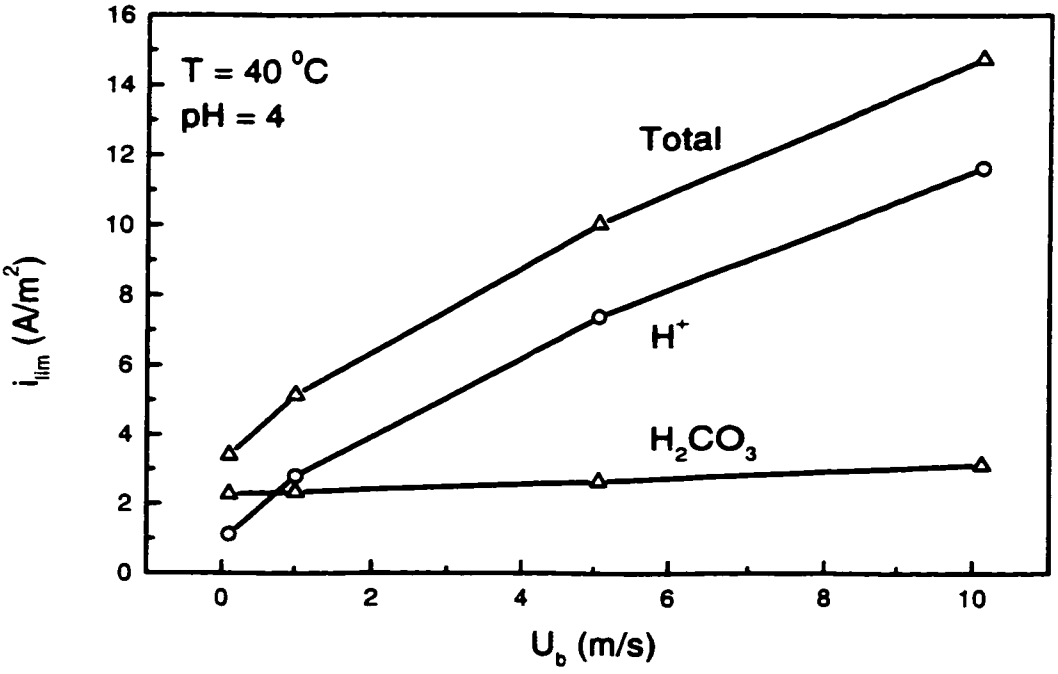

Figure 7.27 Cathodic limiting currents as a function of mean flow. T = 40 ^{0}C; pH = 4; P_{CO_2} = 0.1 MPa.

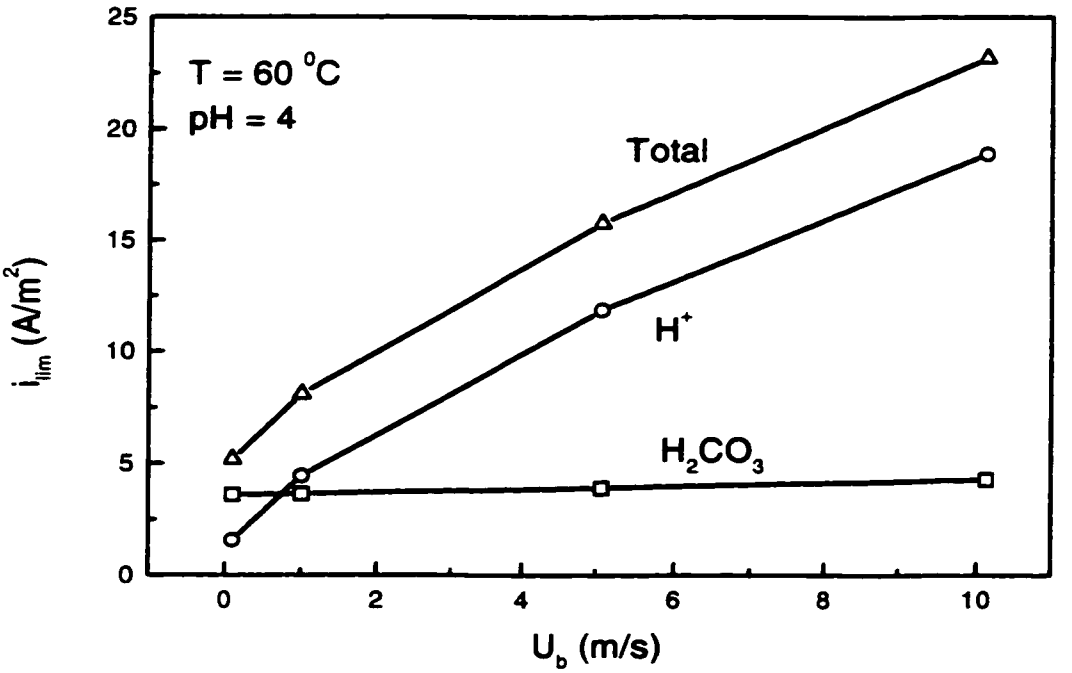

Figure 7.28 Cathodic limiting currents as a function of mean flow. T = 60 ^{0}C; pH = 4; P_{CO_2} = 0.1 MPa.

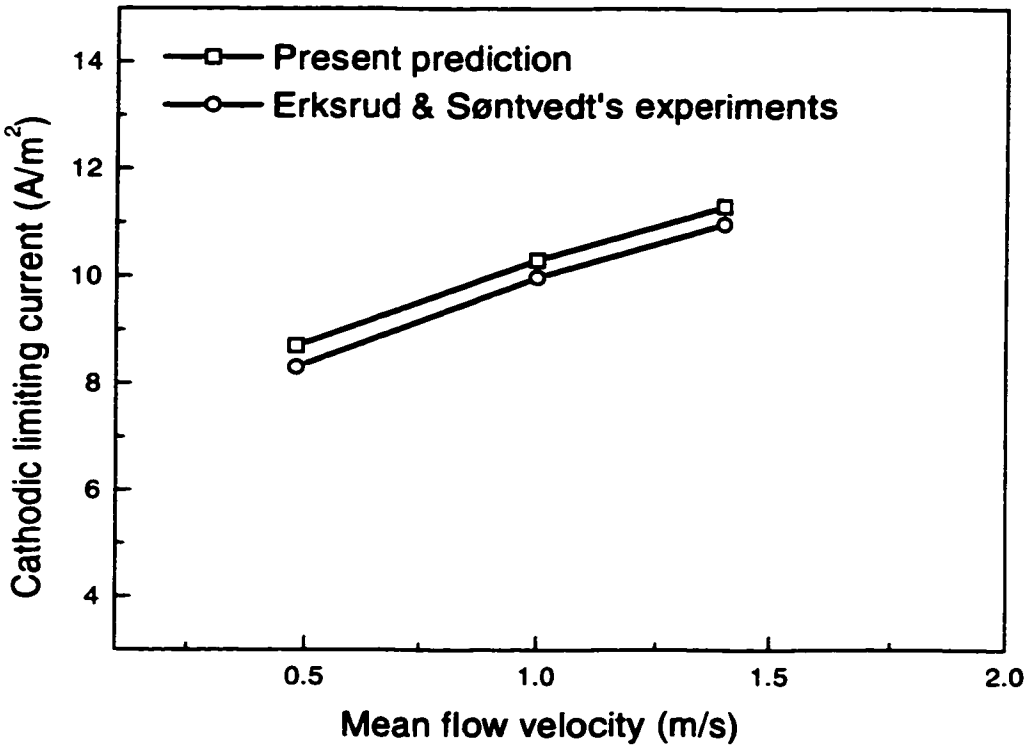

Figure 7.29 Comparison of model predictions with Eriksrud and Søntvedt (1984) experimental results. $T = 60\ ^{0}C$; $pH = 4$; $P_{CO_2} = 0.156$ MPa; No protective films present.

7.2.5 Effect of CO_2 Hydration on the Cathodic Reactions

As described earlier, the slow homogeneous chemical reaction of CO_2 hydration plays an important role in CO_2 corrosion. Carbonic acid is generated throughout the concentration boundary layer through CO_2 hydration. This, for H_2CO_3, is felt as having the same effect as enhancing mass transfer through conventional mass transport modes such as diffusion or convection. Since carbonic acid is an extra source of H^+ and both species are interconnected through rapid chemical equilibria, it is expected that the generation of carbonic acid will also impact the H^+ mass transport.

Figures 7.20 – 7.23 show that the generation of carbonic acid through the slow chemical reaction of CO_2 hydration increases the H_2CO_3 limiting current at all flow velocities though the effect is more remarkable at lower velocities. As shown in Figures 7.30 – 7.31, it also moderately increases the H^+ limiting current at relatively low velocities. At high velocities the impact is negligible because the enhanced mass transport at high velocities far outstrip the effect of CO_2 hydration.

The effect of CO_2 hydration can be looked at from another perspective – the species developing mass transfer boundary layer. As shown in Figure 7.32, generation of H_2CO_3 through the slow chemical reaction hastens the development of the mass transfer boundary layer and reduces the H_2CO_3 mass transfer entrance length. Mass transfer

entrance lengths are important when considering maximum corrosion rates that can occur when small patches of protective film are removed (Postlethwaite *et al.*, 1992). The fully developed value of H_2CO_3 mass transfer coefficient increases as a result of the carbonic acid generation through CO_2 hydration. For H^+ (Figure 7.33), the mass transfer entrance length is somewhat reduced and the fully developed mass transfer coefficient is also moderately increased under the given conditions.

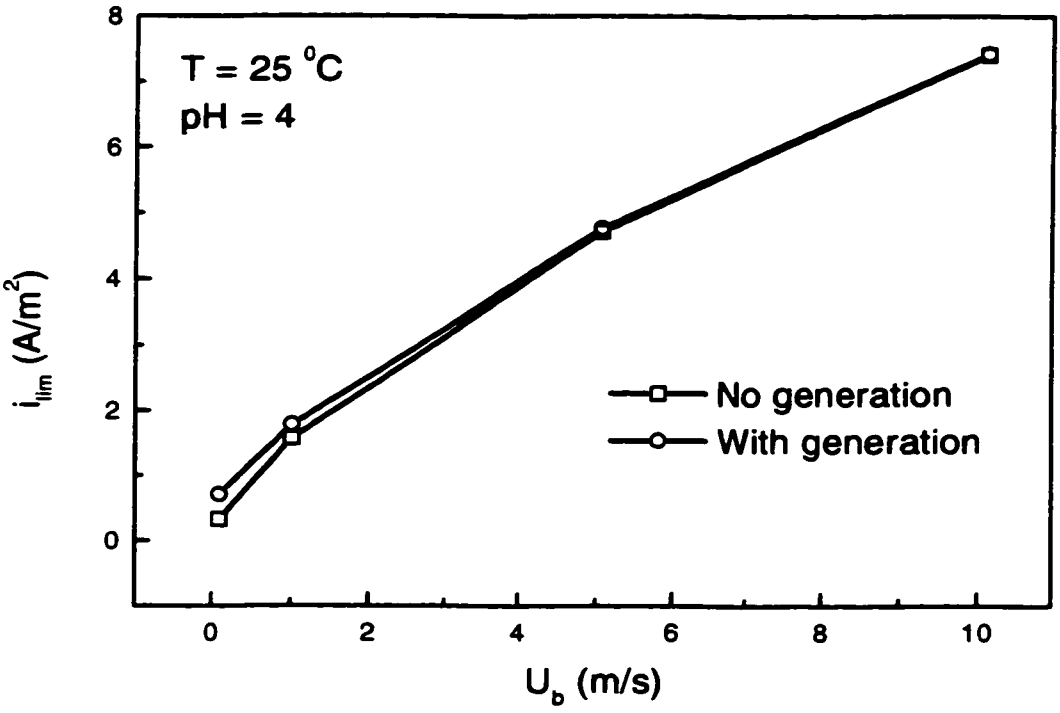

Figure 7.30 Effect of carbonic acid generation through CO_2 hydration on H^+ reduction limiting current. $T = 25\ ^0C$; $pH = 4$; $P_{CO_2} = 0.1$ MPa.

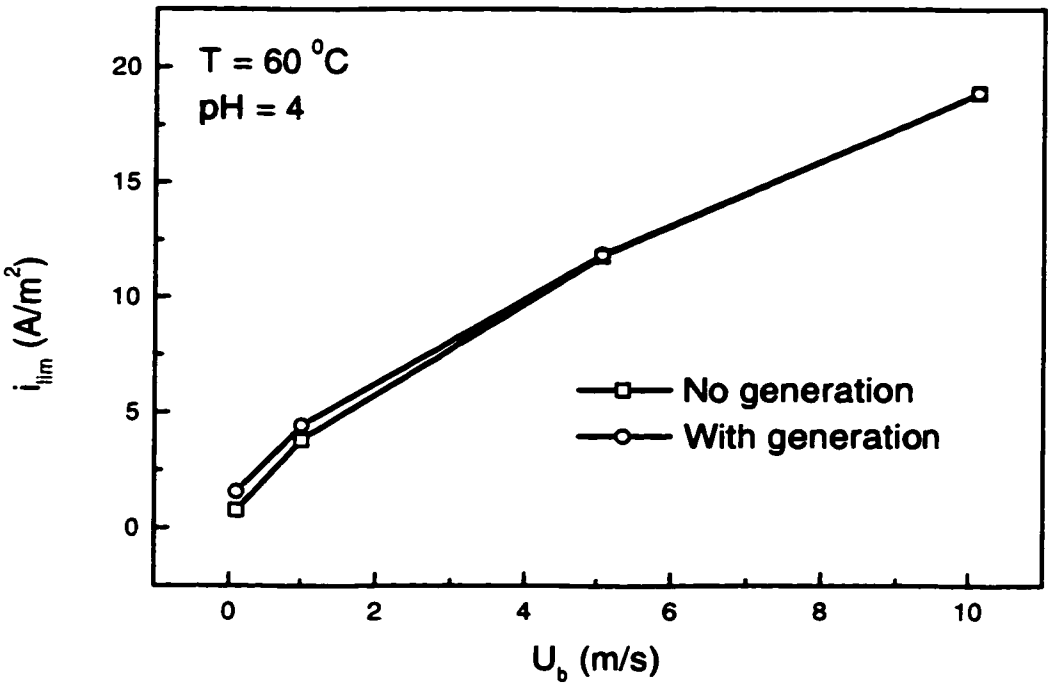

Figure 7.31 Effect of carbonic acid generation through CO_2 hydration on H^+ reduction limiting current. $T = 60\ ^0C$; $pH = 4$; $P_{CO_2} = 0.1$ MPa.

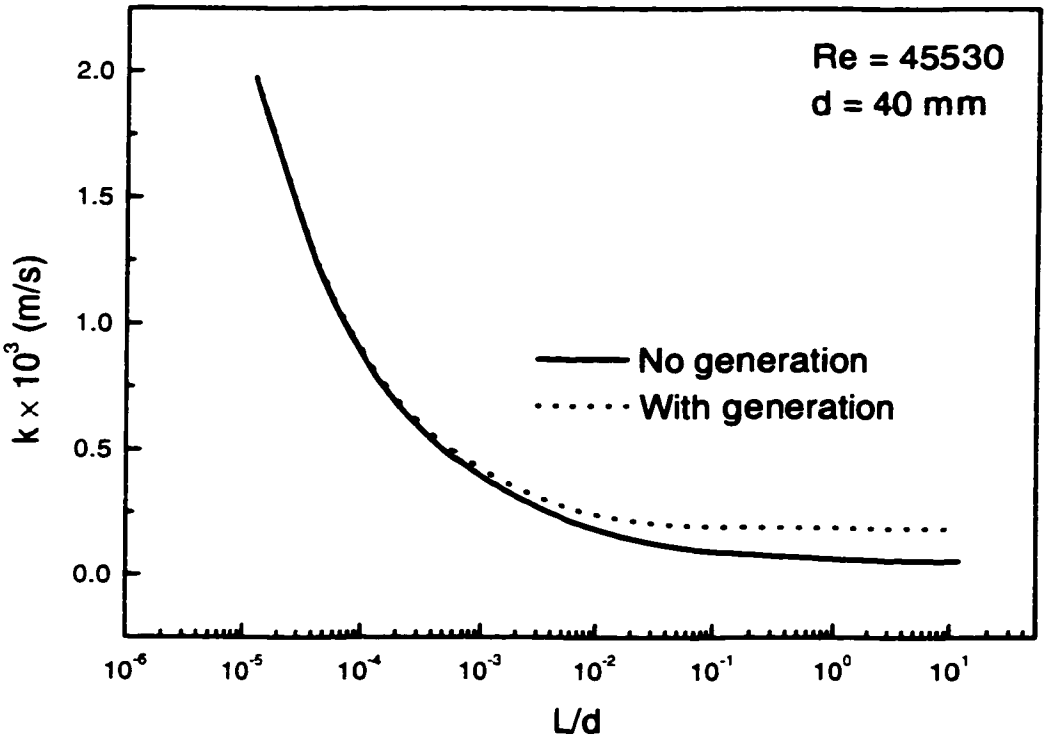

Figure 7.32 Variation of local H_2CO_3 mass transfer coefficient with L/d. $T = 25\ ^0C$; U_b = 1.01 m/s; $pH = 4$; $P_{CO_2} = 0.1$ MPa.

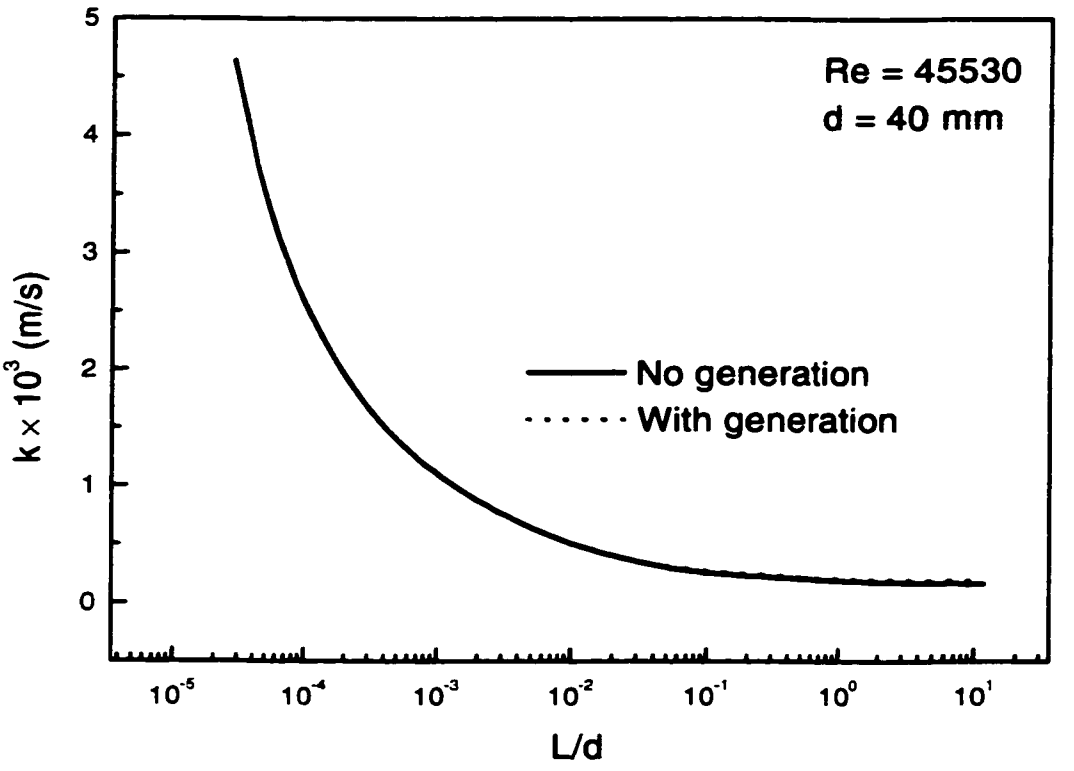

Figure 7.33 Variation of local H^+ mass transfer coefficient with *L/d*. T = 25 ^{0}C; U_b = 1.01 m/s; $pH = 4$; P_{CO_2} = 0.1 MPa.

7.3 Modelling of CO_2 Corrosion – A Numerical Model

7.3.1 Introduction

The ultimate goal of a corrosion model is to be able to predict corrosion rates under various conditions. In the previous section, the cathodic reactions are studied. In this section, the anodic reaction of iron dissolution is introduced in an attempt to calculate the corrosion rates and to present the complete numerical model.

The electrochemical reactions that are now dealt with are iron dissolution, reduction of carbonic acid, reduction of hydrogen ion, and reduction of water. Rapid solution chemical equilibria are preserved throughout the solution. As described in Chapter 6, an iterative procedure is employed to calculate the corrosion rate. The present model is capable of producing species concentration profiles from which kinetic corrosion diagrams can be constructed.

7.3.2 Concentration Profiles

7.3.2.1 Ferrous Ion

The concentration profiles of various dissolved species in the corrosion system are determined from the bulk solution to the corroding surface. Figure 7.34 shows the

ferrous ion profiles under four different flow velocities for 25 ^{0}C and pH 4. The bulk concentrations of Fe^{2+} ions are assumed to be 1×10^{-6} M. It is seen that within the concentration boundary layer, ferrous ion concentration increases towards the wall surface. The surface Fe^{2+} concentration varies from 1.46×10^{-3} M at 0.1 m/s to 4.23×10^{-4} M at 10.1 m/s. Surface ferrous ion concentrations at 25 ^{0}C and pH 6 (Figure 7.35) are lower than those at 25 ^{0}C and pH 4. The Fe^{2+} concentration profiles for other temperatures (10, 40, and 60 ^{0}C) are presented in Figures 7.36 – 7.38.

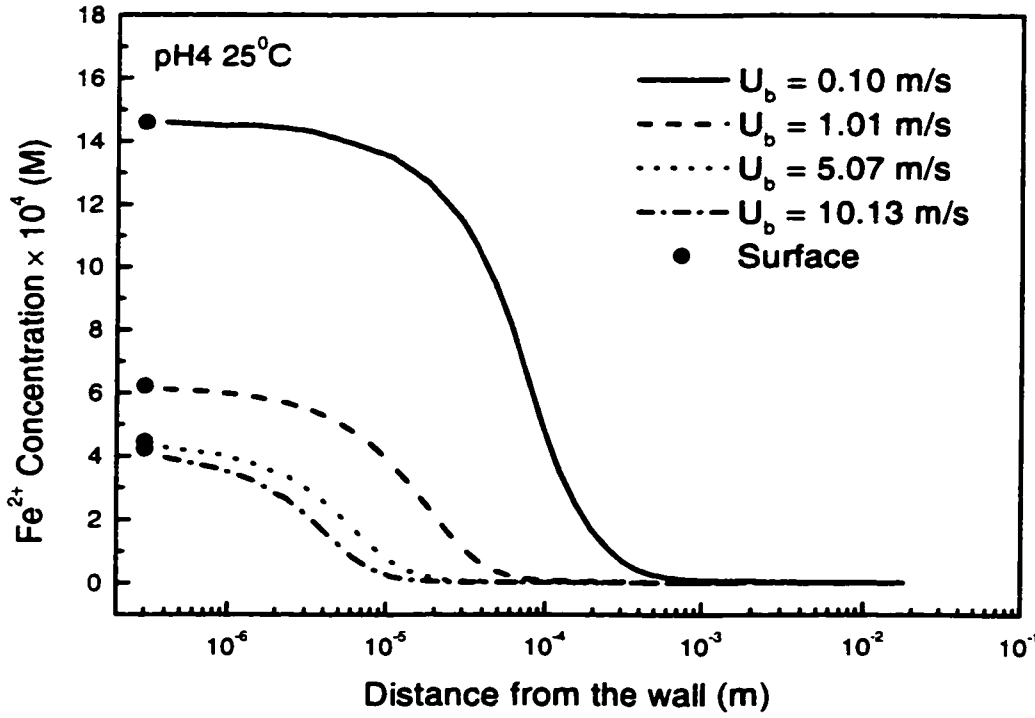

Figure 7.34 Ferrous ion concentration profiles as a function of mean flow. $pH = 4$; $T = 25\ ^0C$; $P_{CO_2} = 0.1$ MPa.

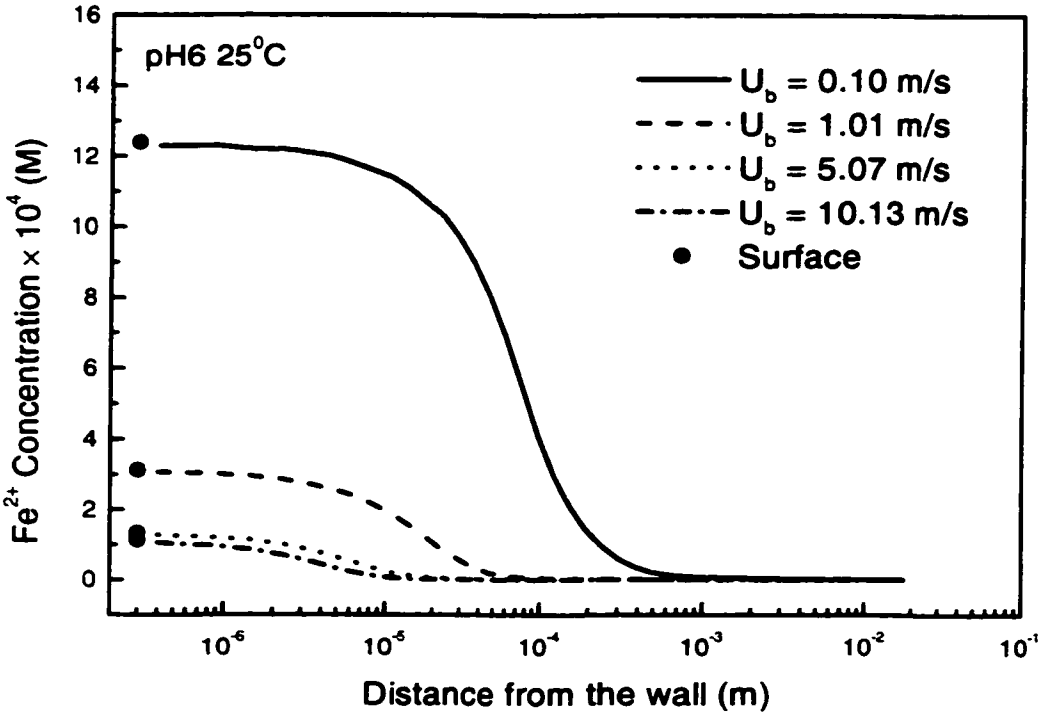

Figure 7.35 Ferrous ion concentration profiles as a function of mean flow. $pH = 6$; $T = 25\ ^0C$; $P_{CO_2} = 0.1$ MPa.

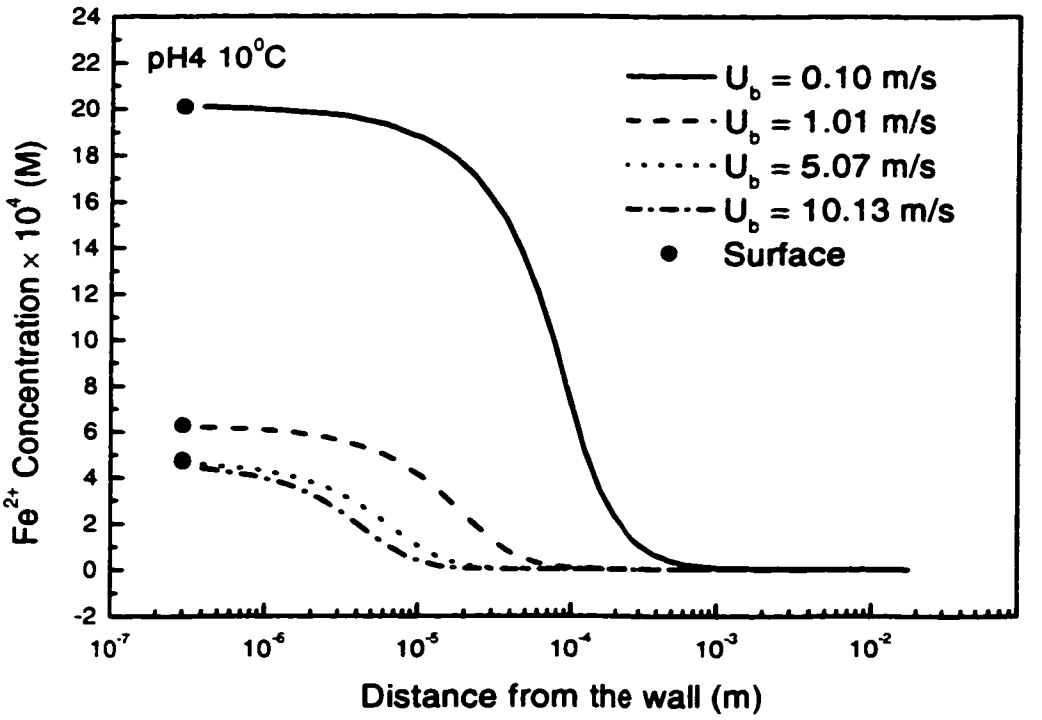

Figure 7.36 Ferrous ion concentration profiles as a function of mean flow. pH = 4; T = 10 ^{0}C; P_{CO_2} = 0.1 MPa.

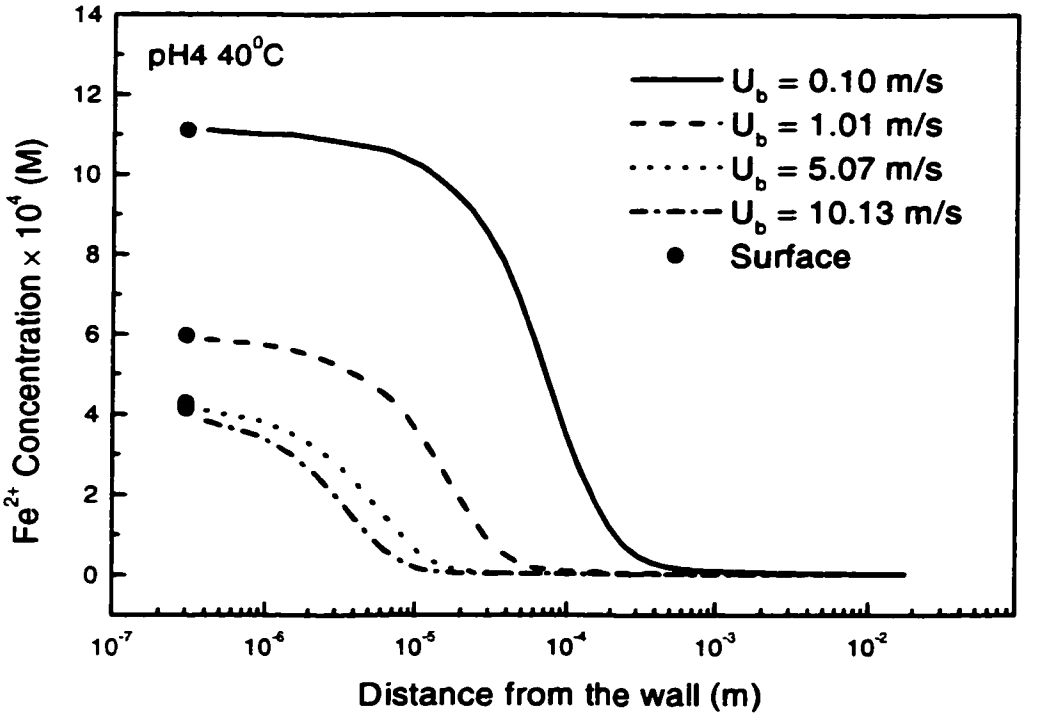

Figure 7.37 Ferrous ion concentration profiles as a function of mean flow. pH = 4; T = 40 ^{0}C; P_{CO_2} = 0.1 MPa.

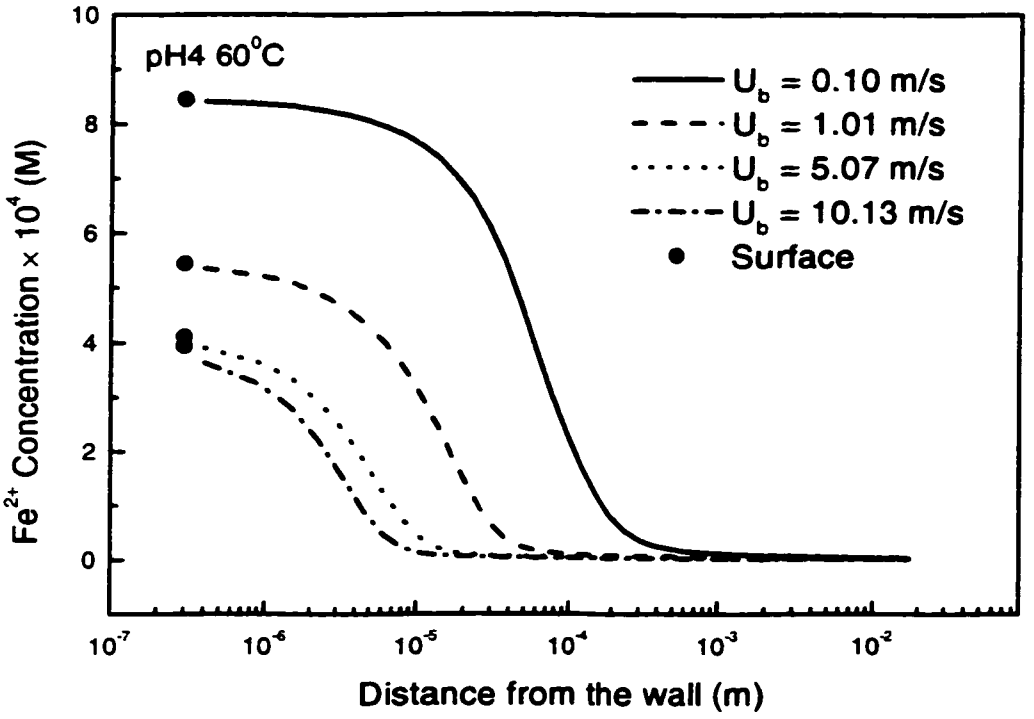

Figure 7.38 Ferrous ion concentration profiles as a function of mean flow. pH = 4; T = 60 ^{0}C; P_{CO_2} = 0.1 MPa.

7.3.2.2 Carbonate Species

The concentration profiles for different species (H_2CO_3, H^+, HCO_3^-, CO_3^{2-}, etc.) as differences between local and bulk concentrations for pH 4, 25 ^{0}C and U_b = 1.01 m/s are presented in Figure 7.39. Unlike ferrous ions which are produced at the wall surface, H_2CO_3 and H^+ are reduced (consumed) on the surface and their concentrations decrease towards the wall. Bicarbonate and carbonate species concentrations change as a result of the changes in carbonic acid and hydrogen ion concentrations. All the species concentration changes occur in a narrow region close to the wall. The corresponding concentration profiles for different pH (pH 6), temperatures (40 and 60 ^{0}C), and mean flow velocities (5.07 and 10.13 m/s) are also obtained and shown in Figures 7.40 – 7.44, respectively.

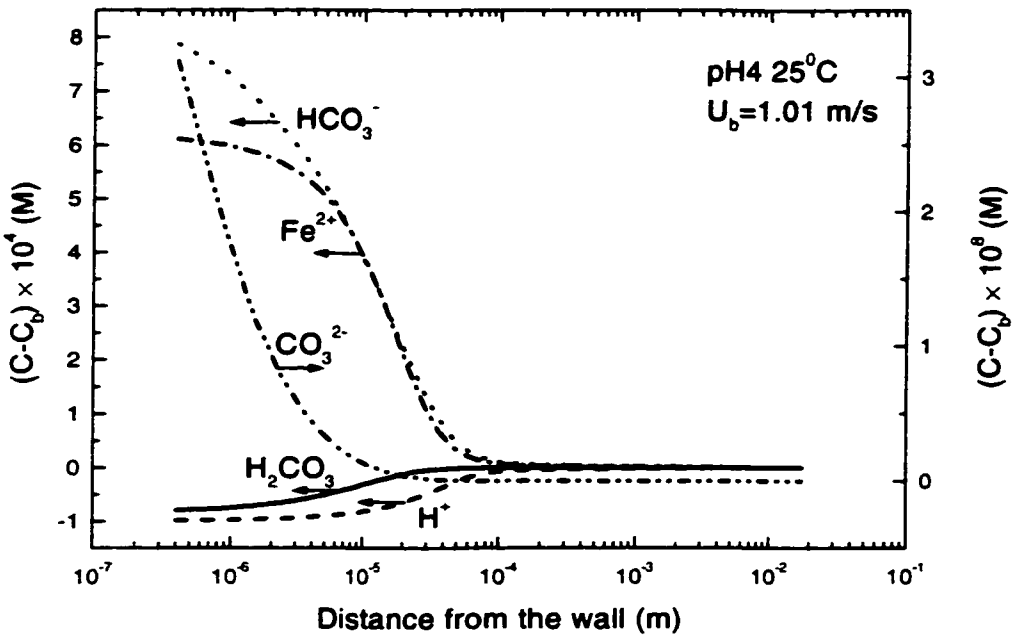

Figure 7.39 Concentration profiles of various species. $pH = 4$; $T = 25\ ^{0}C$; $U_b = 1.01$ m/s.

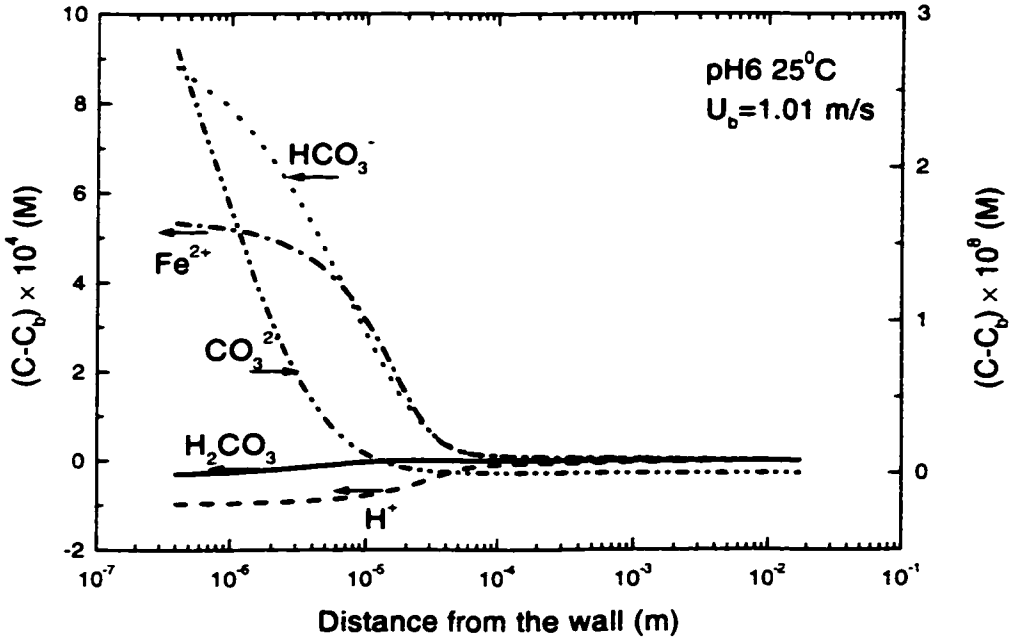

Figure 7.40 Concentration profiles of various species. $pH = 6$; $T = 25\ ^0C$; $U_b = 1.01$ m/s.

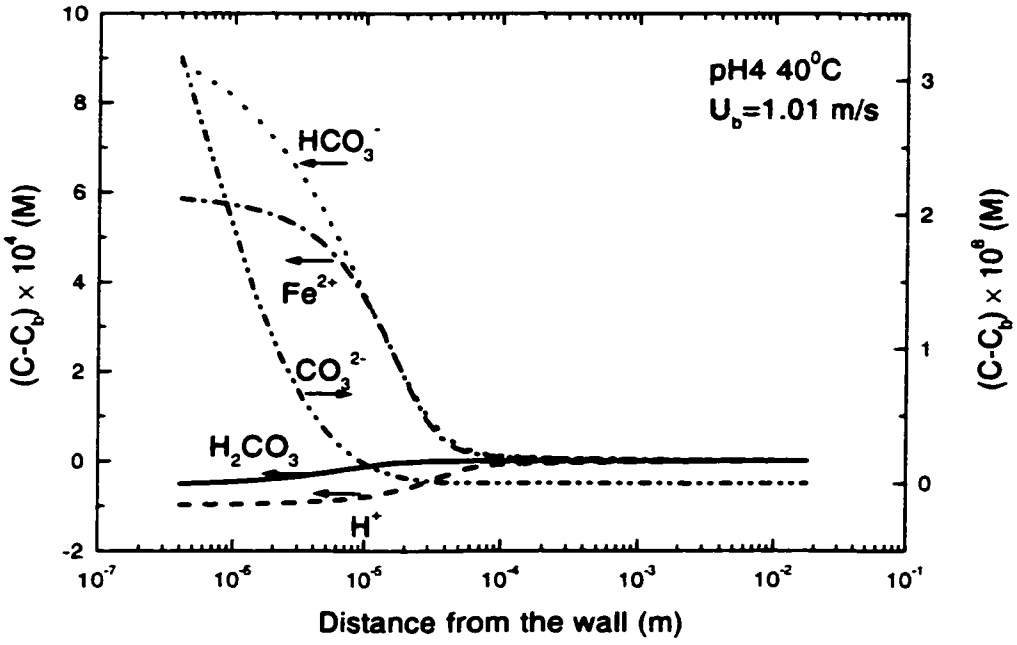

Figure 7.41 Concentration profiles of various species. $pH = 4$; $T = 40\ ^0$C; $U_b = 1.01$ m/s.

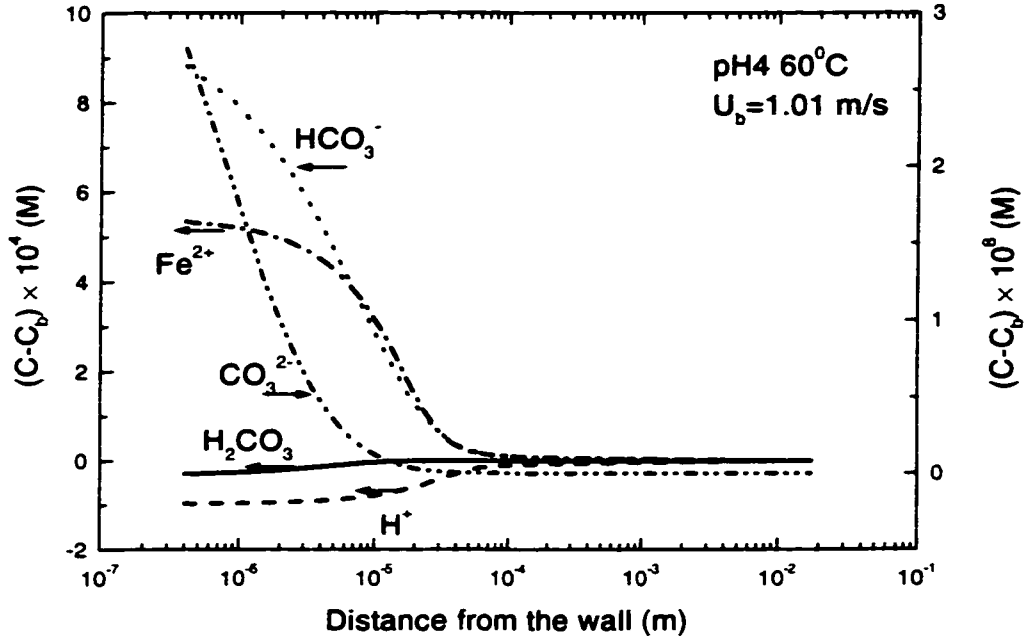

Figure 7.42 Concentration profiles of various species. $pH = 4$; $T = 60\ ^{0}C$; $U_b = 1.01$ m/s.

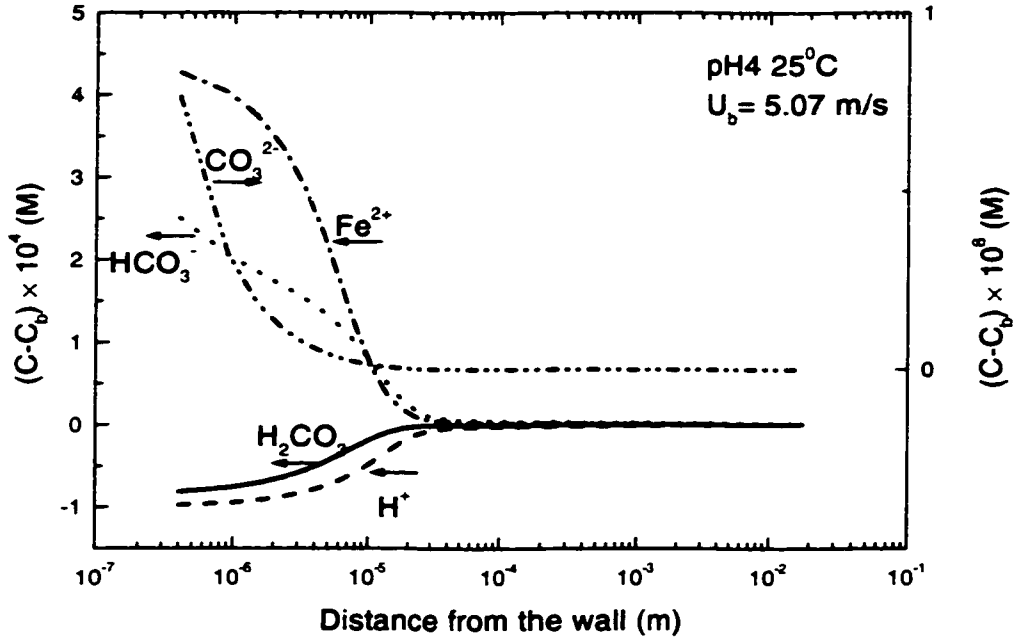

Figure 7.43 Concentration profiles of various species. $pH = 4$; $T = 25\ ^0C$; $U_b = 5.07$ m/s.

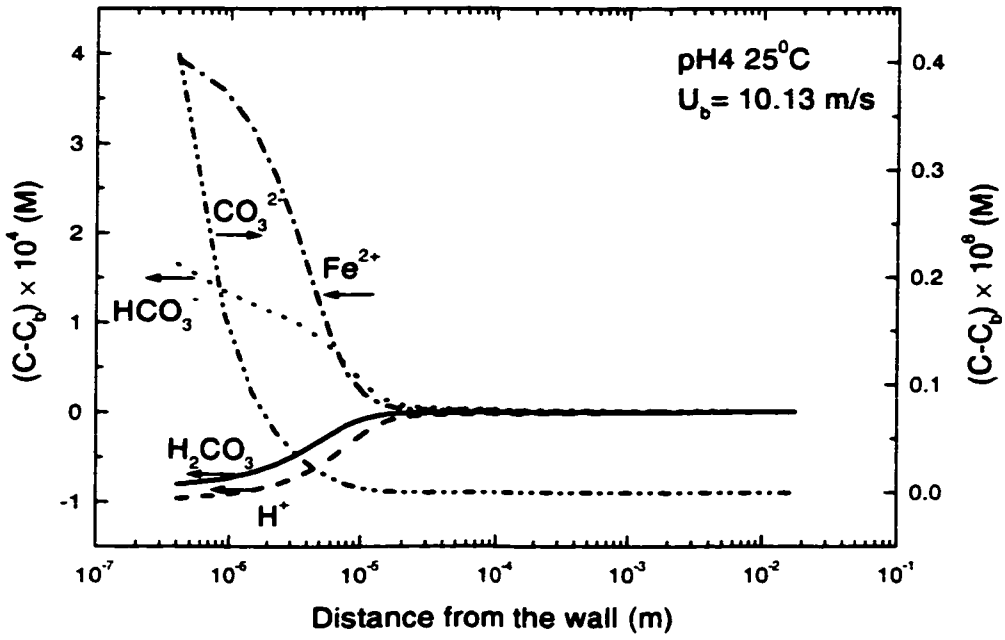

Figure 7.44 Concentration profiles of various species. pH = 4; T = 25 ^{0}C; U_b = 10.13 m/s.

7.3.3 Kinetic Corrosion Diagrams

Corrosion diagrams provide an effective and efficient way of understanding the corrosion phenomenon. Once the concentration profiles of the electroactive species have been obtained, corrosion diagrams can be constructed with the reversible potentials and exchange current densities determined from the surface concentrations of the reacting species.

Figures 7.45 and 7.46 show the corrosion diagrams for mean velocity of 1.01 m/s but under two different pH values, 4 and 6. In the plots, E_{corr} and i_{corr} are the corrosion potential and the corrosion current, respectively. It is seen that at pH 4, the contribution of the H^+ reduction to the total cathodic current is comparable to that of the H_2CO_3 reduction. The effect of water reduction is negligible. At pH 6, however, the H_2CO_3 reduction is the dominant cathodic reaction due to the limited availability of H^+ ions. Also the contribution of water reduction is insignificant compared to that of carbonic acid reduction.

It is seen from Figure 7.45 that at 1.01 m/s, the contribution of H_2CO_3 reduction to the total cathodic current is greater than that of H^+ reduction. This is not the case at higher velocities as illustrated in Figure 7.47 which gives the corrosion diagrams for U_b = 5.07 m/s, pH 4 and 25 ^{0}C. Because of the fact that H^+ reduction is much more flow-

dependent than carbonic acid reduction, higher velocities result in higher H^+ contribution to the cathodic current.

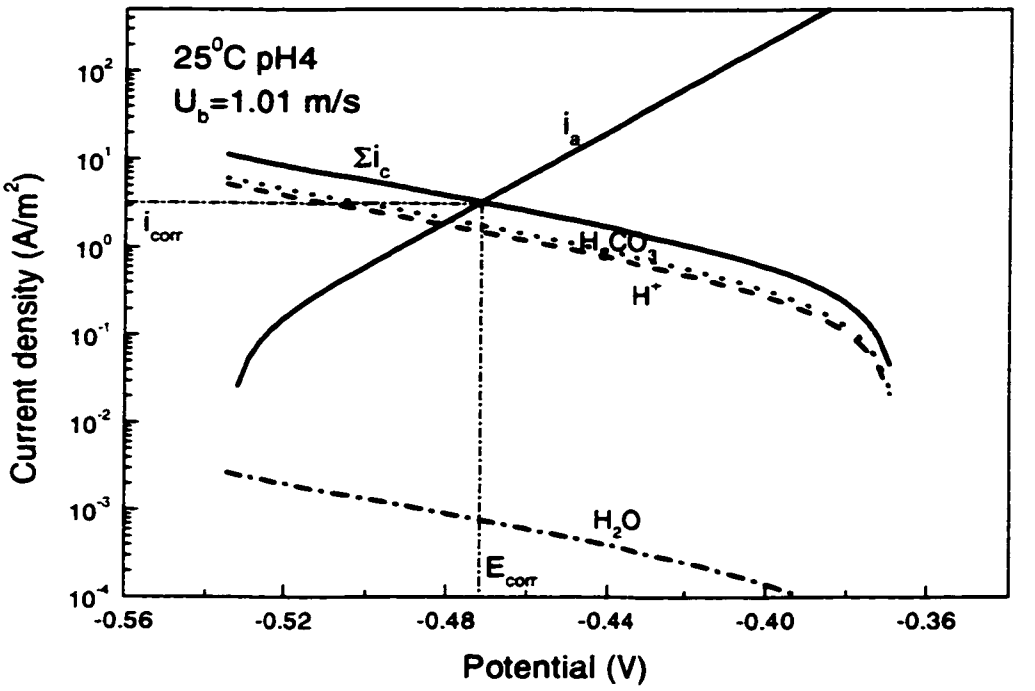

Figure 7.45 Corrosion diagram for bulk $pH = 4$, $U_b = 1.01$ m/s and 25 ^{0}C. Calculations based on surface concentrations.

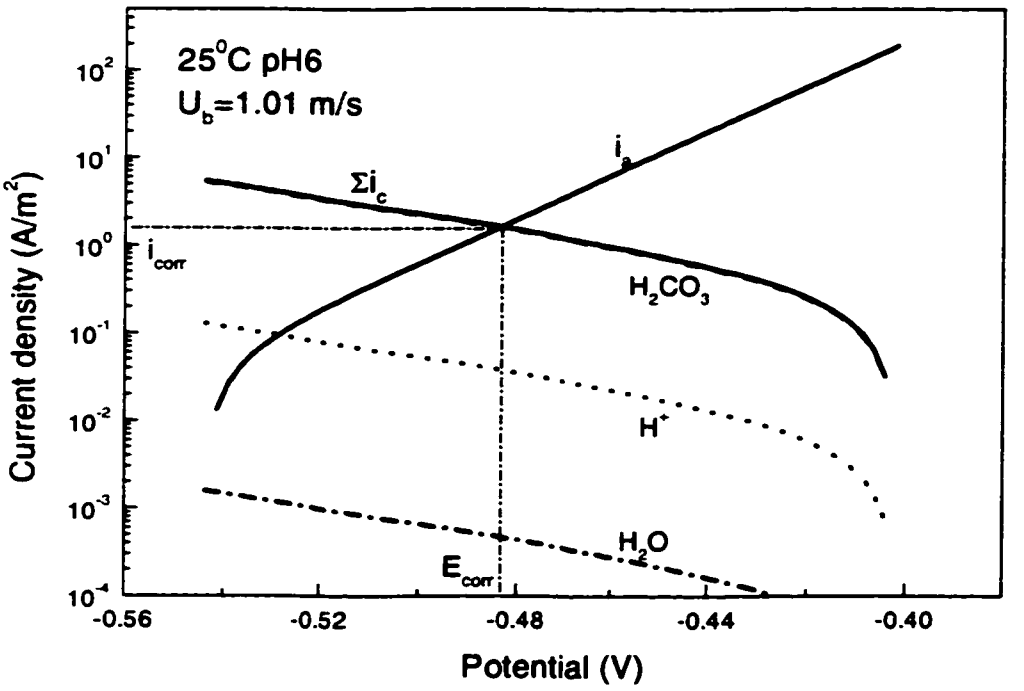

Figure 7.46 Corrosion diagram for bulk $pH = 6$, $U_b = 1.01$ m/s and 25 ^{0}C. Calculations based on surface concentrations.

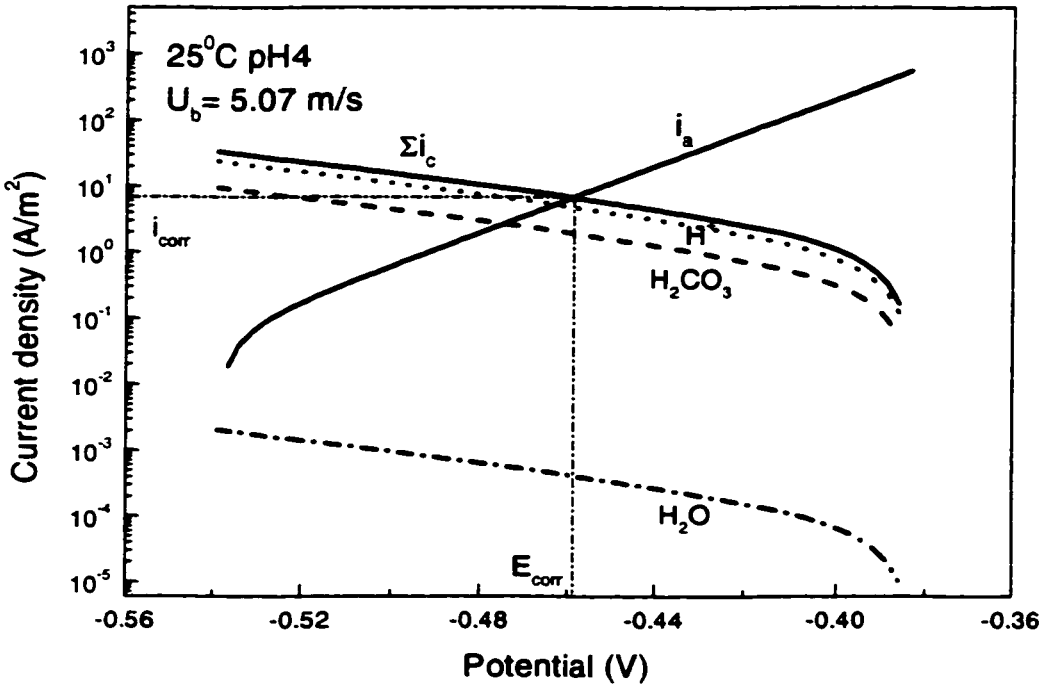

Figure 7.47 Corrosion diagram for bulk $pH = 4$, $U_b = 5.07$ m/s and 25 ^{0}C. Calculations based on surface concentrations.

7.3.4 Parametric Studies

7.3.4.1 Flow and pH

For corrosion without protective films present, turbulent flow is normally regarded to act through its influence on mass transfer. The corrosion rate should be accelerated by flow as expressed below:

$$Corrosion\ rate = C \times (flow\ rate)^n \tag{7.1}$$

The value of the exponent, n, depends on the corrosion mechanism. It is 0.8 for a convective diffusion controlled transport in a smooth tube with developed flow in the turbulent region (Manner and Heitz, 1978). In CO_2 corrosion, the flow acceleration effect can be attributed to the flow-sensitive nature of the cathodic reactions. The reduction of H^+ is very flow sensitive at the low H^+ concentrations found in carbonic acid corrosion. The reduction of carbonic acid is under mixed homogeneous-chemical-reaction and mass transfer (diffusion) control and is less flow-sensitive than the H^+ reduction reaction (Nesic *et al.*, 1995).

Figure 7.48 presents the CO_2 corrosion rate versus mean flow velocity in a double logarithmic plot for 25 ^{0}C and 0.1 MPa CO_2 and two different pH values. At pH 4 the exponent, n, has a value of about 0.4. This indicates that the corrosion rate is not

purely mass transport controlled. This is not surprising given the fact that the H_2CO_3 reduction reaction is partially chemical-reaction controlled and that electrochemistry also plays an important role in the corrosion process. This finding is in excellent agreement with Videm and Dugstad (1989) who experimentally found an exponent value of 0.4 on steel St. 52 for pH 4 and 90 ^{0}C when no protective films were present. Protective surface films (scales) are not taken into account in this study. While films do form at low temperatures (below 60^{0}C), it is known that such surface films are not protective (Videm and Dugstad, 1988; Dugstad, 1992).

It can be seen from Figure 7.48 that at pH 6, the exponent n is even smaller. This indicates a smaller flow effect. As shown earlier in the corrosion diagrams, both H^+ and H_2CO_3 reductions are important at pH 4; whereas, at pH 6, H_2CO_3 reduction is the dominant cathodic reaction. Given the fact that H^+ reduction is far more flow sensitive than H_2CO_3 reduction, a stronger flow effect is expected at lower pH values.

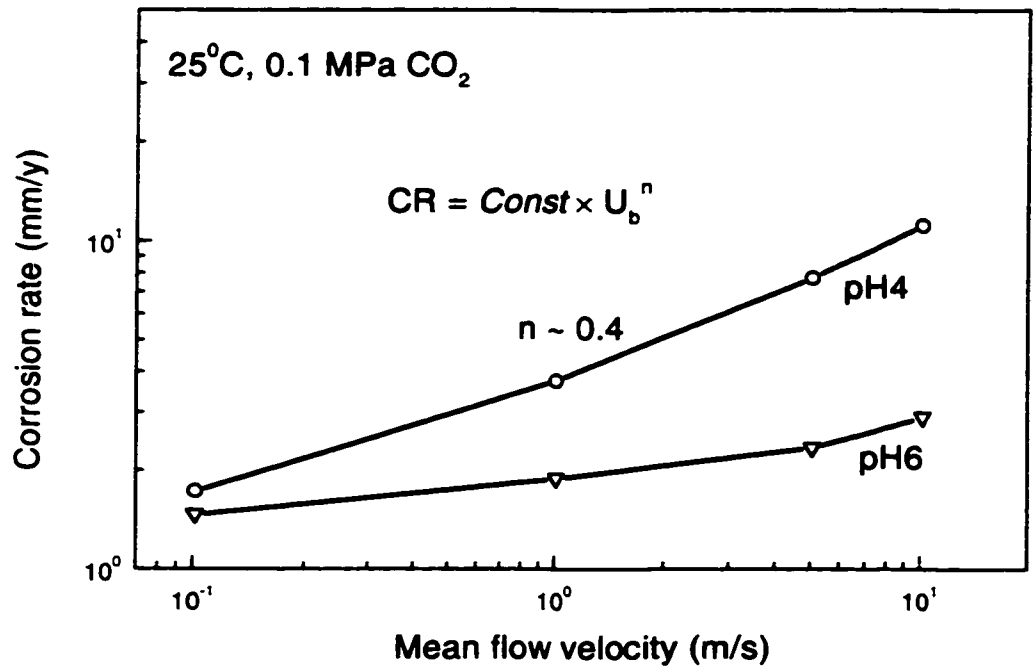

Figure 7.48 Variation of CO_2 corrosion rate with mean flow at bulk pH 4 and 6. $T = 25$ ^{0}C; $P_{CO_2} = 0.1$ MPa.

7.3.4.2 CO_2 Partial Pressure

Corrosion rates are dependent on the CO_2 partial pressure. The widely referenced de Waard-Lotz (1993) equation correlates the two with the following expression:

$$\log(Vcor) = 5.8 - \frac{1710}{273+t} + 0.67\log(P_{CO_2}) \tag{7.2}$$

where Vcor is the corrosion rate in mm/y and P_{CO_2} is the CO_2 partial pressure in bar (10^5 Pa). The equation indicates that when other conditions remain constant, log(Vcor) is proportional to $\log(P_{CO_2})$ and the proportionality factor is 0.67. It was found experimentally that CO_2 corrosion rate increases with CO_2 partial pressure by a power of 0.5 to 0.8 (e.g., Videm and Dugstad, 1989; Ikeda *et al.*, 1983; Schmitt, 1983). Figure 7.49 shows the predicted CO_2 corrosion rates with CO_2 partial pressure in a double logarithmic plot. A straight line is obtained with a slope of 0.7. The value of the slope falls between the experimental values and it agrees well with the de Waard-Lotz equation.

7.3.4.3 Temperature

Corrosion rates generally increase with increasing temperatures when no protective surface films are present. Figure 7.50 shows the corrosion rate in logarithmic scale versus 1/T. A straight line is obtained and the slope is about −1041. This value is

the same order of magnitude as −1710 which is proposed in the de Waard-Lotz (1993) equation.

It should be pointed out that because of the nature of mass transfer, experimental limiting currents can be predicted satisfactorily. However, this is not true of sub-limiting conditions where corrosion currents are controlled by both mass transport and electrochemistry. While it would be desirable to compare experimental corrosion rates values with model predictions, the extreme variability of exchange current densities and their heavy dependence on the state of the surface in question makes the task difficult. Under such conditions experimental exchange current densities for the system under study are required. Literature values should be used only for parameter studies.

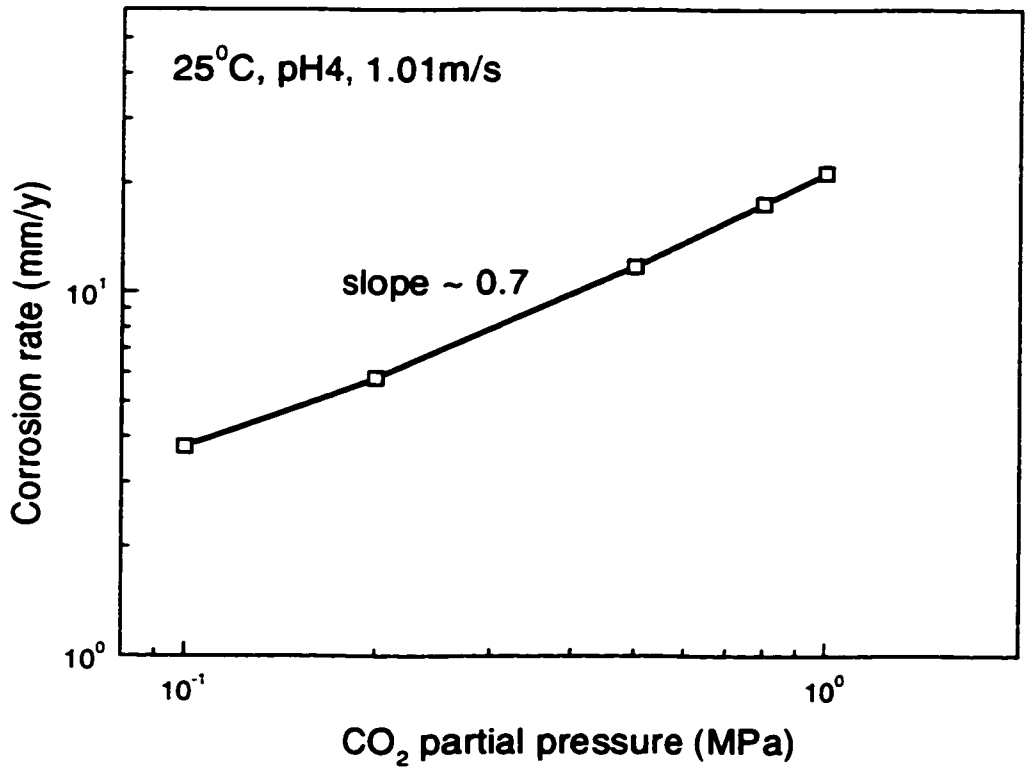

Figure 7.49 Variation of CO_2 corrosion rate with CO_2 partial pressure. $pH = 4$; $T = 25\ ^0C$; $U_b = 1.01$ m/s.

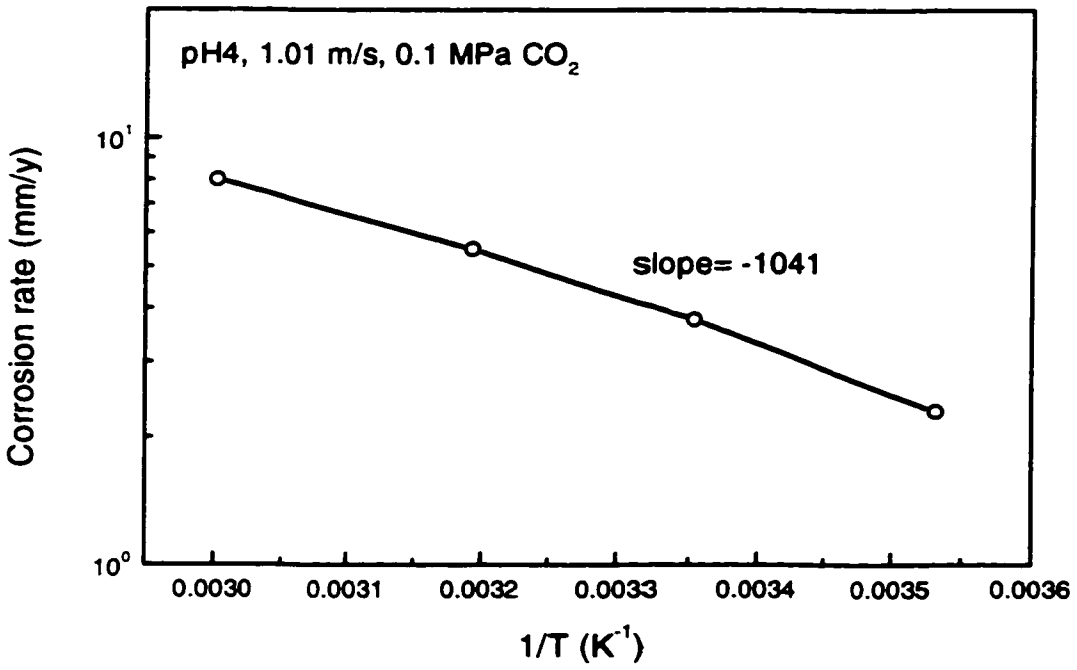

Figure 7.50 Variation of CO_2 corrosion rate with the inverse of temperature (1/T). pH = 4; U_b = 1.01 m/s; P_{CO_2} = 0.1 MPa.

7.3.5 Species Mass Transfer Boundary Layers

The predicted transport coefficients, the effective viscosity, μ_{eff}, and the effective diffusivity, D_{eff}, for the three species Fe^{2+}, H_2CO_3 and H^+ are shown in Figures 7.51 – 7.53 for 25 ^{0}C and U_b = 1.01 m/s. The corresponding Reynolds number is 45530 and the Schmidt numbers are 1251, 445, and 96 for Fe^{2+}, H_2CO_3 and H^+, respectively. It is observed that far from the wall, the effective viscosity is far greater than the molecular value. For example, at 1 mm from the wall, the effective viscosity is about 22 times greater than the molecular viscosity. This indicates that the flow is dominated by turbulent transport. As the wall is approached, the value of the effective viscosity becomes comparable to the value of the molecular viscosity indicating that the turbulence is gradually being damped. At about 50 μm from the wall, the value of the effective viscosity is almost equal to the molecular viscosity. This is the edge of the viscous sublayer. In the wall region of viscous sublayer, flow is controlled by viscous forces.

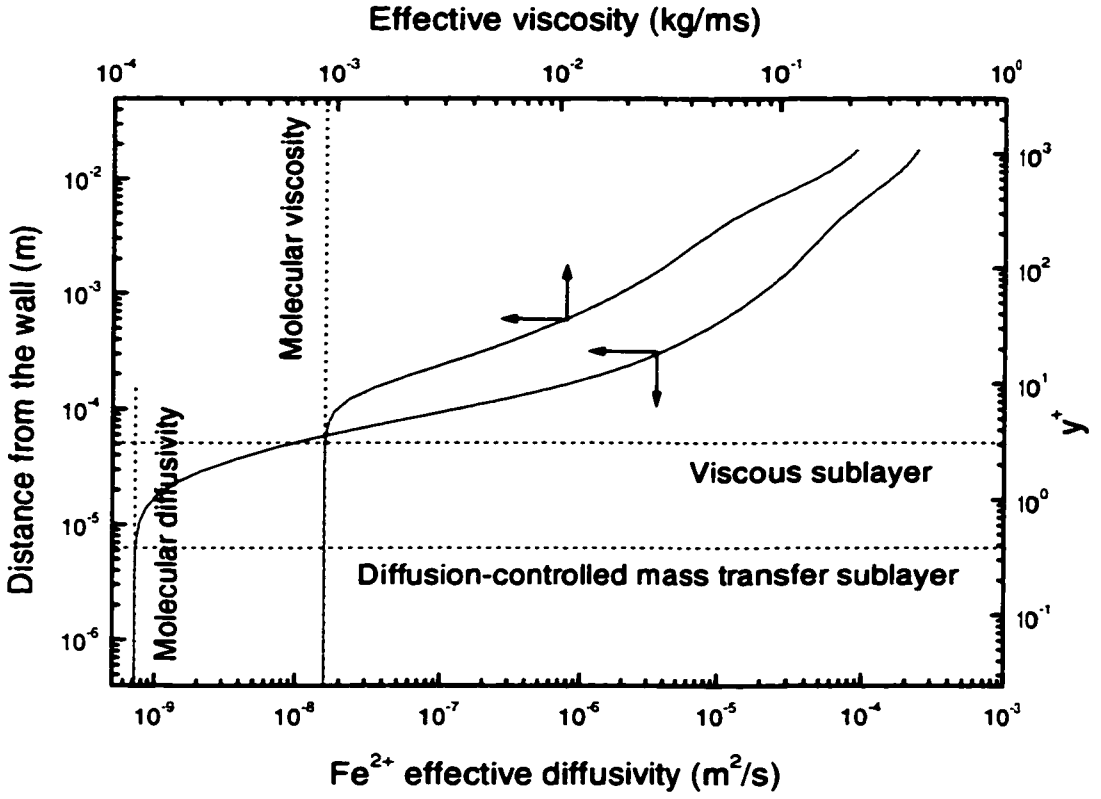

Figure 7.51 Variation of Fe^{2+} transport coefficients with distance from the wall. U_b = 1.01 m/s; T = 25 ^{0}C; Re = 45530; Sc = 1251; d = 40 mm.

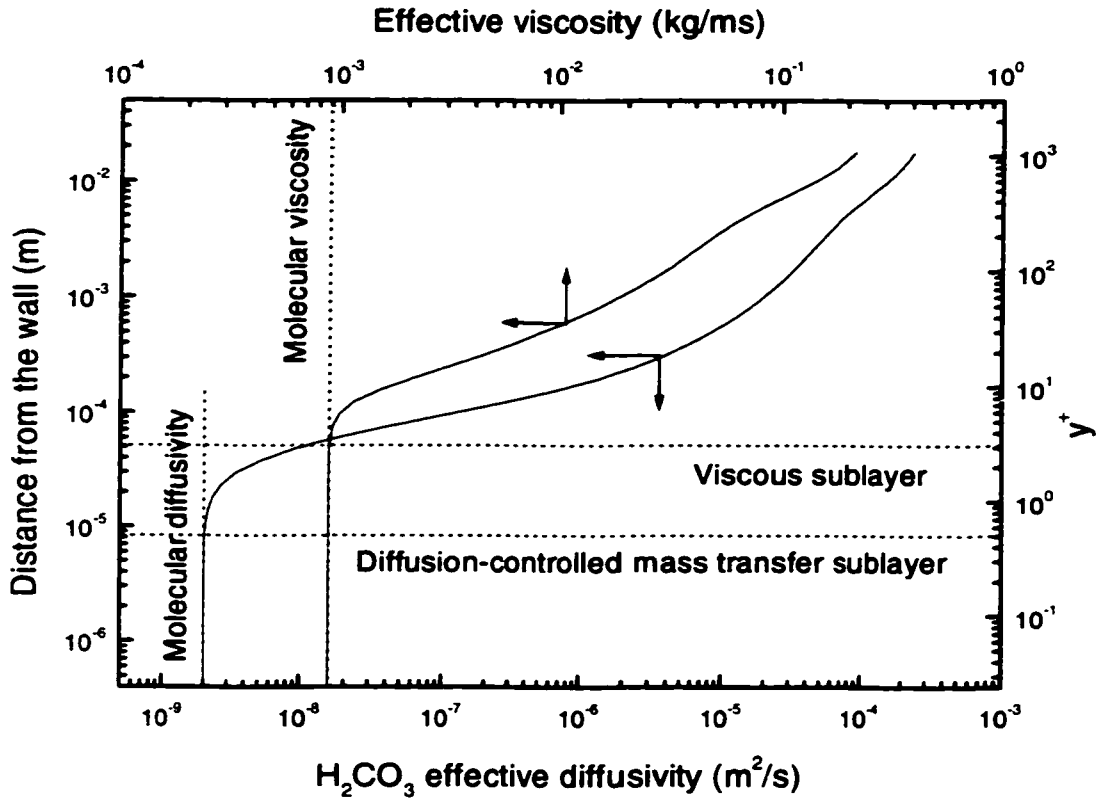

Figure 7.52 Variation of H_2CO_3 transport coefficients with distance from the wall. U_b = 1.01 m/s; T = 25 ^{0}C; Re = 45530; Sc = 445; d = 40 mm.

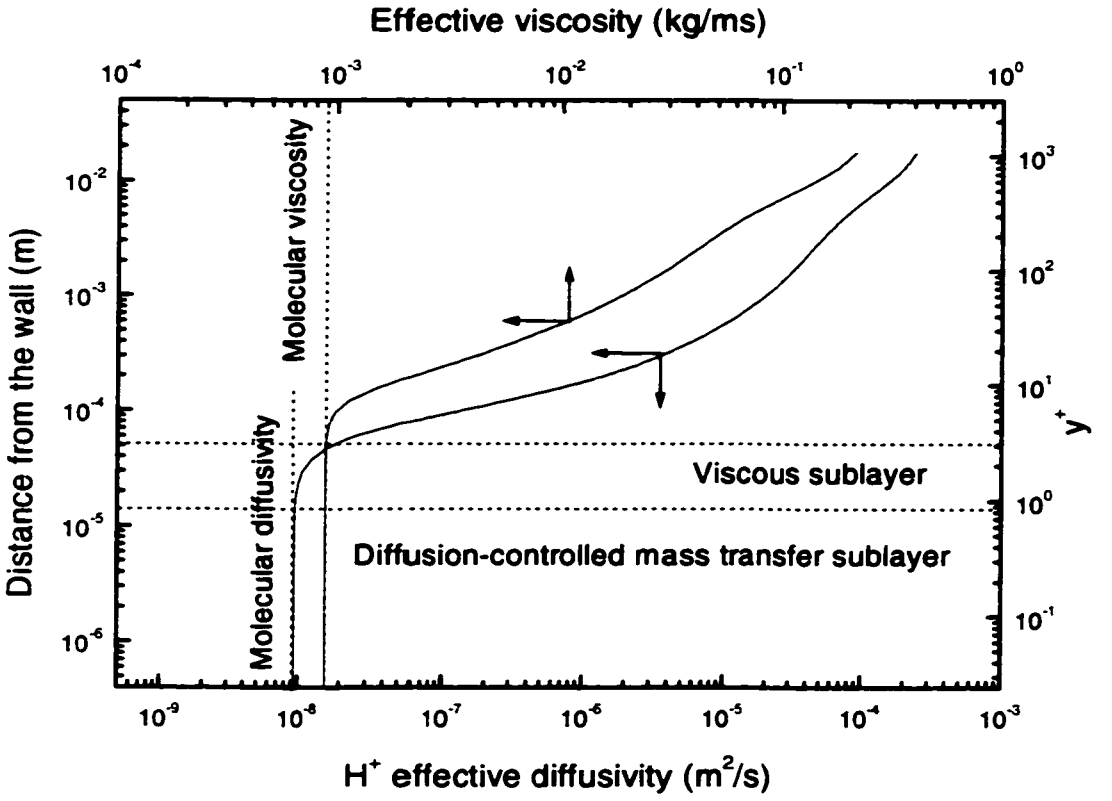

Figure 7.53 Variation of H^+ transport coefficients with distance from the wall. U_b = 1.01 m/s; T = 25 ^{0}C; Re = 45530; Sc = 96; d = 40 mm.

Figure 7.51 (Fe^{2+}) shows that in the outer portion of the viscous sublayer, the turbulent viscosity is less than 1% of the effective viscosity indicating that very little turbulence is retained. However, the effective diffusivity is still at least one order of magnitude greater than the molecular diffusivity. This illustrates that although the residual turbulence has a negligible effect on momentum transport, it still has considerable impact on the mass transport. The turbulent diffusivity is diminished as the wall is approached. At about 6 μm from the wall, effective diffusivity is reduced to molecular diffusivity. This is the edge of the diffusion controlled mass transfer sublayer where mass is transported exclusively by molecular diffusion. Far away from the wall, the effective diffusivities for the three species are the same because the turbulent contribution to effective diffusivity is predominant. It is observed that the diffusion controlled mass transfer sublayer is imbedded deep inside the viscous sublayer. This is expected of fluids with large Schmidt numbers (Levich, 1962). The diffusion-controlled mass transfer sublayer for Fe^{2+} is the thinnest among the three electroactive species due to the fact ferrous ion has the smallest molecular diffusion coefficient and thus the biggest Schmidt number.

It is seen that the viscous sublayer and the diffusion-controlled mass transfer sublayer for the same species and under the same conditions except at a higher flow

velocity of 10.13 m/s (Figures 7.54 – 7.56) are thinner than those at 1.01 m/s. This is to be expected and is due to more vigorous turbulence and mixing at higher velocities.

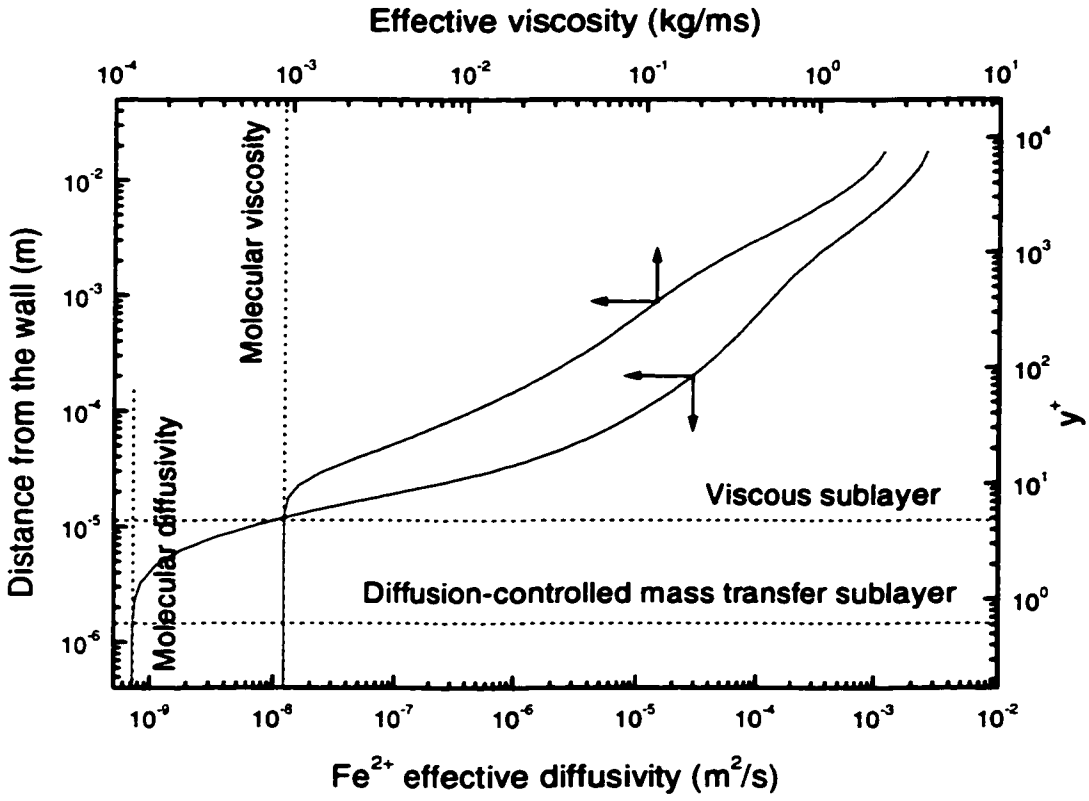

Figure 7.54 Variation of Fe^{2+} transport coefficients with distance from the wall. U_b = 10.13 m/s; T = 25 ^{0}C; Re = 455300; Sc = 1251; d = 40 mm.

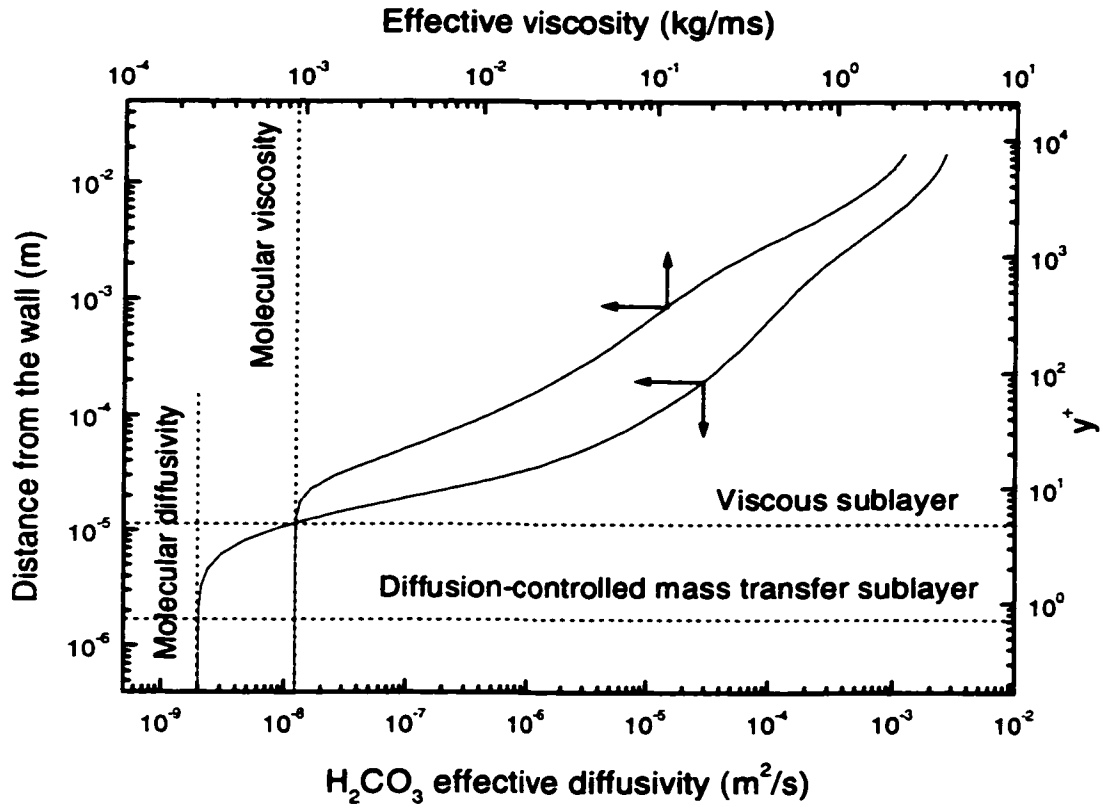

Figure 7.55 Variation of H_2CO_3 transport coefficients with distance from the wall. U_b = 10.13 m/s; T = 25 ^{0}C; Re = 455300; Sc = 445; d = 40 mm.

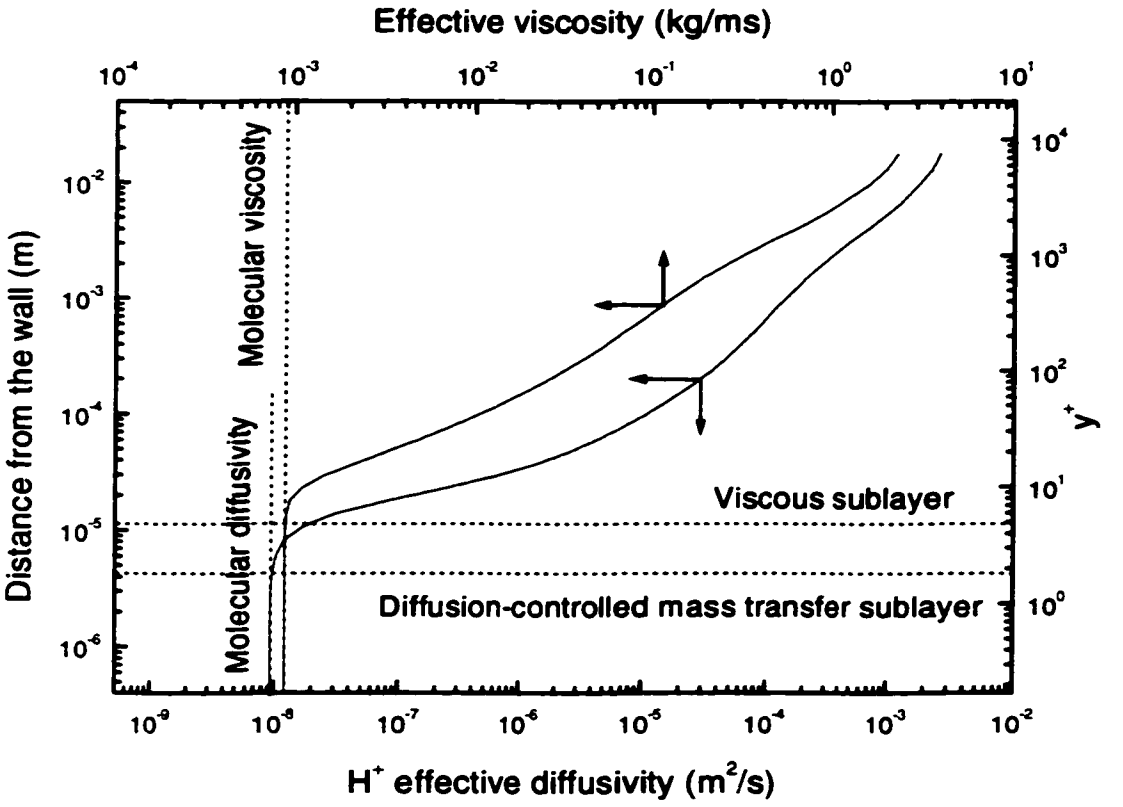

Figure 7.56 Variation of H^+ transport coefficients with distance from the wall. U_b = 10.13 m/s; $T = 25\ ^0C$; $Re = 455300$; $Sc = 96$; $d = 40$ mm.

7.4 Development of an Electrochemical CO_2 Corrosion Model

7.4.1 Introduction

The numerical model presented so far is unique in that it incorporates the three major aspects into the model, namely the turbulent flow, chemical reactions (equilibria), and electrochemical reactions. Mass transfer was modelled using a two dimensional low Reynolds number turbulence model. The species concentration profiles were determined from the corroding surface to the bulk solution and individual electrochemical reaction currents were calculated based on the species surface concentration. The model is of significant academic value and useful in conducting comprehensive investigations of carbon dioxide corrosion. On the other hand, we are also interested in developing a simplified electrochemical model which is simple to use, easy to understand, and yet still firmly based on the fundamental electrochemical principles.

The electrochemical model presented in this section is based on the mixed potential theory. It is built upon the Nesic-Postlethwaite (1994) model with structured Visual Basic programming used to automate the model calculation process. Modelled electrochemical reactions include the cathodic reactions of hydrogen ion reduction,

carbonic acid reduction, water reduction, and dissolved oxygen reduction. The anodic reaction is the dissolution of iron. Mass transport was treated in a simplified way by assuming independent diffusion of the species and by using well established overall mass transfer coefficients for pipe flow.

7.4.2 The Mathematical Model

As the first step, all relevant electrochemical reactions are modelled and quantified. For hydrogen ion reduction, the reaction rate is calculated by the following expression:

$$i_{H^+} = i_{0,H^+}\left[\frac{[H^+]_s}{[H^+]_b}\exp\left(-\frac{\tilde{\alpha}F\eta}{RT}\right)\right] \tag{7.3}$$

Equation (7.3) takes into account the effect of resistance to both charge transfer and mass transfer. The H^+ surface concentration $[H^+]_s$ can be determined from the mass transfer equation:

$$i_{H^+} = KF\left([H^+]_b - [H^+]_s\right) \tag{7.4}$$

where K is the mass transfer coefficient. After eliminating $[H^+]_s$ from equations (7.3) and (7.4), the following current density versus overpotential relationship for H^+ reduction is obtained:

$$\frac{1}{i_{H^+}} = \frac{1}{i_0 10^{-\frac{\eta}{b_c}}} + \frac{1}{i_{\lim}^d} \tag{7.5}$$

The exchange current density, i_0, and the overpotential, η, are based on the *bulk* H^+ concentration. The Tafel slope, b_c, and other relevant information have been detailed in Chapter 6 and are omitted here. The diffusion limiting current density, $i_{\lim}^d$, is:

$$i_{\lim}^d = KF[H^+]_b \tag{7.6}$$

The mass transfer coefficient is calculated from the straight pipe correlation of Berger and Hau (1977):

$$Sh = \frac{Kl}{D} = 0.0165 \times \mathrm{Re}^{0.86} \times Sc^{0.33} \tag{7.7}$$

For H_2CO_3 reduction, a similar relationship to equation (7.5) is used to calculate the reaction current:

$$\frac{1}{i_{H_2CO_3}} = \frac{1}{i_0 10^{-\frac{\eta}{b_c}}} + \frac{1}{i_{\lim}^r} \tag{7.8}$$

The exchange current density and overpotential are also evaluated based on the *bulk* concentrations of H_2CO_3 and/or H^+. The chemical reaction limiting current density, $i_{\lim}^r$, is calculated as (Vetter, 1967; Hurlen *et al.*, 1984):

$$i_{\lim}^{r} = F \times [CO_2]_b \times (D_{H_2CO_3} K_{hyd} k_f)^{0.5} \tag{7.9}$$

where K_{hyd} is the equilibrium constant for the CO_2 hydration reaction and k_f is the forward reaction rate constant for CO_2 hydration.

Pure Tafel behavior can be assumed for the reduction of water:

$$i_{H_2O} = i_0 \times 10^{-\frac{\eta}{b_c}} \tag{7.10}$$

For the reduction of dissolved oxygen:

$$O_{2(aq)} + 4H^+ + 4e^- \rightarrow 2H_2O \tag{7.11}$$

pure mass transfer (diffusion) control can be assumed because of the very low concentration of dissolved oxygen:

$$i_{O_2} = i_{\lim}^{d} = 4KF[O_{2(aq)}]_b \tag{7.12}$$

The dissolved oxygen mass transfer coefficient can be determined from the Berger-Hau correlation presented earlier. The reference oxygen diffusion coefficient is 2.09×10^{-9} m^2/s at 20 ^{0}C (Atkins, 1986).

7.4.3 Implementation of the Model

Now that the reaction currents of all the electrochemical reactions are determined, the corrosion potential, E_{corr}, and the corrosion current, i_{corr}, can be calculated. According to the mixed potential theory, at the corrosion potential, E_{corr}, the total anodic current is equal to the total cathodic current and both are equal to the corrosion current i_{corr}:

$$i_a = \sum i_c = i_{corr} \tag{7.13}$$

The electrochemical model is implemented in Microsoft® Excel 97. Equation (7.13) can be solved by the Solver add-in in Excel. Corrosion rates are predicted based on the input data such as temperature, pH value, solution velocity, CO_2 partial pressure, and pipe diameter.

7.4.4 Automation of the Calculation Procedure Using Visual Basic Programming

Through Visual Basic programming, macros and controls are used to automate the calculation process so that getting the model predictions/results is just a click of mouse away. Figure 7.57 illustrates how the model works. It is basically a two step process. Parameters are first input to the model. Then the user can click one of four buttons to get the CO_2 corrosion rate, kinetic corrosion E-i diagrams (Figure 7.58), the

theoretical potential dynamic sweep curve, or the theoretical linear polarization curve for the corrosion system.

The essential computer code written in Visual Basic is attached in Appendix A. There are 7 macros in the code and all are placed in Module 1. Execution of the Return_To_Main_Menu macro makes worksheet Main_Menu the active worksheet. The Calculate_Now macro calculates forcibly all open workbooks and worksheets. The Calc_Corrosion_Rate macro uses the Solver functions to solve for the corrosion potential and the corrosion current. If after calculation the net current, which is defined as $\left|\left\{\left(\left|i_a\right|\right)-\left(\left|\sum i_c\right|\right)\right\}\right|$, is found to be greater than 0.0001 A/m^2, a message appears cautioning that more time or more iterations are needed and that calculation results may not be reliable. A current of 0.0001 A/m^2 corresponds to a corrosion rate of approximately 1.2×10^{-4} mm/yr. The remaining four macros (Corrosion_Rate, E_i_Diagram, Sweep_Chart, and Linear_Polarization_Chart) have similar code structures. First, the Calculate_Now macro is called if the workbook calculation mode is not set to "automatic". Next, if the net current is greater than 0.0001 A/m^2, the Calc_Corrosion_Rate macro is called. Finally the appropriate results are tabulated or plotted and the relevant worksheet is made the active worksheet.

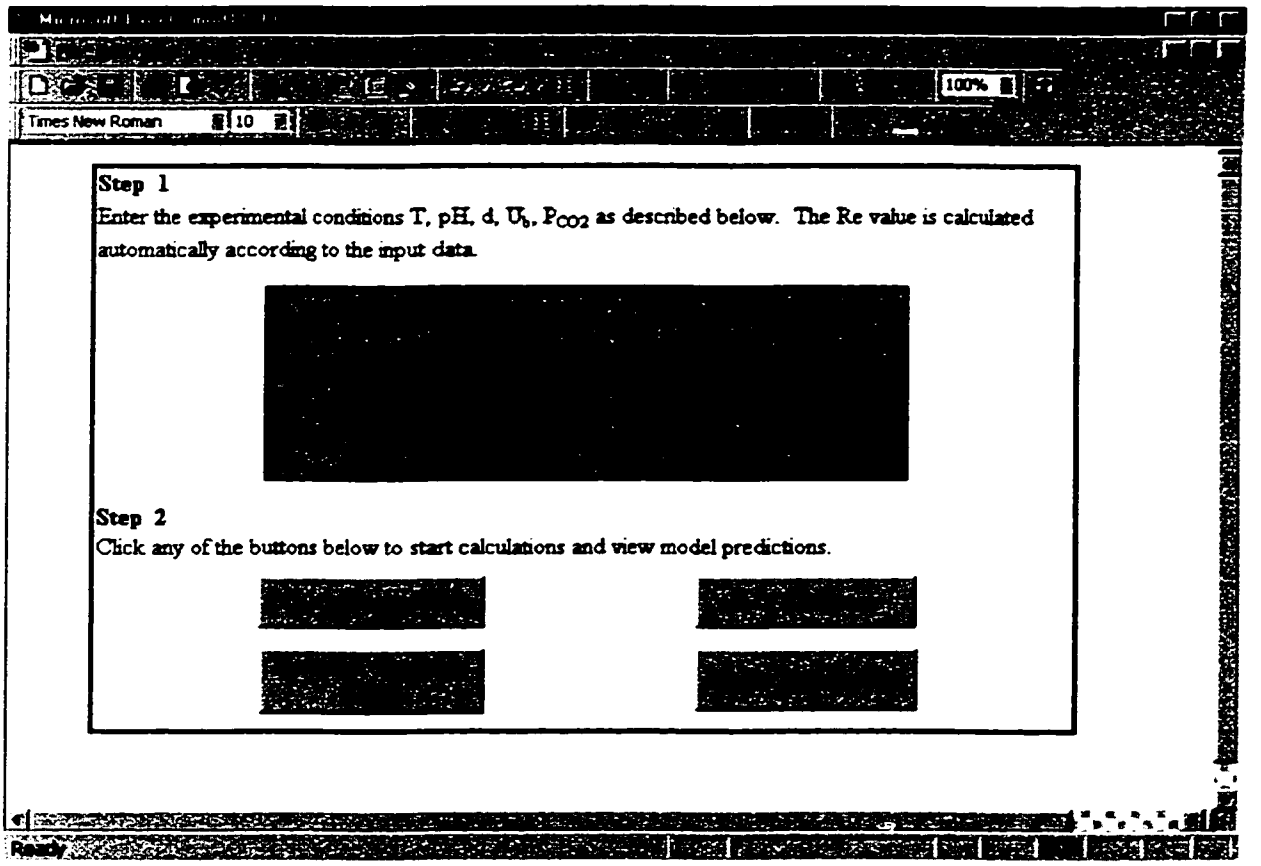

Figure 7.57 Illustrative input and control screen of the electrochemical model.

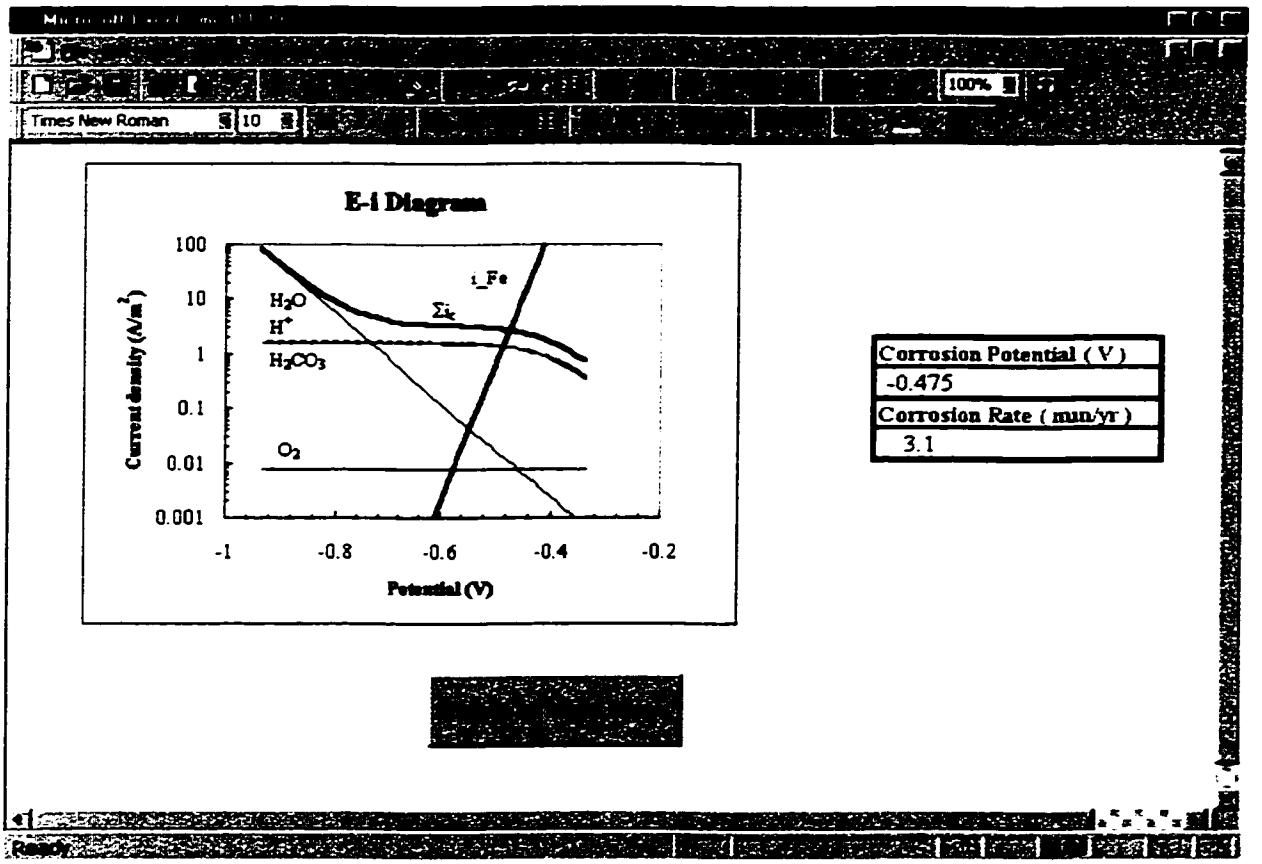

Figure 7.58 Illustrative E-i corrosion diagram generated by the electrochemical model.

7.4.5 Validation of the Electrochemical Model

The present electrochemical model is validated by comparing model predictions with those of two well-known semi-empirical models, the de Waard and Lotz model (1993) and the Dugstad *et al.* model (1994).

Figure 7.59 illustrates the effects of flow on predicted corrosion rates for pH 4, 20 ^{0}C and 0.1 MPa of CO_2 partial pressure. It is seen that the present predictions are somewhat in between the two other models at low flow velocities (< 2 m/s) and at high velocities (> 7 m/s). At intermediate velocities the present model agrees better with the Dugstad *et al.* model.

The pH effects on the CO_2 corrosion are shown in Figure 7.60. In the pH range of 3.9 to 5.5, the present model predictions are again in between the predictions from the other two models. At very low pH values (< 3.9), the hydrogen ion reduction is the predominant cathodic reaction. Therefore the present model predicts sharp increases in corrosion rates with decreasing pH values. At high pH values (> 5.5), the H_2CO_3 reduction is dominant and the contribution from the H^+ reduction is insignificant due to the limited availability of H^+ ions. Therefore the corrosion rates are almost unaffected by the increase in pH values.

The predicted temperature dependence of the corrosion rates are plotted in Figure 7.61. The present model performs similarly as the de Waard and Lotz model except at higher temperatures (> 60 ^{0}C) due to the formation of protective films. The presence of protective films slows down corrosion rate. Both the de Waard-Lotz model and the Dugstad *et al.* model have used a correction factor for protective film formation.

Figure 7.62 shows the predicted effects of CO_2 partial pressure on corrosion rates. It is seen that at $P_{CO_2} \geq 1$ bar (10^5 Pa) the present model reproduces the power law dependence exhibited by the other two models. The exponent is approximately 0.7. At CO_2 partial pressure less than 1 bar, the present model predicts slight decrease in the corrosion rates with decreasing CO_2 partial pressures.

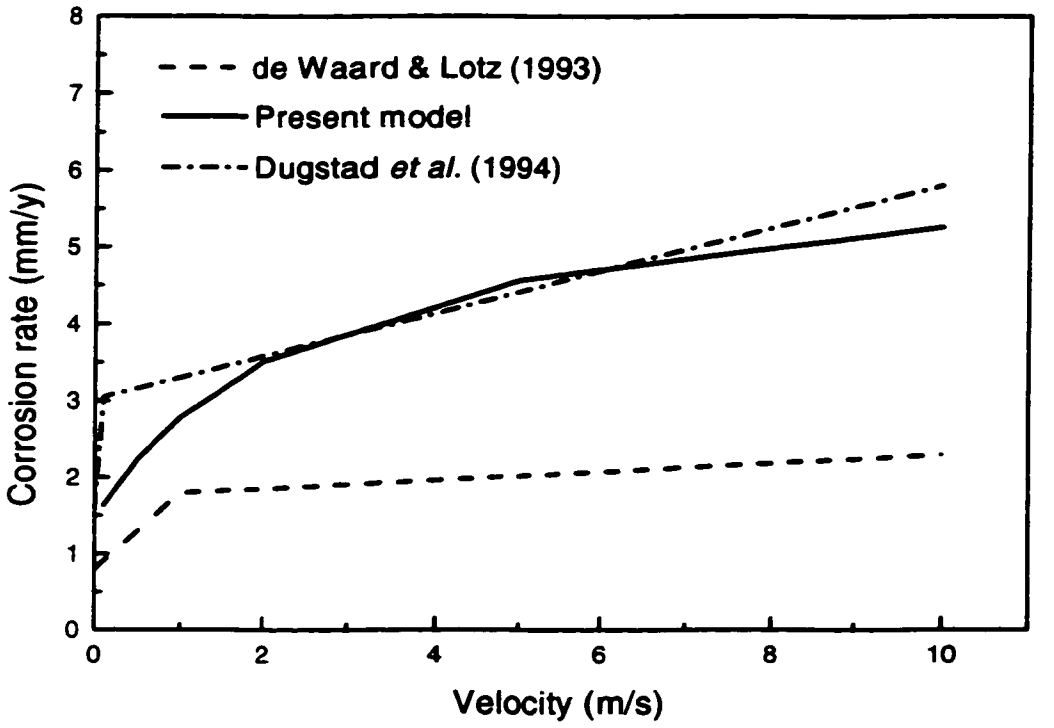

Figure 7.59 Comparison of predicted effects of flow on CO_2 corrosion rate. P_{CO_2} = 0.1 MPa; $pH = 4$; $T = 20\ ^0C$.

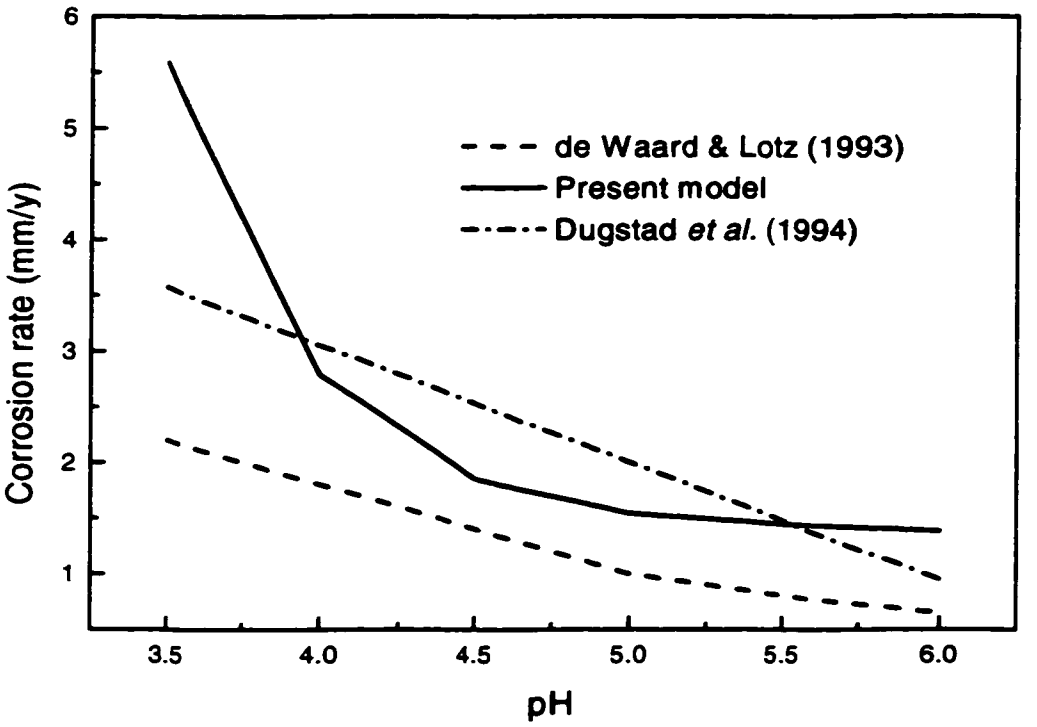

Figure 7.60 Comparison of predicted pH effects on CO_2 corrosion rate. P_{CO_2} = 0.1 MPa; T = 20 ^{0}C; U_b = 1.0 m/s.

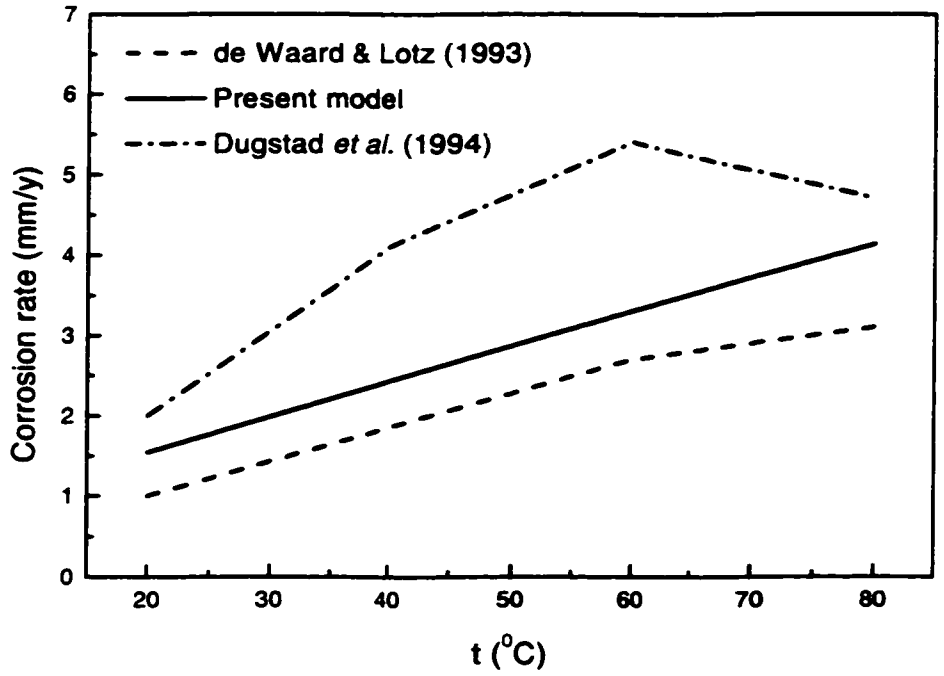

Figure 7.61 Comparison of predicted effects of temperature on CO_2 corrosion rate. P_{CO_2} = 0.1 MPa; pH = 5; U_b = 1.0 m/s.

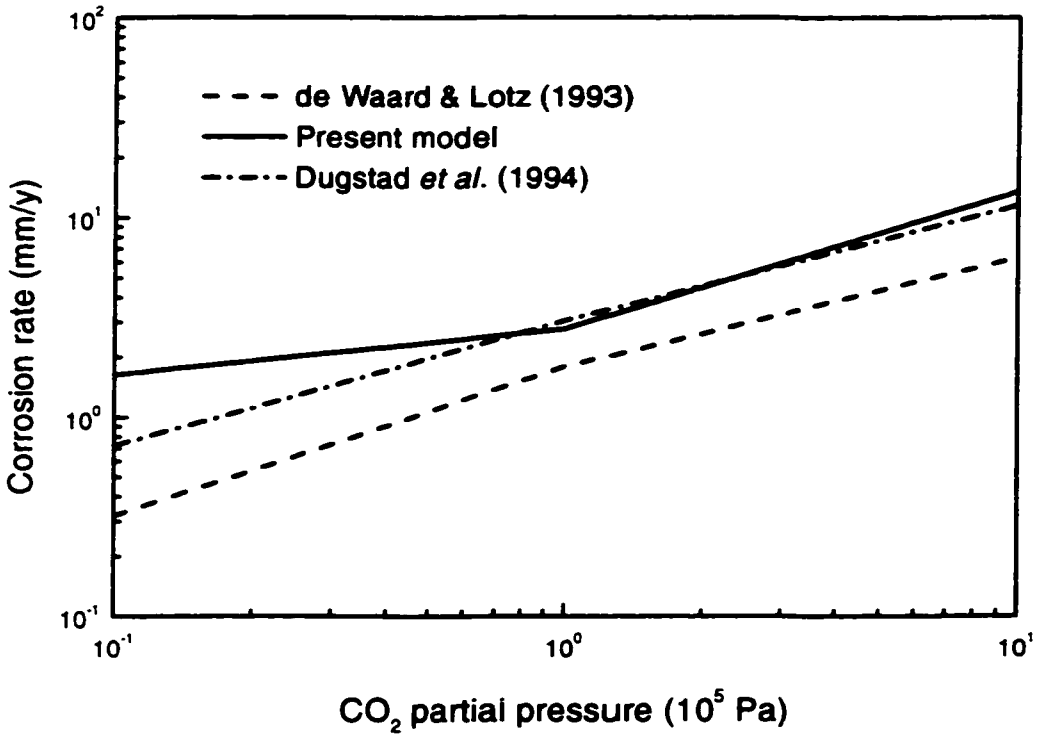

Figure 7.62 Comparison of predicted effects of CO_2 partial pressure on the corrosion rate. $pH = 4$; $T = 20\ ^0C$; $U_b = 1.0$ m/s.

7.4.6 Applications of the Electrochemical Model

The present electrochemical model is straightforward, easy and inexpensive to run, and yet still theoretically sound and keeps the user informed of all the reactions and processes taking place inside the corrosion system. It can be used to predict the CO_2 corrosion rates under different experimental conditions. Alternatively, it can be used to study the effects of various parameters on CO_2 corrosion. The model provides E-i diagrams with individual and total electrochemical reaction currents. Therefore, it can also be used to study the effects of various parameters on individual electrochemical reactions, and to investigate the relative importance of the cathodic currents to the corrosion rate.

Some final words on the differences between the numerical model (Sections 7.2 and 7.3) and the simplified electrochemical model (Section 7.4) are in order. With a low Reynolds number turbulence model used in the modelling of turbulent flow and mass transport, the numerical model can be employed to study carbon dioxide corrosion under developing, fully-developed or disturbed flow conditions. The simplified electrochemical model, on the other hand, can only be used to estimate the corrosion rate in developed flows with fully-developed concentration boundary layers as overall mass transfer coefficients for the electroactive species are used in the model.

8. Conclusions

8.1 The Numerical CO_2 Corrosion Model

A predictive model is developed to simulate the aqueous carbon dioxide corrosion of iron in turbulent pipe flow. It takes into account diffusion, convection, and charge transfer. The model also allows for the slow homogeneous chemical reaction of CO_2 hydration and various rapid solution equilibria.

The mass transfer is modelled with a two dimensional low Reynolds number k-ε turbulence model by simultaneously solving the conservation equations for mass, axial momentum, radial momentum, kinetic energy of turbulence and its dissipation rate, along with the concentrations of various dissolved species. The effect of the slow homogeneous chemical reaction of CO_2 hydration is incorporated into the model by including an extra source term in the transport equation for carbonic acid. Other homogeneous chemical reactions are assumed to be in equilibrium with the equilibrium adjusted after each iteration. The cathodic reactions considered are the reduction of H_2CO_3, the H^+ reduction and the reduction of H_2O. The anodic reaction is the iron dissolution.

An iterative procedure is employed to calculate the CO_2 corrosion rates. It involves the determination of surface concentrations of dissolved species and the fluxes of all the reacting species at the surface. The iteration ensures that mixed potential theory is satisfied and that the various surface chemical equilibria are preserved. The simulation results show that:

- At bulk pH 4 and very low flow velocities the reduction of carbonic acid is controlled by the slow homogeneous chemical reaction of CO_2 hydration. The reduction limiting current agrees well with the chemical reaction limiting current given by the Vetter equation (Vetter, 1967). At higher velocities and in the high current density region where Tafel behavior is no longer observed, H_2CO_3 reduction is controlled by the interaction of chemical reaction and mass transfer. At higher current densities, hydrogen ion reduction is controlled by the mass transport of H^+ from the bulk solution to the surface.

- The relative contributions of H_2CO_3, H^+, and H_2O reduction to the corrosion current depend on the solution pH. At bulk pH 4, hydrogen ion reduction and H_2CO_3 reduction are both important. The contribution of water reduction is negligible. At pH 6, the carbonic acid reduction is the dominant cathodic reaction. The contribution of H_2O reduction is small compared to that of H_2CO_3 reduction.

- The H^+ reduction is more flow sensitive than the H_2CO_3 reduction. H_2O reduction is assumed to be charge transfer controlled and flow independent. CO_2 corrosion rates

are more flow sensitive at bulk pH 4 than at higher pH values due to the fact that the H^+ reduction is the dominant cathodic reaction at pH 4.

- Generation of H_2CO_3 through the slow homogeneous chemical reaction of CO_2 hydration enhances the H_2CO_3 mass transport and reduces the H_2CO_3 mass transfer entrance length. The H_2CO_3 generated through CO_2 hydration also serves as an extra source of hydrogen ions. As a result, CO_2 hydration increases the H_2CO_3 limiting current at all flow velocities though the effect is more remarkable at lower velocities. It also moderately increases the H^+ limiting current at relatively low velocities. At high velocities, the impact is negligible.

- The corrosion rates in the developing section of the mass transfer boundary layer will be much larger than those determined for fully developed mass transfer.

- The CO_2 corrosion rate is accelerated by flow through an approximate power law: $CR = C \times U_b{}^n$. At bulk pH 4, the exponent, n, has a value of about 0.4 which is less than 0.8 indicating that the corrosion process is not purely mass transfer controlled but rather it is under the mixed control of mass transfer and charge transfer. At pH 6, the value of the exponent n is smaller than that for pH 4 which indicates a smaller flow effect at higher pH values. The corrosion rate increases with increasing CO_2 partial pressure. Their relationship is found to be $CR \propto \left(P_{CO_2}\right)^{0.7}$.

- Present model predictions were tested against experimental results and the de Waard-Lotz model (1993). Good agreement is achieved.

8.2 The Electrochemical Model

A simplified electrochemical model is developed for the corrosion of iron in CO_2-water system. It takes into account the following electrochemical reactions: hydrogen ion reduction, carbonic acid reduction, water reduction, dissolved oxygen reduction and the anodic dissolution of iron. The electrochemical reactions are quantified by using the rate equation which takes into account the effect of resistance to both charge transfer and mass transfer. The species overall mass transfer coefficients are calculated from the straight pipe correlation of Berger and Hau (1977). Corrosion rates are calculated based on the mixed potential theory.

The model is implemented in Microsoft® Excel 97. Corrosion rates are predicted based on the input data such as temperature, pH value, solution velocity, CO_2 partial pressure, and pipe diameter. Through Visual Basic programming, macros and controls are used to automate the calculation process.

Predictions of the present electrochemical model were compared to those of other well-known CO_2 corrosion models and generally good agreement was achieved. The present model is easy to use and, unlike the semi-empirical models, provides the

user with a clear picture of all the reactions and processes taking place inside the corrosion system. It can be used to study the governing corrosion mechanisms under specified conditions.

9. Recommendations

This study has been focused on CO_2 corrosion in constant geometry straight pipes. When the geometry changes abruptly such as in a sudden pipe expansion, the flow separates and develops a recirculation region. Such regions are of considerable practical relevance and are often where severe corrosion problems occur. With minor modifications, the present numerical model could be applied to study CO_2 corrosion under these disturbed flow conditions.

The numerical model can be extended by taking into account the protective film formation and growth. This could be accomplished in two stages. First, by implementing the solubility limits for $FeCO_3$, it is possible to account for the formation of protective iron carbonate films. In the second stage, species such as Na^+, Cl^-, Ca^{2+}, Br^-, Ba^{2+}, and Sr^{2+} could be added to achieve a more realistic modelled system and to account for the formation of complex scales.

For model validation and calibration, more experimental data are needed. An extensive experimental program should be pursued to study the CO_2 corrosion under various flow conditions, in a variety of aqueous solution conditions and on various steels.

Bibliography

Abe, K., Kondoh, T., Nagano, Y., "A New Turbulence Model for Predicting Fluid Flow and Heat Transfer in Separating and Reattaching Flows – I. Flow Field Calculations," *Int. J. Heat Mass Transfer*, Vol. 37, No. 1, p. 139-151 (1994).

Adams, C.D., Garber, J.D., Fang, C.S., Perkins, R., Reinhardt, J.R., "Methods of Prediction of Tubing Life for Gas Condensate Wells Containing CO_2," *23rd Annual Offshore Technology Conference*, Houston, Texas (1991).

Adams, C.D., Garber, J.D., Walters, F.H., Singh, C., "Verification of Computer Modelled Tubing Life Predictions by Field Data," *CORROSION/93*, paper no. 82 (Houston, TX: NACE, 1993).

American Petroleum Institute, Corrosion of Oil- and Gas-Well Equipment, API, Dallas, Texas (1958).

Atkins, P.W., Physical Chemistry, 2nd ed., Oxford University Press, Oxford, England, p. 905 (1986).

Baes, C.F., Jr., Mesmer, R.E., The Hydrolysis of Cations, John Wiley & Sons, New York, p. 227 (1976).

Bard, A.J., Faulkner, L.R., Electrochemical Methods, Fundamentals and Applications, John Wiley and Sons, Chapters 8 and 11 (1980).

Berger, F.P., Hau, K.-F.F.-L., "Mass Transfer in Turbulent Pipe Flow Measured by the Electrochemical Method", *Int. J. Heat Mass Transfer*, Vol. 20, p. 1185-1194 (1977).

Bockris, J.O.M., Drazic, D., Despic, A.R., "The Electrode Kinetics of the Deposition and Dissolution of Iron", *Electrochimica Acta*, Vol. 4, p. 325 (1961).

Bockris, J.O.M., Reddy, A.K.N., Modern Electrochemistry – An Introduction to an Interdisciplinary Area, Volume 2, Plenum Press, New York (1970).

Boussinesq, J., "Theorie de l'Ecoulement Tourbillant," *Mem. Presentes par Divers Savants Acad. Sci. Inst. Fr.*, Vol. 23, p. 46-50 (1877).

Copson, H.R., *Corrosion*, Vol. 7, No. 4, p. 123 (1951).

Craig, B.D., Anderson, D.S., eds., Handbook of Corrosion Data, ASM International, Metals Park, Ohio, p. 250 (1995).

Davies, J.T., Turbulence Phenomena, Academic Press, New York (1972).

de Waard, C., Lotz, U., "Prediction of CO_2 Corrosion of Carbon Steel," *CORROSION/93*, paper no. 69 (Houston, TX: NACE, 1993).

de Waard, C., Lotz, U., Milliams, D. E., "Predictive Model for CO_2 Corrosion Engineering in Wet Natural Gas Pipelines", *Corrosion/91*, paper no. 577 (Houston, TX: NACE, 1991).

de Waard, C., Milliams, D.E., "Carbonic Acid Corrosion of Steel", *Corrosion*, Vol. 31, p. 131 (1975a).

de Waard, C., Milliams, D.E., "Prediction of Carbonic Acid Corrosion in Natural Gas Pipelines," *First International Conference on the Internal and External Protection of Pipes*, University of Durham, UK (1975b).

Deberry, D.W., Clark, W.S., "Corrosion Due to Use of Carbon Dioxide for Enhanced Oil Recovery," U.S. Dept. of Energy Report, DOE/MC/08442-Ti (1979).

Dugstad, A., "The Importance of $FeCO_3$ Supersaturation on the CO_2 Corrosion of Carbon Steels," *CORROSION/92*, paper no. 14 (Houston, TX: NACE, 1992).

Dugstad, A., Lunde, L., Videm, K., "Parametric Study of CO_2 Corrosion of Carbon Steel," *CORROSION/94*, paper no. 14 (Houston, TX: NACE, 1994).

Dunlop, A.K., Hassell, H.L., Rhodes, P.A., "Fundamental Considerations in Wet Gas Well Corrosion," in Advances in CO_2 Corrosion – Volume 1, Proceedings of the CORROSION/83 Symposium on CO_2 Corrosion in the Oil and Gas Industry, eds. Hausler, R.H., Godard, H.P., p. 52 (Houston, TX: NACE, 1984).

Eriksrud, E., Søntvedt, T., "Effect of Flow on CO_2 Corrosion Rates in Real and Synthetic Formation Waters," in Advances in CO_2 Corrosion – Volume 1, Proceedings of the CORROSION/83 Symposium on CO_2 Corrosion in the Oil and Gas Industry, eds. Hausler, R.H., Godard, H.P., p. 20 (Houston, TX: NACE, 1984).

Graves, J.W., Sullivan, E.H., *Materials Protection*, Vol. 5, No. 6, p. 33 (1966).

Gray, L.G.S., Anderson, B.G., Danysh, M.J., Tremaine, P.G., "Mechanism of Carbon Steel Corrosion in Brines Containing Dissolved Carbon Dioxide at pH 4," *CORROSION/89*, paper no. 464 (Houston, TX: NACE, 1989).

Gray, L.G.S., Anderson, B.G., Danysh, M.J., Tremaine, P.R., "Effect of pH and Temperature on the Mechanism of Carbon Steel Corrosion by Aqueous Carbon Dioxide," *CORROSION/90*, paper no. 40 (Houston, TX: NACE, 1990).

Hausler, R.H., "The Mechanism of CO_2 Corrosion of Steel in Hot, Deep Gas Wells," in Advances in CO_2 Corrosion – Volume 1, Proceedings of the CORROSION/83 Symposium on CO_2 Corrosion in the Oil and Gas Industry, eds. Hausler, R.H., Godard, H.P., p. 72 (Houston, TX: NACE, 1984).

Hinze, J.O., Turbulence, 2nd ed., McGraw-Hill, New York, p. 23 (1975).

Hurlen, T., Gunvaldsen, S., Tunold, R., Blaker, F., Lunde, P.G., "Effect of Carbon Dioxide on Reactions at Iron Electrodes in Aqueous Salt Solutions", *J. Electroanal. Chem.*, Vol. 180, p. 511 (1984).

Ikeda, A., Mukai, S., Ueda, M., "Prevention of CO_2 Corrosion of Line Pipe and Oil Country Tubular Goods," *CORROSION/84*, paper no. 289 (Houston, TX: NACE, 1984).

Ikeda, A., Ueda, M., Mukai, S., "CO_2 Corrosion Behaviour and Mechanism of Carbon Steel and Alloy Steel," *CORROSION/83*, paper no. 45 (Houston, TX: NACE, 1983).

Ikeda, A., Ueda, M., Mukai, S., "Influence of Environmental Factors on Corrosion in CO_2 Source Well," in Advances in CO_2 Corrosion – Volume 2, p. 1 (Houston, TX: NACE, 1985).

Jones, W.P., Launder, B.E., "The Calculation of Low Reynolds Number Phenomena with a Two-Equation Model of Turbulence," *Int. J. Heat Mass Transfer*, Vol. 16, p. 1119-1130 (1973).

Jones, W.P., Launder, B.E., "The Prediction of Laminarization with a Two-Equation Model of Turbulence," *Int. J. Heat Mass Transfer*, Vol. 15, p. 301-314 (1972).

Kays, W.M., Crawford, M.E., Convective Heat and Mass Transfer, McGraw-Hill, New York, p. 225 (1980).

Kern, D.M., *Journal of Chemical Education*, Vol. 37, No. 1, p. 19 (1960).

Launder, B.E., Spalding, D.B., *Computer Methods in Applied Mechanics and Engineering*, Vol. 3, p. 269-289 (1974).

Levich, V., Physicochemical Hydrodynamics, Prentice-Hall, Englewood Cliffs, New Jersey, p. 144-154 (1962).

Lide, D.R., Frederikse, H.P.R., eds., CRC Handbook of Chemistry and Physics, CRC Press, Boca Raton, Florida, p. 6-3 (1997).

Lotz, U., "Velocity Effects in Flow Induced Corrosion," *CORROSION/90*, paper no. 27 (Houston, TX: NACE, 1990).

Manner, R., Heitz, E., *Werkstoffe und Korrosion*, Vol. 29, p. 783 (1978).

Maron, M.J., Numerical Analysis – A Practical Approach, 2nd edition, Macmillan Publishing Company, New York (1987).

Martin, R.L., "Corrosion Control by Inhibitors in Producing Oil Wells in Carbon Dioxide Flooded Fields," in Advances in CO_2 Corrosion – Volume. 2, p. 250 (Houston, TX: NACE, 1985).

Murata, T., Sato, E., Matsuhashi, R., "Factors Controlling Corrosion of Steels in CO_2-Saturated Environments," in Advances in CO_2 Corrosion – Volume 1, Proceedings of the CORROSION/83 Symposium on CO_2 Corrosion in the Oil and Gas Industry, eds. Hausler, R.H., Godard, H.P., p. 64 (Houston, TX: NACE, 1984).

Nagano, Y., Tagawa, M., "An Improved k-ε Model for Boundary Layer Flows," *ASME J. Fluids Eng.*, Vol. 112, p. 33-39 (1990).

Nagy, Z., Thomas, D.A., *J. Electrochem. Soc.*, Vol. 133, p. 2013 (1986).

Nesic, S., "Prediction of Transport Processes in CO_2 Corrosion," in A Working Party Report on Predicting CO_2 Corrosion in the Oil and Gas Industry, The Institute of Metals, London, England, p. 120 (1994).

Nesic, S., Postlethwaite, J., "Modelling of CO_2 Corrosion Mechanisms," in Modelling Aqueous Corrosion, eds. Trethewey, K.R., Roberge, P.R., Kluwer Academic Publishers, The Netherlands, p. 317 (1994).

Nesic, S., Postlethwaite, J., Olsen, S., "An Electrochemical Model for Prediction of Corrosion of Mild Steel in Aqueous Carbon Dioxide Solutions," *Corrosion*, Vol. 52, No. 4, p. 280 (1996).

Nesic, S., Postlethwaite, J., Vrhovac, M., *Corrosion Reviews*, Vol. 15, Nos. 1-2, p. 211-240 (1997).

Nesic, S., Pots, B.F.M., Postlethwaite, J., Thevenot, N., "Superposition of Diffusion and Chemical Reaction Controlled Limiting Currents - Application to CO_2 Corrosion," Journal of Corrosion Science and Engineering, Vol. 1, paper no. 3 (Internet edition, http://www.cp.umist.ac.uk/JCSE/: The Corrosion Information Server, 1995).

Palacios, C.A., "Mechanisms of CO_2 Corrosion Related to Velocity in Two-Phase Flow Systems," Ph.D. Thesis, The University of Tulsa (1990).

Palmer, D.A., Eldik, R.V., *Chem. Rev.*, Vol. 83, p. 651 (1983).

Parsons, R., Handbook of Electrochemical Constants, Academic Press, New York, p. 85 (1959).

Patankar, S.V., Numerical Heat Transfer and Fluid Flow, Hemisphere Publishing Corp., New York, p. 126 (1980).

Patankar, S.V., Spalding, D.B., *Int. J. Heat Mass Transfer*, Vol. 15, p. 1787 (1972).

Postlethwaite, J., Nesic, S., Adamopoulos, G., "Modelling Local Mass-Transfer Controlled Corrosion at Geometrical Irregularities," *Materials Science Forum*, Vols. 111 – 112, p. 53-62 (1992).

Postlethwaite, J., Wang, F., "Modelling Mass Transport in Aqueous CO_2 Corrosion in Turbulent Pipe Flow," *Electrochemical Methods in Corrosion Research 97: Sixth*

International Symposium on Electrochemical Methods in Corrosion Research, Trento, Italy (1997).

Pots, B.F.M., "Mechanistic Models for the Prediction of CO_2 Corrosion Rates Under Multi-Phase Flow Conditions," *CORROSION/95*, paper no. 137 (Houston, TX: NACE, 1995).

Prandtl, L., "Uberdie ausgebildete Turbulenz," *ZAMM*, Vol. 5, p. 136 (1925).

Press, W.H., Teukolsky, S.A., Vetterling, W.T., Flannery, B.P., Numerical Recipes in FORTRAN – The Art of Scientific Computing, Cambridge University Press, New York (1992).

Reid, R.C., Prausnitz, J.M., Sherwood, T.K., The Properties of Gases and Liquids, McGraw-Hill, New York (1977).

Reynolds, O., "On the Dynamic Theory of Incompressible Viscous Fluids and the Determination of the Criterion," *Philosophical Transactions of the Royal Society of London*, Series A, Vol. 186, p. 123 (1895).

Roberts, B.E., Tremaine, P.R., "Vapor Liquid Equilibrium Calculations for Dilute Aqueous Solutions of CO_2, H_2S, NH_3 and NaOH to 300 ^{0}C", *The Canadian Journal of Chemical Engineering*, Vol. 63, p. 294 (1985).

Rogers, W.F., Shellshear, W.A., *Ind. Eng. Chem.*, Vol. 29, No. 2, p. 160 (1937).

Schlichting, H., Boundary-Layer Theory, 7th ed., McGraw-Hill, New York (1979).

Schmitt, G., "Fundamental Aspects of CO_2 Corrosion," *CORROSION/83*, paper no. 43 (Houston, TX: NACE, 1983).

Schmitt, G., Rothmann, B., *Werkstoffe und Korrosion*, Vol. 28, p. 816 (1977).

Schmitt, G., Rothmann, B., *Werkstoffe und Korrosion*, Vol. 29, p. 98 (1978).

Schwenk, W., *Werkstoffe und Korrosion*, Vol. 25, p. 643 (1974).

Singer, P.C., Stumm, W., "The Solubility of Ferrous Iron in Carbonate-Bearing Waters," *Jour. AWWA*, Vol. 62, p. 198-202 (1970).

Stern, M., "The Electrochemical Behavior, Including Hydrogen Overvoltage, of Iron in Acid Environments," *J. Electrochem. Soc.*, Vol. 102, No. 11, p. 609-616 (1955).

Stern, M., Geary, L., *J. Electrochem. Soc.*, Vol. 104, p. 56 (1957).

Sweeton, F.H., Mesmer, R.E., Baes, C.F., Jr., "Acidity Measurements at Elevated Temperatures. VII. Dissociation of Water", *J. Solution Chem.*, Vol. 3, p. 191-214 (1974).

Tennekes, H., Lumley, J.L., A First Course in Turbulence, MIT Press, Cambridge, Mass. (1972).

Turgoose, S., Cottis, R.A., Lawson, K., "Modelling of Electrode Processes and Surface Chemistry in Carbon Dioxide Containing Solutions", *ASTM Symposium on Computer Modelling for Corrosion*, San Antonio, Texas (1990).

Vetter, K.J., Electrochemical Kinetics: Theoretical and Experimental Aspects, trans. eds. Bruckenstein, S., Howard, B., Academic Press, New York, p. 231-244 (1967).

Videm, K., Dugstad, A., "Film Covered Corrosion, Film Breakdown and Pitting Attack of Carbon Steels in Aqueous CO_2 Environments," *CORROSION/88*, paper no. 186 (Houston, TX: NACE, 1988).

Videm, K., Dugstad, A., *Materials Performance*, Vol. 28, No. 3, p. 64 (1989).

Wagner, C., Traud, W., *Z. Electrochem.*, Vol. 44, p. 391 (1938).

Wang, Y., Postlethwaite, J., Bergstrom, D.J., *J. Electrochem. Soc.*, Vol. 26, p. 471 (1996).

Wilcox, D.C., Turbulent Modelling for CFD, DCW Industries, California (1993).

Appendix A. The Computer Source Code Used in the Electrochemical Model

```
' Return_To_Main_Menu Macro
Sub Return_To_Main_Menu()
    ActiveWindow.ScrollWorkbookTabs Position:=xlFirst
    Sheets("Main Menu").Select
End Sub

' Calculate_Now Macro
Sub Calculate_Now()
    Application.MaxChange = 0.001
    ActiveWorkbook.PrecisionAsDisplayed = False
    Application.Calculate
End Sub

' Calc_Corrosion_Rate Macro
Sub Calc_Corrosion_Rate()
    Sheets("Data_Pipe").Select
    Range("A400").Select
```

```
    SolverReset
    SolverOptions Iterations:=10000, Precision:=0.00001, Convergence:=0.00001
    SolverOk SetCell:="$F$76", MaxMinVal:=2, ValueOf:="0", ByChange:="$F$64"
    SolverSolve UserFinish:=True
    If Cells(76, 6).Value > 0.0001 Then
      MsgBox ("More time or iterations are needed.  Calculation results may not be
reliable.")
    End If
End Sub


' Corrosion_Rate Macro
Sub Corrosion_Rate()
    If Application.Calculation <> xlAutomatic Then
      Calculate_Now
    End If
    If Sheets("Data_Pipe").Cells(76, 6).Value > 0.0001 Then
      Calc_Corrosion_Rate
    End If
    Sheets("Corrosion_Rate").Select
End Sub


' E_i_Diagram Macro
Sub E_i_Diagram()
```

```
    If Application.Calculation <> xlAutomatic Then
        Calculate_Now
    End If
    If Sheets("Data_Pipe").Cells(76, 6).Value > 0.0001 Then
        Calc_Corrosion_Rate
    End If
    Sheets("E- i _ Chart").Select
End Sub

' Sweep_Chart Macro
Sub Sweep_Chart()
    If Application.Calculation <> xlAutomatic Then
        Calculate_Now
    End If
    If Sheets("Data_Pipe").Cells(76, 6).Value > 0.0001 Then
        Calc_Corrosion_Rate
    End If
    Sheets("Sweep_Chart").Select
End Sub

'Linear_Polarization_Chart Macro
Sub Linear_Polarization_Chart()
    If Application.Calculation <> xlAutomatic Then
```

```
    Calculate_Now
  End If
  If Sheets("Data_Pipe").Cells(76, 6).Value > 0.0001 Then
    Calc_Corrosion_Rate
  End If
  Sheets("LinearPolar_Chart").Select
End Sub
```